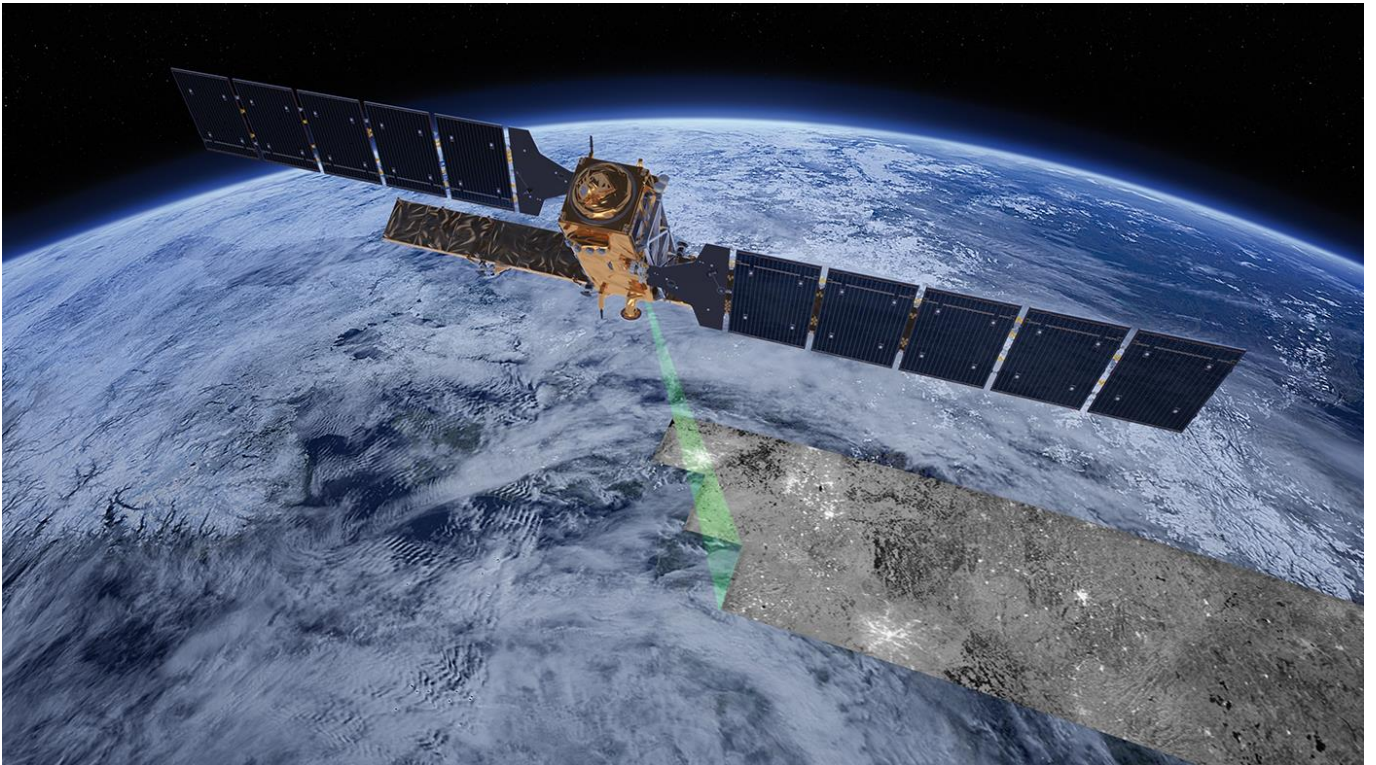


Comparison of deformation and surface water level time series from different locations at the Port of Rotterdam



*Developing an analysis methodology to correlate InSAR vertical deformation time series and
fluctuating surface water levels*

Kevin Ochieng

BSc. Graduation thesis

Faculty: Land and Water management

Specialization: Hydrology

Van Hall Larenstein University of Applied Sciences

Comparison of deformation and surface water level time series from different locations at the Port of Rotterdam

by

Kevin Ochieng

to obtain the degree of Bachelor of Science in Land and Water
management at the Van Hall Larenstein University of Applied
Sciences in 2018

Company: SkyGeo

Location: Oude Delft 175, 2611 HB Delft

Educational institution: VHL University of Applied Sciences

Faculty: Land and Water management

Location: Larensteinselaan 26-A, 6882 CT Velp

Supervision from SkyGeo:

Martijn Houtepen | Customer Access Manager

Contact: martijn.houtepen@skygeo.com

Supervision from VHL University of Applied Sciences

Ir. J.C.M. (Jack) Schoenmakers | Land use Planning and GIS

Contact: jack.schoenmakers@hvhl.nl

kevin.ochieng@hvhl.nl

Registration number: 000004656

Date of Publication: 21-06-2018

Photo cover: SkyGeo



Acknowledgements

I express my deepest gratitude to the CEO of SkyGeo Pieter Bas Leezenberg who gave me the opportunity to do my Bachelor's thesis internship at the company. I am grateful for the chance I received from you to learn and develop myself in a company that uses the most advanced technique in SAR Interferometry for deformation monitoring. I would also like to show sincere appreciation to my supervisor from SkyGeo Martijn Houtepen who guided me through the internship. I wish to acknowledge the development and engineering teams for the feedback that they provided on the two presentations that I gave at the company. I am also thankful to my fellow interns Marco and Alex I value the discussions and recommendations that come out from our weekly intern meetings. Last but not least I thank Shaoqing Lu who always showed the willingness to help me with programming in R, whenever I faced difficulties. As last, I thank my supervisor from my university Jack Schoenmakers whose guidance played an important role in the writing of this report.

Nomenclature

List of Acronyms

Asc	Ascending
DEM	Digital Elevation Model
Desc	Descending
DInSAR	Differential Interferometric Synthetic Aperture Radar
DS	Distributed Scatterers
EM	Electromagnetic
ERS	European Remote Sensing
ESA	European Space Agency
FOV	Field Of View
GNSS	Global Navigation Satellite System
IFOV	Instantaneous Field Of View
InSAR	Interferometric Synthetic Aperture Radar
LOS	Line of Sight
NAP	Normaal Amsterdamse Peil
NASA	National Aeronautics and Space Administration
NDE	Non- Destructive Examination
OTL	Ocean Tidal Loading
PS	Persistent Scatterers
PSI	Persistent Scatterer Interferometry
Radar	Radio Detection and Ranging
RS	Remote Sensing
RTE	Residual Topographic Error
SAR	Synthetic Aperture Radar

Glossary

Amplitude: measure of the strength of a signal, and in particular the strength or height of an electromagnetic wave (ESA Earthnet Online, 2014).

Dielectric property: property related to the ability of a material to be polarized by an electrical field (EESemi.com, 2005).

Doppler frequency: frequency that depends on the component of satellite velocity in the line-of-sight direction to the target (ESA Earthnet Online, 2014).

Frequency: number of oscillations per unit time or number of wavelengths that pass a point per unit time (ESA Earthnet Online, 2014).

Ground resolution cell: area on the terrain that is covered by the IFOV of a detector (Lamont-Doherty Earth Observatory, 1998).

Incidence angle: the angle formed between an imaginary line normal to the surface and another connecting the antenna and the target (Lamont-Doherty Earth Observatory, 1998).

Instantaneous field of view: solid angle through which a detector is sensitive to radiation. In a scanning system, the solid angle subtended by the detector when the scanning motion is stopped (Lamont-Doherty Earth Observatory, 1998).

Master image: the first image (reference image) registered in repeat-pass interferometry. The second image is called slave image (Zhou, Chang, & Li, 2009).

Non-Destructive Examination (testing): quality control method that does not damage or destroy the material or product being tested (Business Dictionary, 2018).

Phase: a property of a periodic phenomenon, for example a wave, referring to its starting point or advancement (fraction) relative to an arbitrary origin (ESA Earthnet Online, 2014).

Pixel: contraction of picture element (Lamont-Doherty Earth Observatory, 1998).

Polarisations: the direction of orientation in which the electrical field vector of electromagnetic radiation vibrates (Lamont-Doherty Earth Observatory, 1998).

Repeat pass interferometry: method based on two image acquisitions of the same scene from slightly displaced orbits of a satellite (ESA Earthnet Online, 2014).

Resolution: ability to separate closely spaced objects on an image or photograph. Resolution is commonly expressed as the most closely spaced line-pairs per unit distance that can be distinguished. Also called spatial resolution (Lamont-Doherty Earth Observatory, 1998).

Resolution cell: the volume of space that is occupied by a radar pulse and that is determined by the pulse duration and the horizontal and vertical beam widths of the transmitting radar (ITS, 1996).

(Slant) range resolution: the spatial resolution in the range direction, which is determined by the pulse length of the transmitted microwave energy (Lamont-Doherty Earth Observatory, 1998).

Swath width (ground swath): width of the strip of terrain that is imaged by a scanner system (Lamont-Doherty Earth Observatory, 1998).

Wavelength: the distance between two points of corresponding phase in consecutive cycles (ESA Earthnet Online, 2014).

Table of Contents

Summary

1. Introduction	1
1.1 Background	1
1.2 SAR Interferometry and sustainability	2
1.3 Problem statement	2
1.4 Study area	3
1.5 Objective	4
1.6 Research question and sub questions	4
1.7 Research methods	5
1.8 Delimitations	5
1.9 Reader's guide.....	5
1.10 Target audience	5
2. Remote sensing.....	6
2.1 The Electromagnetic spectrum	6
2.2 Atmospheric window	6
2.3 Remote sensing sensors.....	7
2.4 Microwave remote sensing.....	8
3. Radar remote sensing	10
3.1 Basic radar principles	10
3.2 Radar satellites.....	11
4. Synthetic Aperture Radar.....	12
4.1 Basic principles of SAR	12
4.2 Permanent and Distributed Scatterers	14
4.3 SAR Interferometry	15
5. Methodology.....	19
5.1 Data acquisition	19
5.1.1 Water level time series	19
5.1.2 Deformation time series	19
5.2 Data Analysis.....	20
5.2.1 Correlation and regression analysis	20
5.2.2 DInSAR and ocean tide loading.....	22
5.2.3 Difference with previous study.....	23

Table of Contents

5.2.4 Workflow.....	23
6 Results.....	26
6.1 Correlation between spatially averaged deformation time series and water level time series.....	26
6.2 Correlation between unaveraged deformation time series and water level time series.....	32
7 Conclusions and discussions	33
7.1 Conclusions	33
7.2 Discussion and recommendations	35
Appendices.....	38
Appendix I: Port of Rotterdam cargo handling/industries at the harbours.....	38
Appendix II: Port of Rotterdam development over the years	38
Appendix III: Image pre-processing	39
Appendix IV: Remote sensing chain.....	39
Appendix V: InSAR systems and characteristics	41
Appendix VI: Applications of InSAR in different disciplines.....	42
Appendix VII: Study areas at the Port of Rotterdam	43
Appendix VIII: Surface water measuring locations in the project area	43
Appendix IX: Measured surface water levels.....	44
Appendix X: TerraSAR-X.....	45
Appendix XI: Deformation points at study areas.....	47
Appendix XII: Acquisition times TerraSAR-X (2009-2010)	49
Appendix XIII: Spatial averages of vertical deformation time series	50
Appendix XIV: Vertical deformation on dates when connection with water levels were established	51
Appendix XV: Water levels on dates when connection with averaged deformation were established.....	52
Appendix XVI: Results Donauhaven and 7e Petroleumhaven (7e PH); regression and correlation plots	53
Appendix XVII: Frequency histograms Donauhaven and 7e Petroleumhaven	54
Appendix XVIII: Frequency histograms Londenhaven	55
Appendix XIX: Frequency histograms Brittaniëhaven.....	56
Appendix XX: Frequency histograms Hartelkanaal.....	57
Appendix XXI: Frequency histograms Prinses Beatrixhaven and Prins Johan Friso haven	58
Appendix XXII: Frequency histograms Waalhaven	59
Appendix XXIII: Correlation per point Donauhaven and 7e Petroleumhaven (using Descending PS time series).....	60

Table of Contents

References	61
------------------	----

Summary

This study was conducted to develop an analysis methodology for analysing correlation between water level and vertical deformation time series obtained from different locations at the Port of Rotterdam. The study areas include seven harbours and one kanal: Donauhaven, 7e Petroleumhaven, Londenhaven, Brittaniëhaven, Hartelkanaal, Prinses Beatrixhaven, Prins Johan Friso haven and Waalhaven. SkyGeo is specialised in delivering products acquired through InSAR, a special radar technique used in geodesy and remote sensing. Using the most advanced and innovative technique in InSAR, the company provides millimetre accuracy measurements of up to one million measurements per square kilometres for infrastructure monitoring. It also provides constant semi-continuous updates on subsidence and uplift of infrastructure and has data from the last twenty-five years. The data archive covers seventy percent of the Earth's surface. The company works with data from satellites such as Radarsat2, Envisat, Sentinel- 1, Sentinel- 2 and TerraSAR-X. In its ambition to explore the application possibilities of InSAR for research purposes, SkyGeo takes initiatives to conduct independent research such as in the field of earth and environmental studies.

Data and information from a previous study conducted by SkyGeo played an important role in this research. These were used as a starting point to find out different factors that could be of influence in the correlation between vertical deformation and water level time series at the mentioned study areas. Using literature review, the basic concepts and principles of radar, SAR and InSAR together with its applications in various fields of research were studied. This study used vertical deformation time series that had already been pre- and post-processed by SkyGeo using the Persistent Scatter Interferometry (PSI) technique. The time series were generated from satellite data acquired from the earth observation satellite TerraSAR-X (also referred to as TSX or TSX-1) between 2009 and 2014. Using the programming language and software R, correlation and regression analyses were conducted. The Pearson's Product Momentum Correlation Coefficient (Pearson's r) was used to calculate the magnitude of correlation between the deformation and water level time series. The correlation results were then presented in tables, plots and visualizations created in the Geographic Information System software QGIS.

Two methods, based on conducting or not conducting spatial averages of deformation time series were used in this study. Conducting no spatial averaging enables comparisons of classes that give the strength and direction of correlation of multiple points. Furthermore, correlation coefficients can be visualized based on the location (x-y coordinates) of the deformation point being considered. Spatial averaging of deformation time series allows different factors that possibly influence the correlation between deformation and water levels time series to be tested in a quick and efficient way due to the short computation time and less time needed to develop the scripts to compute them. Using a classification table with positive and negative divisions, correlation coefficients were classified based on their strength and direction.

Most of the correlation coefficients calculated from the two methods are negative. This infers that most of the time when surface water levels get higher, downward vertical deformation increases. Using the method that involves spatial averaging, the following factors were found to be of influence on the correlation results: the distance of the measuring station (from which a time series are obtained) to a particular study area, the frequency of the water level time series, the rounding off time of the acquisition time of the satellite, the length of the time series (number of observations) and differences in time series acquired from either descending or ascending orbits of the satellite.

1. Introduction

1.1 Background



Figure 1.1 An aerial view of Waalhaven, one of the harbours at the Port of Rotterdam (Havenbedrijf Rotterdam, 2018).

All over the world, ports create vital economic activities in coastal areas. Not only are they part of the primary components of transportation, but they are also a connecting medium for expanding the world economy. The bigger the *throughput* of goods time after time at port areas, the more provisions, infrastructure and associated services are needed. This brings a manifold of benefits to the economy and to a country (Dwarakish & Salim, 2015). Ports lower the costs of trade and provide value added through the economic practices that port authorities and firms related to ports conduct; they play a key role in global supply chains making them facilitators of trade between port-regions and countries; they also act as places for research, innovation and development. By providing jobs, ports also have a social function (Merk, 2010; Dwarakish & Salim, 2015).

Monitoring the deformation of large scale man-made infrastructure such as ports is important to avert catastrophic loss of infrastructure and human life (Sousa et al., 2014). Furthermore, accurate monitoring procedures of structures and their environment are vital to determine instability of structures in time and take prevention actions (Roque et al., 2015). In recent decades, there has been a rapid development of space technologies that has enabled the development of surface motion detection of the Earth's surface from space, with a high precision scale. This advancement has been possible due to data obtained by Synthetic Aperture Radar (SAR) sensors that are carried on board satellites. Another contributing factor is the development of new *interferometric* processing techniques using time series analysis of SAR images (Sousa et al, 2016).

SAR interferometry is a space-based technology that uses microwave active sensors carried in satellites to image the Earth's surface. The sensors emit microwave radiation towards the Earth which are then reflected and return to the sensor. Both the *amplitude* and *phase* information are registered for each *resolution cell*, forming SAR images. Applications of radar interferometry are very broad and it can be for instance used to measure deformation due to volcanoes and earthquakes, and land subsidence due to mining activities or groundwater extraction (Zhou, Chang, & Li, 2009). Time-series InSAR technique provides means to estimate displacements at millimetres level from using a series of SAR images with the same *acquisition geometry*. Time series InSAR techniques are a cost-effective means for measuring precise displacements on the Earth's surface at a regional scale.

1. Introduction

These techniques can be applied as an early warning system for the safety of structures and their surroundings (Roque et al., 2015).

1.2 SAR Interferometry and sustainability

The monitoring and measuring of deformation of man-made structures is a key task of geomatics and applied geodesy. The techniques used by the disciplines are however based on detecting changes at specific locations with prior interest and investment in human resources or special equipment (Sousa et al., 2014). This is normally done using (combined) techniques such as visual inspection by experts with aid of some *Non-Destructive Examination (NDE)*, in built-sensors, fibre optic sensors and other geodetic instruments (Sousa et al., 2014). Satellite based monitoring using radar interferometry on the other hand offers a viable source of independent products that can be used to remotely monitor structural health of structures to feed decision support models. Over the last three decades the technique has proven to be a valuable method for measuring both natural and human induced deformation. A very key advantage is that a single radar image, which can be acquired in any weather and even in darkness, can cover an area of up to 100 km by 100 km including all the numerous infrastructure within (Sousa et al., 2014). Compared to the conventional methods mentioned above, SAR Interferometry is more sustainable since it helps in better scheduling of maintenance cycles; better expenditure allocation for maintenance; more accurate mapping of subsidence and it can be used as the basis for efficient long-term planning (SkyGeo, 2018).

1.2.1 About SkyGeo

By using innovative techniques within InSAR, SkyGeo provides a continuous and global view of deformation processes. Among the clients of SkyGeo are municipal governments and oil and gas companies. These clients use the InSAR processed data for maintenance purposes of structures such as pipelines, buildings, roads, sewers and bridges. In a single view, clients can determine where inspection is most urgently required using deliverables provided by SkyGeo (SkyGeo, 2018). The company started in 2008 as a spin-off from the Technical University of Delft, with the aim to apply InSAR technique to dam and dike stability problems. Over the years it has gradually expanded its area of expertise and in 2014 it changed its focus from being an InSAR service company to being more of a data-driven company. The company has over the years built a data archive that covers 70% of the earth's land. This archive is used to provide insights in the historical movements of infrastructure. SkyGeo has offices in Delft, Houston (Texas), San Mateo (California) and Calgary (Canada) (SkyGeo, 2018).

1.3 Problem statement

Quay walls are earth retaining structures beside a river or sea (ports) at which ships can dock and get loaded or unloaded. These long platforms are used for the handling of goods by cranes and other equipment that move alongside ships. They can be made from varied materials and are equipped with fenders and bollards (Richwien, 2008). Apart from docking purposes, quay walls also have functions such as retaining soil behind the quay area and providing capacity to carry loads imposed by the transshipment of the crabs and freight storage facilities. Besides, they can serve as a water barrier for areas lying behind them during periods with high water levels (De Gijt & Broeken, 2014). Located partly on the North Sea and at the mouth of the river Rhine, water levels at the Port of Rotterdam have high fluctuations due to influences from ocean tides. Ocean tides refer to the rise and fall of ocean waves according to certain cycles caused by gravitational attraction from celestial bodies. Tidal phenomena are dominated by the gravitational attraction of the Moon and to a lesser extent the Sun. Ocean tides generally rise and fall twice per day, with the duration of each cycle depending on the place of observation (Yeh et al., 2011). The elastic response of the earth due to the redistribution of water mass from ocean tides is called Ocean Tide Loading (OTL). In coastal

1. Introduction

areas, OTL vertical displacement may reach several centimetres (Lei et al., 2017; Peng, Wang, & Cao, 2017). From a previous investigation conducted by SkyGeo, it was observed that there is some level of correlation between vertical deformation time series derived from InSAR measurements and measured surface water levels at various harbours at the Port of Rotterdam, mainly at places near the quay wall areas and structures on water. When there are high surface water levels, detected vertical deformation near the quay wall areas is generally expected to be high, due to the high pressure exerted downwards on the ocean bed. On the other hand, when the surface water levels are low, the vertical deformation is expected to be low. Results from the investigation showed a good correlation (between moderate and high negative using Pearson's Correlation coefficient) at some areas of the harbours of the port. At other harbours, the results were inconclusive. A proper analysis methodology that tackles different factors that could be of influence in the correlation results is however missing.

1.4 Study area

The Port of Rotterdam, figure 1.2, is located in the province of Zuid-Holland in the south-west region of the country and it extends from the city of Rotterdam to the North Sea. The port is the largest in Europe and 30,000 vessels dock at the port every year. The port is managed by the Port of Rotterdam Authority, an unlisted public limited company. The shareholders of the port are: the Dutch government (about 30 %) and the Municipality of Rotterdam (about 70%) (The Port of Rotterdam, 2018).

The Port of Rotterdam

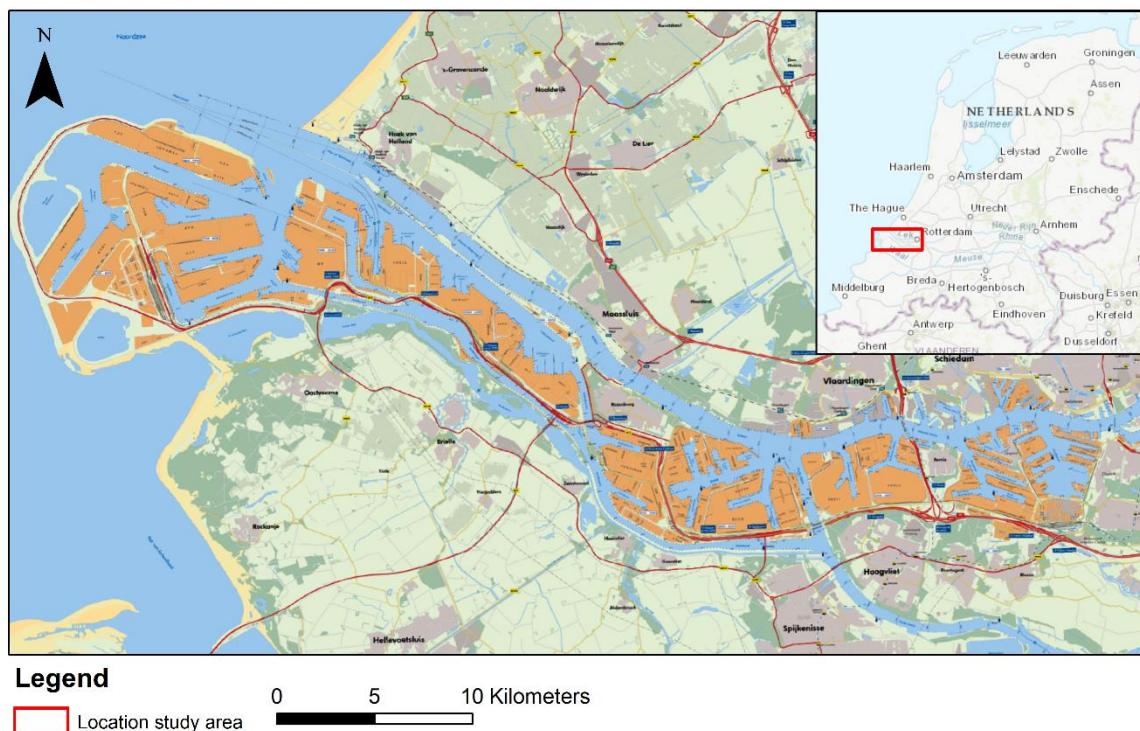


Figure 1.2 The Port of Rotterdam, adapted from (Port of Rotterdam, 2018)

1. Introduction

Short history

The city of Rotterdam began as a fishing village in the second half of the 13th century. After attaining its municipal rights in 1328, Rotterdam gradually developed into a prosperous merchant port and industries at the port thrived as well. The first harbours at the port were constructed between the years 1600 and 1620. The French occupation from 1795 to 1813 led to disappearance of industries and decline in trade. Later on, the entrance to the port silted up and the port became inactive. At the beginning of the last century a series of new harbours got constructed by the municipality and the port expanded significantly. The digging of the Waalhaven harbour in 1922 was one of the biggest achievements. The Waalhaven harbour has a surface water area of 219 hectares, making it the biggest man-made dock in the world (The Port of Rotterdam, 2018).

The port reached its milestone in 1938, after the creation of the Rotterdam Municipal Port Management (since 2004 the Port of Rotterdam Authority), and became the largest Port in Rotterdam. The growth of the port continued and it became the world's largest port in 1962, after exceeding the cargo tonnage of the Port of New York. Several Asian ports, such as the Port of Shanghai, later surpassed the Port of Rotterdam and the port lost its global number one position. Around the year 2000, there were expectations that the port would soon reach its maximum capacity. To maintain its leading position in Europe, a decision was made to create more land on the sea. This led to the construction of Maasvlakte 2, which ended in 2012. The construction of Maasvlakte 2 enabled the port to grow by 20 percent. Furthermore, it enabled the capacity for container handling to triple (The Port of Rotterdam, 2018). Appendix I shows the type of cargo handling and current industries located on various harbours at the port. Appendix II shows the different construction periods of port sections dating back to 1400.

1.5 Objective

The aim of this study was to develop an analysis methodology that considers several factors that possibly influence the magnitude of correlation between measured surface water levels and vertical deformation time series, especially at areas around quay walls, measured at several harbours at the Port of Rotterdam. Knowing more about different factors causing variations in structure deformation such as on quay walls can contribute to a better understanding of stressors on structures. Such kind of information can possibly indicate locations under greater stress, and this information could be incorporated into maintenance plans. The objectives of this study were to: (1) calculate correlation between (averaged and unaveraged) vertical deformation time series and water level time series obtained from a measuring station closest to each study area in this project, (2) compare correlation results in cases whereby water level time series are obtained from different measuring stations (3) compare correlation results calculated for individual years and (4) calculate correlations between water level and deformation time series at events with peak water levels.

1.6 Research question and sub questions

Main research question: 'What are the most influential factors that possibly influence correlation between measured surface water levels and detected vertical deformation at the Port of Rotterdam?'

Sub questions

1. What are the principles and concepts of InSAR?
2. What are the applications of InSAR?
3. How well do water level time series from various measuring stations at the Port of Rotterdam correlate to deformation time series?
4. What level of correlation is observed during peak water levels?
5. How accurate are the correlation results analysed in this study and can they be confirmed?

1. Introduction

1.7 Research methods

A literature review was conducted to understand the basic key concepts of remote sensing, radar remote sensing, SAR remote sensing and SAR Interferometry together with its applications. Information regarding these topics were mainly gained from existing publications and online portals directly or indirectly operated by NASA and ESA. The Geographic Information System Software QGIS was used to select key areas in the study areas for obtaining relevant vertical deformation time series. Spatial averaging of the vertical deformation time series was done in Microsoft Office Excel. Using the programming language and software R, correlation and regression analyses were conducted. In the software, different packages for data restructuring, plotting and statistical analyses were downloaded and used. Both QGIS and R were used to visualize the results of this study. Discussions with InSAR engineers at SkyGeo were also occasionally held.

1.8 Delimitations

The magnitude of water pressure difference over a quay wall mainly depends on (i) the soil condition, (ii) the intensity of water level fluctuations at the outer side (ii) the existence of a reliable drainage system. Tidal areas, such as the Port of Rotterdam, have dynamic geohydrological system and water levels in the aquifer can correspond to the outer surface water level with some delay (De Gijt & Broeken, 2014). Quay wall areas being a major point of interest, this study focusses only on surface water levels and does not pay attention to the groundwater, geo-hydrological or drainage system of the project area. Furthermore, the technical consequences of vertical deformation on structures are not considered in this study. Besides, the study only works with deformation time series of vertical deformation and not horizontal deformation since only vertical deformation time series were available for this study. Due to time constraints, correlation analysis could not be performed at events with peak water levels.

1.9 Reader's guide

Chapters two to four of this report are literature review. Chapter two summarizes the basic concepts of remote sensing. Chapter three handles the basic principles and concepts of radar, radar satellites and image pre-processing. Chapter four explains the basic concepts and principles of SAR and SAR Interferometry. Methods used in this study are described in chapter 5. The correlation results are analysed and presented in tables and graphs in chapter 6. The last chapter contains discussion and conclusion from the work discussed in this report.

1.10 Target audience

This study was conducted as a final Bachelor's thesis project within the major Applied Hydrology, Faculty of Land and Water management at the VHL University of Applied Sciences. The thesis report of this study targets students and lecturers of the mentioned faculty, as wells as engineers at SkyGeo.

2. Remote sensing

The term “remote sensing” was first used in the United States Office of Naval Research in the 1950’s. Nowadays the term is commonly used to describe the science and art of identifying, observing and measuring an object without coming into contact with it (NASA Earth Observatory, 2018). It is a process that involves the detection and measurement of electromagnetic radiation of different *wavelengths* reflected or emitted from distant materials or objects (NASA Earth Observatory, 2018). It also encompasses the group of techniques for collecting images or other forms of data, the processing, the analysis and interpretation (ESA Earthnet Online, 2014; Lamont-Doherty Earth Observatory, 1998). Wavelengths may be identified and categorized based on type or class, substance and spatial distribution (NASA Earth Observatory, 2018).

2.1 The Electromagnetic spectrum

The first requirement for remote sensing is the availability of an energy source to illuminate a target or the target to emit energy that can be sensed. This energy is in the form of electromagnetic radiation. Electromagnetic (EM) radiation comprises of an electrical field (E) which can vary in magnitude in a direction perpendicular to the direction in which the radiation is travelling, a magnetic field (M) oriented at right angles to the electrical field. Both these fields travel at the speed of light (C) (Natural Resources Canada, 2015). A representation of EM radiation is shown in figure 2.1.

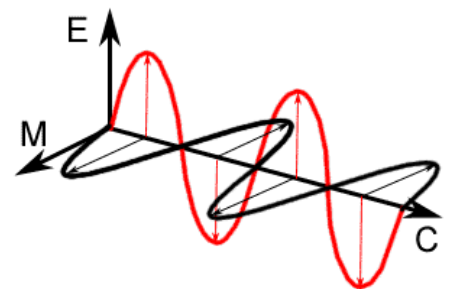


Figure 2.1 A representation of EM radiation (Natural Resources Canada, 2015)

The EM spectrum is described as an array of known EM waves of the electromagnetic radiation arranged according to *wavelength* (or *frequency*). These waves are considered to be EM because they are made up of combined electric and magnetic waves that result when charged particles accelerate. The shorter the wavelength, the higher the frequency. The EM spectrum, shown in figure 2.2, is divided into intervals to which descriptive names have been applied. These include gamma rays (highest frequency, shortest wavelength), ultraviolet, visible (red, green blue), infra-red, microwaves and radio (lowest frequency, longest wavelength) (NASA Earth Observatory, 2018). In the ultraviolet region the wavelengths extend from about one nanometer (nm) to 0.36 micrometres (μm), the visible part spans between 0.4 and 0.7 (μm) (400 to 700 nm), the infrared region occupies the region between 0.7 and 100 μm , the microwave region ranges from 1 nm to 100 (μm). This region includes all the intervals used by man-made radar systems, which generate their own radiation towards intended targets. The radio region which has the longest wavelength goes beyond 1 meter (NASA Earth Observatory, 2018).

2.2 Atmospheric window

Some types of electromagnetic radiation can easily pass through the atmosphere as solar radiation whereas some cannot. The Earth’s atmosphere consists of gasses (such as ozone (O_3), carbon dioxide (CO_2) and water vapour (H_2O)) that absorb radiation in some wavelengths while allowing radiation with differing wavelength to pass through. Areas of the electromagnetic spectrum that get absorbed by atmospheric gases are referred to as the absorption bands. Absorption bands are represented in figure 2.3 by a low transmission value that is related to specific range of wavelengths. Areas of the electromagnetic spectrum where there is limited or no absorption of radiation to specific wavelengths are known as atmospheric windows because they permit the radiation to easily go through the atmosphere to the surface of the Earth (NASA Earth Observatory, 2018).

2. Remote sensing

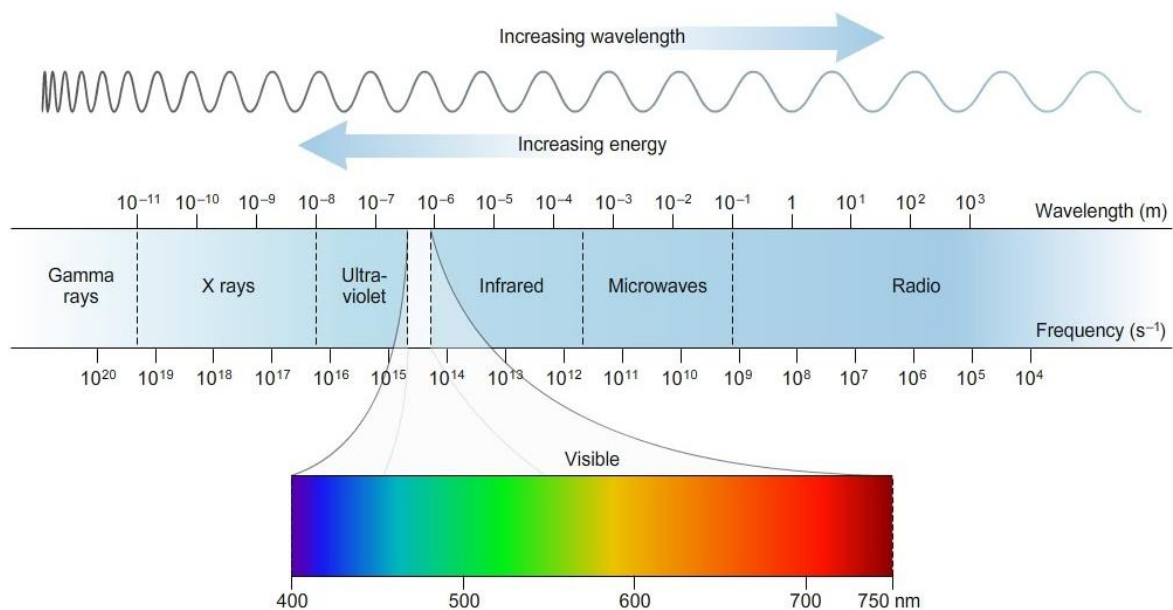


Figure 2.2 The EM spectrum (Sapling Learning, 2018)

A majority of remote sensing tools on satellites or on aircrafts operate in one or more of the atmospheric windows by conducting their measurements with detectors tuned to specific wavelengths (and frequencies) that penetrate through the atmosphere. The entire atmosphere is almost non-transparent to electromagnetic radiation in the middle infrared and all of the far infrared regions. In contrast, most of radiation passes through the atmosphere unhindered in the microwave region (NASA Earth Observatory, 2018).

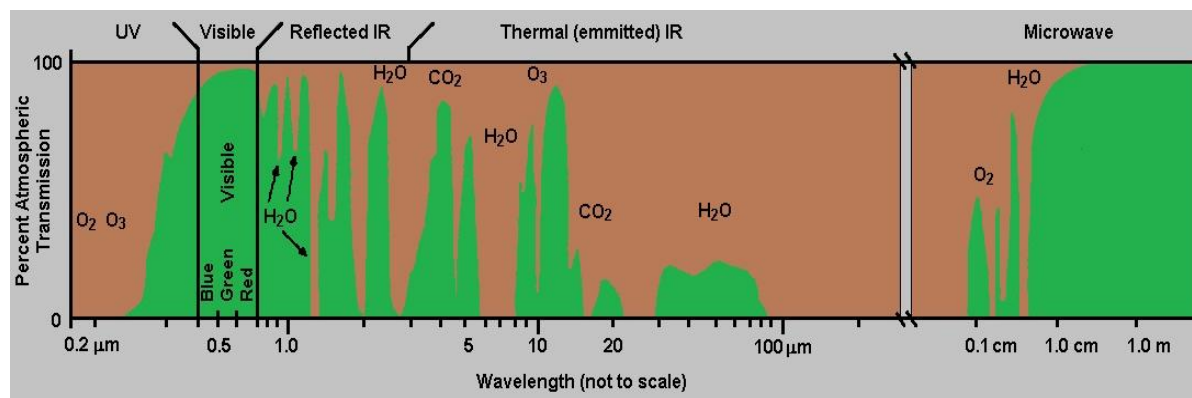


Figure 2.3 Atmospheric window in remote sensing (Baumann, 2010)

2.3 Remote sensing sensors

Remote sensing instruments can be classified into two groups: (i) active and (ii) passive instruments (sensors). Passive instruments only sense natural radiation (energy) that is released by an object being viewed, or radiation being reflected by the object from a source different than the instrument. The most common source of external radiation sensed by passive instruments is reflected sunlight (NASA Earth Observatory, 2018). Most of the passive sensors utilized in remote sensing applications operate in the visible, infrared, thermal infrared and microwave regions of the electromagnetic spectrum. Examples of passive remote sensors are radiometers, imaging radiometers, accelerometers and spectrometers (NASA Earth Observatory, 2018; EARTHDATA, 2018). Active sensors on the other hand provide their own source of radiation and irradiate this electromagnetic radiation in the direction of the object being investigated. Examples of active sensors include scatterometers, laser altimeters, lidar sensors and radar sensors. These sensors operate in the

2. Remote sensing

microwave region of the electromagnetic spectrum allowing them to pass through the atmosphere under most conditions (EARTHDATA, 2018).

2.4 Microwave remote sensing

Based on the type of sensor, remote sensing can be classified into three two types; active and passive remote sensing. Another classification can be made based on which part of the electromagnetic spectrum the technique utilizes. These include: (i) optical (ii) thermal and (ii) microwave remote sensing. Optical remote sensing uses the visible and near infrared portion of the electromagnetic spectrum, thermal remote sensing operates from the middle infrared to far infrared region, while microwave remote sensing operates in the microwave region (1 cm to 1m in wavelength) (Natural Resources Canada, 2015). The concepts of passive microwave remote sensing are similar to those of thermal remote sensing; all objects emit microwave energy of some magnitude. The amounts however are generally small. Passive microwave sensors detect the naturally emitted microwave energy within its field of view (FOV) (Natural Resources Canada, 2015). The detected energy is then related to the moisture and temperature properties of the targeted surface or object. In active microwave remote sensing, figure 2.4, an antenna emits (artificial) electronically generated microwaves to a pre-determined direction. The antenna produces regular pulses of energy of a known wavelength (ESA, 2018; Natural Resources Canada, 2015). As shown in figure 2.3 most of the radiation in the Earth's atmosphere penetrates through the atmosphere unimpeded in the microwave region of the EM spectrum. Because of their longer wavelengths (compared to visible and infrared), microwave wavelengths are very advantageous since they can penetrate through gases, clouds, haze, dust, even solids to a limited degree and all but the heaviest rainfall, as opposed to visible and infrared wavelengths. This allows data collection to be done at any time (ESA, 2018; NASA Earth Observatory, 2018; Natural Resources Canada, 2015).

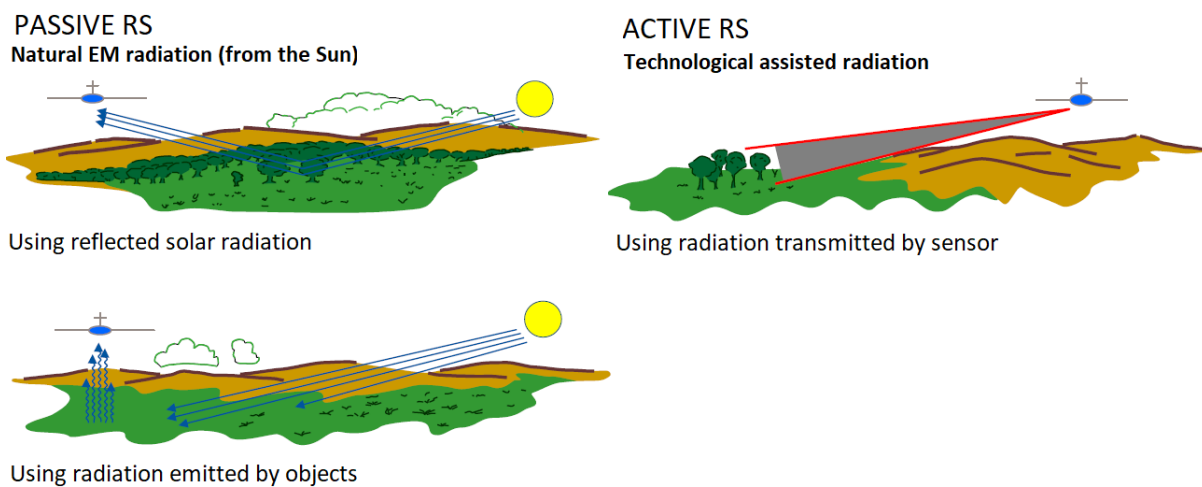


Figure 2.4 Active vs Passive remote sensing. Adapted from (Brinkman, 2016)

3. Radar remote sensing

Active microwave sensors are generally classified into two groups; imaging and non-imaging radars. Radar, an acronym of **R**adio **D**etection and **R**anging, is the most common form of imaging radars (active microwave sensors) (Natural Resources Canada, 2015). Imaging radars are used to produce two-dimensional images (ESA Earthnet Online, 2014). Radar can refer to both a tool and a technique. As a tool, radar is the instrument that emits electromagnetic waves (signals) and measures the signal that returns from a target and also the distance between the radar emitter and the target (Natural Resources Canada, 2015; Zhou, Chang, & Li, 2009). As mentioned earlier on, microwave wavelengths can penetrate through clouds. There are however weather radars that can detect precipitation and clouds because they are tuned to observe backscattered radiation from ice particles and liquid (NASA Earth Observatory, 2018).

3.1 Basic radar principles

The fundamental parts of a radar instrument include a transmitter, a receiver, an antenna and an electronic system to process and record data. The transmitter generates short pulses of microwave (A) at consistent intervals. The antenna focusses the pulses into a beam (B). The beam illuminates the surface slantwise (always sideways) at a right angle to the motion of the platform. The antenna receives the portion of the transmitted energy that gets backscattered from various targets within the illuminated beam (C). The strength of the backscattered signal is measured to distinguish different objects. Figure 3.1 gives a representation of the radar technique, applied from an aeroplane. The time delay between the emitted and backscattered signal is used to determine the range or distance to the target, making it possible to determine their location. As the sensor platform moves forward, the backscattered signals are recorded and processed to build up a two-dimensional image of the surface (Natural Resources Canada, 2015). Recorded signals provide information on magnitude, phase, the interval between signal emission and return from target, *polarization* and *Doppler frequency* (ESA Earthnet Online, 2018). Factors that influence radar backscatter include frequency of radiation, polarization, roughness of target, the *incidence angle* and moisture of the target (ESA Earthnet Online, 2018). The radar backscattering coefficient (σ) gives information about the imaged surface. It is a function of two parameters: (1) radar observation parameters: Incidence angle, polarisation(p) and frequency (f) of the transmitted electromagnetic waves and (2) surface parameters: roughness, geometric shape and dielectric properties of the target. Figure 3.2 gives examples of radar images.

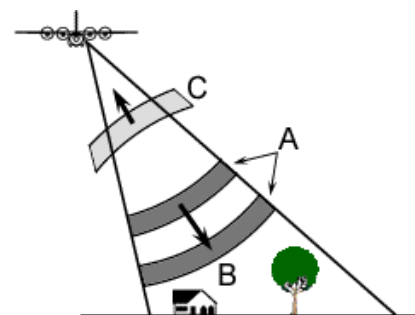


Figure 3.1 A simplified representation of a radar system (Natural Resources Canada,

2015). Recorded signals provide information on magnitude, phase, the interval between signal emission and return from target, *polarization* and *Doppler frequency* (ESA Earthnet Online, 2018). Factors that influence radar backscatter include frequency of radiation, polarization, roughness of target, the *incidence angle* and moisture of the target (ESA Earthnet Online, 2018). The radar backscattering coefficient (σ) gives information about the imaged surface. It is a function of two parameters: (1) radar observation parameters: Incidence angle, polarisation(p) and frequency (f) of the transmitted electromagnetic waves and (2) surface parameters: roughness, geometric shape and dielectric properties of the target. Figure 3.2 gives examples of radar images.



Figure 3.2 Examples of radar images (Kyluchevskaya Volcano eruption in Russia in 1994) (NASA Earth Observatory, 2018)

3. Radar remote sensing

Radar equation

The radar range equation represents the physical dependencies of the transmit power, from the transmission of signals up to the receiving of backscattered signals. The Power P_E that returns to the receiving antenna is given by the radar equation, depending on the transmitted power P_S , the slant range R , and the reflecting characteristics of the target (referred to as the radar cross section σ). R_{max} is the maximum range from the radar platform to the target (radartutorial.eu, 2018). Equation 1 gives a simplified formula of the basic radar range equation.

$$R_{max} = \sqrt[4]{\frac{P_S * G^2 * \lambda^2 * \sigma}{P_{Emin} * (4\pi)^3}}$$

Equation 1 Radar range equation

Table 1 Parameter definitions and units of the radar range equation

Parameter symbol	Definition	Unit
R_{max}	maximum radar range	km
P_S	transmitted power	Watts (W)
G	gain of the transmitting antenna	dimensionless
λ	transmitted wavelength	meters (m)
σ	target radar cross section	m^2
P_{Emin}	minimum detectable signal of receiver	Watts (W)

3.2 Radar satellites

Radar satellites orbit the Earth at an altitude between 500 and 800 kilometres with a velocity of about 7.5 kilometres per second. They scan the whole Earth and due to the rotation of the Earth and their *orbits* (moving path), they repeat the same cycle after a certain amount of days (revisit time), depending on the satellite. A satellite passes a certain location, both from south to north (ascending orbit) and from north to south (descending orbit). Since a satellite faces the Earth under an angle and the viewing angle is generally fixed (mostly right-looking), the Earth can thus be observed from two different locations. Using the InSAR technique, these two measurements can be combined to estimate vertical and horizontal deformation (SkyGeo, 2018). Figure 3.3 gives a representation of descending and ascending orbits of a satellite.

After data is received from a satellite, it needs to go through several pre-processing steps before it can be analysed. Basic pre-processing operations are discussed in Appendix III.

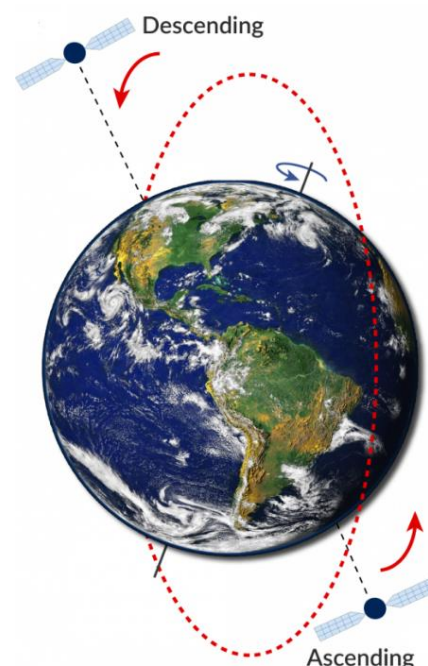


Figure 3.3 A representation of descending (Desc) and ascending (Asc) orbits of a satellite (SkyGeo, 2018)

4. Synthetic Aperture Radar

One of the most commonly used types of imaging radars is the Synthetic Aperture Radar (SAR). Synthetic aperture is referred to as a virtual antenna that consists of a long array of successive coherent (having a constant phase) radar signals that are emitted and received physically by a short real antenna as it moves to a pre-determined flight (ESA Earthnet Online, 2014). An aperture is a RS system that admits electromagnetic radiation to the film in radar systems (Lamont-Doherty Earth Observatory, 1998).

4.1 Basic principles of SAR

In SAR an EM wave pulse is emitted continually in the direction perpendicular to the moving direction of the antenna (cross-track direction), figure 4.1, as the satellite moves. The wave travels through the atmosphere, interacts with the target/ground surface and then part of the signal is scattered back and received by the antenna. To form an image from the backscattered signals from each emitted pulse in the long track direction (azimuth direction), the signals are sorted by their round-trip travel time, resulting in *slant range resolution*. The distance from the antenna to the ground is recorded in a rough form of slant range with additional information in the form of phase in the SAR image (Zhou, Chang, & Li, 2009).

SAR images are formed by recording the amplitude (energy intensity) and the phase (time delay) of reflected signals and assigning them the locations in the image based on their frequency shift and return time (Smith, 2002). An amplitude image records information about surface roughness and terrain slope whereas a phase image records information about the distance between the Earth's surface and the satellite (Geoscience Australia, 2018). The phase measured by each antenna is related to the to the number of wavelengths required to travel across the round-trip distance between the ground surface and the antenna (Smith, 2002).

A representation of radar signal transmission of a SAR antenna is given in figure 4.2.

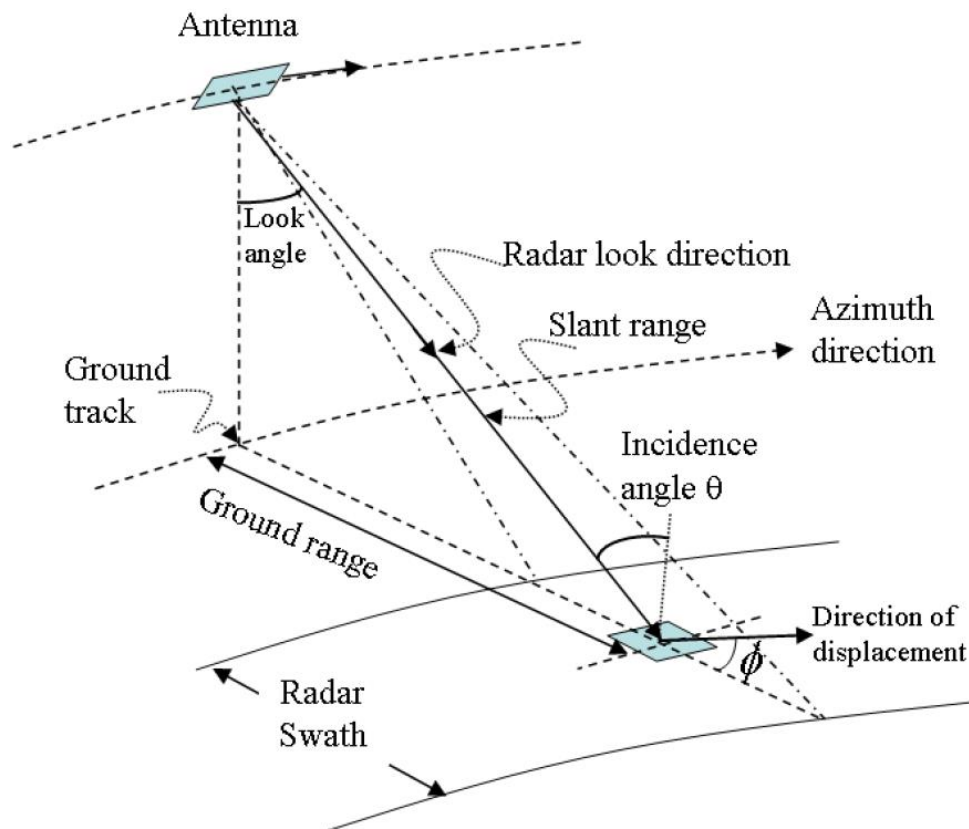


Figure 4.1 A geometrical model for a SAR system (Zhou, Chang, & Li, 2009).

4. Synthetic Aperture Radar

Table 2 Definitions belonging to the SAR geometrical model

Term	Definition
Look angle	The angle between the vertical plane containing a radar antenna and the direction of radar.
Look direction	Direction in which pulses of microwave energy are transmitted by a radar system. The look direction is normal to the azimuth direction.
Slant range	An imaginary line running between the antenna and the target.
Azimuth direction	The direction in which the aircraft is heading (flight direction)
Ground range	The distance from the ground track to an object.
Incidence angle	The angle formed between an imaginary line normal to the surface and another connecting the antenna and the target.
Ground track	The path on the earth's surface below an aircraft, missile, rocket, or spacecraft. ¹

Source: (Lamont-Doherty Earth Observatory, 1998)

As earlier mentioned, the backscatter received by an antenna of an imaging radar from a ground pixel is characterised by two quantities: (i) amplitude and (ii) phase, figure 4.3. The phase records the history of the signal from its emission to its return (Smith, 2002; Zhou, Chang, & Li, 2009; Ferretti et al., 2007)

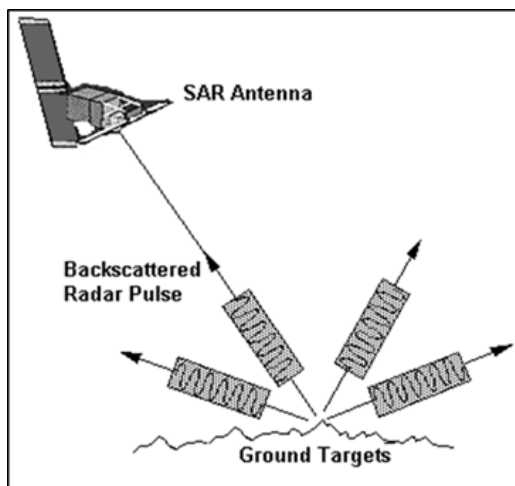


Figure 4.2 A representation of radar signal transmission from the radar platform to the target (left) and backscattering of the signal to the antenna (CRISP, 2001).

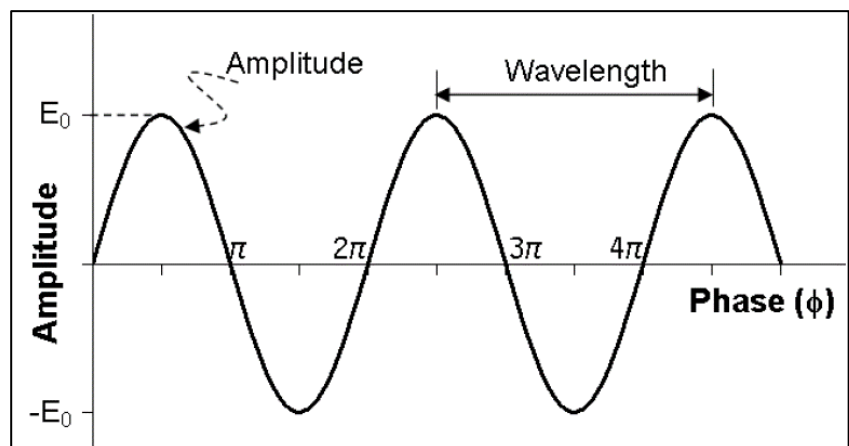


Figure 4.3 A representation of the relationship between amplitude, phase and wavelength of a radar signal (Zhou, Chang, & Li, 2009)

¹ (Dictionary.com, 2018)

4. Synthetic Aperture Radar

Figure 4.4 shows an example of a SAR image acquired by the SAR satellite Sentinel 1A. As it can be seen there is notable linear structure, a river, in the image since radar is sensitive to water/soil moisture. On the right is the Sentinel 1A radar satellite launched by the European Space Agency in April 2014. Appendix IV presents a list of SAR sensors for acquisition of InSAR data.

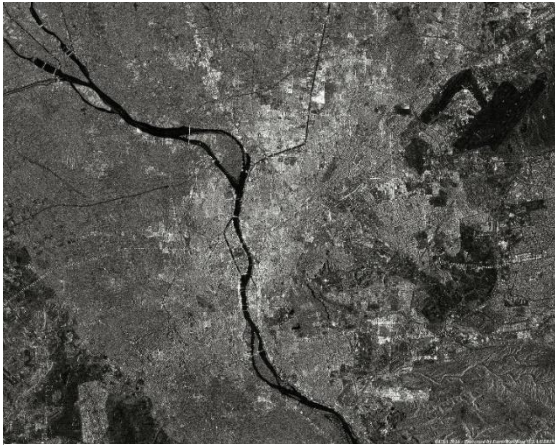


Figure 4.4 SAR image taken by radar satellite Sentinel 1A showing the Nile flowing through Cairo in Egypt (ESA Earth Watching, 2018)



Figure 4.5 Sentinel 1A satellite (ESA Sentinel Online, 2018)

4.2 Permanent and Distributed Scatterers

Data resolution determines the amount of measurements that can be conducted. In a photo camera for instance, only one value can be obtained from one pixel. Multiple objects reflecting a radar signal can however be present in one pixel, these are called scatterers. Different methods are used to measure deformation depending on the reflectance properties of objects within a pixel, not forgetting that pixels hold multiple scatterers. The main types of scatterers are Distributed Scatterers (DS) and Permanent/Persistent Scatterers (PS) (SkyGeo, 2018).

DS are pixels where multiple objects display a weaker backscatter, to a certain degree of similar strength. Examples of DS is a road (pixel). Deformation derived using DS are from a larger homogeneous area and not from a single reflector. PS on the other hand are pixels that contains objects that have high backscatter properties and the backscatter remains consistent throughout time. These objects reflect most of the radar signal received by the satellite. PS are usually found in urban areas, such as on buildings, monuments, exposed rocks and other man-made structures (SkyGeo, 2018; Crosetto et al., 2016). If a pixel contains one scatterer that reflects much stronger compared to others the weaker scatterers are negligible for the measured values (SkyGeo, 2018). Figures 4.6 and 4.7 give representations of DS and PS respectively.

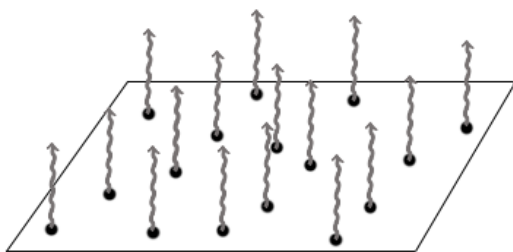


Figure 4.6 A representation of DS: the pixel contains multiple similar reflections (SkyGeo, 2018)

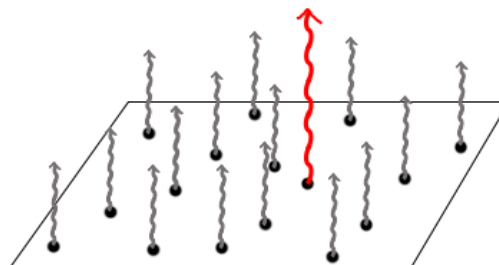


Figure 4.7 A presentation of PS; the pixel contains one dominant reflection (in red) (SkyGeo, 2018)

4. Synthetic Aperture Radar

4.3 SAR Interferometry

Interferometry is a technique that uses phase difference (interference) of backscattered radar signals to detect slight changes on the Earth's surface. It involves the combination of radar measurements of the same geographic area, acquired at the same time, but from slightly different angles to produce stereo images/height data (ESA Earthnet Online, 2014).

4.3.1 Basic InSAR principles

The InSAR technique uses two or more SAR phase images, of the same exact location to generate maps to detect and map surface movement and/or di-electric properties of the ground surface (Zhou, Chang, & Li, 2009; ESA, 2010; Geoscience Australia, 2018). A SAR satellite can observe and acquire images of the same area from slightly different view angles. There are two possibilities: (i) acquisition using one flight, by using two radar antennas separated perpendicularly to the flight direction (with different look angles) mounted on the same satellite, (ii) acquisition using two satellite flights (*repeat-pass-interferometry*) by making use of the repeated orbit of the same radar satellite, the two flights having different look angles (Ferretti et al., 2007). There are thus two methods used in SAR interferometry which are based on these acquisition methods. Measurements of the travel path variations of a satellite as function of its position and acquisition time enables the creation of Digital Elevation Models (DEM) (using the first method) and topographic measurements of up to centimetre scale of the terrain (Ferretti et al., 2007). The InSAR principle is summarized with the equations 2, 3 and 4.

Considering a single pixel footprint on the ground P, the satellite sensors acquires a first SAR image from a certain satellite position M, measuring a phase φ_M then:

$$\varphi_M = \varphi_{geom-M} + \varphi_{scatt-M} = \frac{4 * \pi * MP}{\lambda} + \varphi_{scatt-M}$$

Equation 2 Simplified equation to derive the phase of first SAR image (Crosetto et al., 2016)

Where MP is the distance from sensor to the target, φ_{scatt} is the phase shift generated during interaction between the microwave signals and the target P, λ is the radar wavelength, and 4π is related to way path, radar-target-radar (Crosetto et al., 2016).

When the radar sensor acquires a second image from a satellite position S, measuring the phase φ_S over the same pixel footprint P, then:

$$\varphi_S = \varphi_{geom-S} + \varphi_{scatt-S} = \frac{4 * \pi * SP}{\lambda} + \varphi_{scatt-S}$$

Equation 3 Simplified equation to derive the phase of second SAR image (Crosetto et al., 2016)

The InSAR technique exploits the phase difference $\varphi_S - \varphi_M$

$$\Delta\varphi_{int} = \varphi_S - \varphi_M = \frac{SP - MP}{\lambda} + \varphi_{scatt-S} - \varphi_{scatt-M}$$

Equation 4 Simplified equation of derive phase difference (Crosetto et al., 2016)

The phase difference is related to the distance SP -MP, which is important for the generation of a DEM, to estimate topography of the observed scene (Crosetto et al., 2016).

4. Synthetic Aperture Radar

4.3.2 Differential InSAR

The Differential InSAR (DInSAR), a type of InSAR technique, uses two images of the same area acquired at different times (ascending and descending orbit) by the same satellite to observe phase changes in two images. If the distance between the satellite and the ground changes between the two acquisition times because of surface movement, a phase shift will occur in the radar backscatter signals and this can be mapped, enabling to measure the changes of the surface (Geoscience Australia, 2018; National Research Council of Italy, 2018). This is done by calculating the phase differences (interference) of the waves being reflected to the satellite (Zhou, Chang, & Li, 2009; ESA, 2010). A phase difference image (of the same area) is called an interferogram. An interferogram appears as an image with rainbow-coloured patterns which can show small surface displacements that are not visible to the naked eye (Zhou, Chang, & Li, 2009; ESA, 2010). The phase difference in an interferogram is depicted by the colour of the pixels. A line of equal phase is referred to as a fringe. The number of fringes is counted from a reference point at which the surface displacement is assumed to be zero (Zhou, Chang, & Li, 2009). Figures 4.8 and 4.9 give examples of an interferogram. Interferogram of Figure 4.9 is of the Kenyan section of the Great Rift Valley. It shows small surface displacement of Mt. Longonot (top right), a volcanic mountain. Mt. Suswa, (in the background) another volcanic mountain shows no surface displacement (as in 2010) (ESA, 2010). The interferogram in figure 4.8, is of an earthquake. Each colour contour represents 28 mm motion towards the satellite, or about 70 mm of horizontal displacement. The thick black lines mark the fault rupture derived from SAR images whereas the thin red lines show the locations of fault breaks mapped on the surface during the magnitude 7.6 earthquake. The white areas are possibly lakes or water bodies or areas outside the SAR images (Photojournal, 2001).

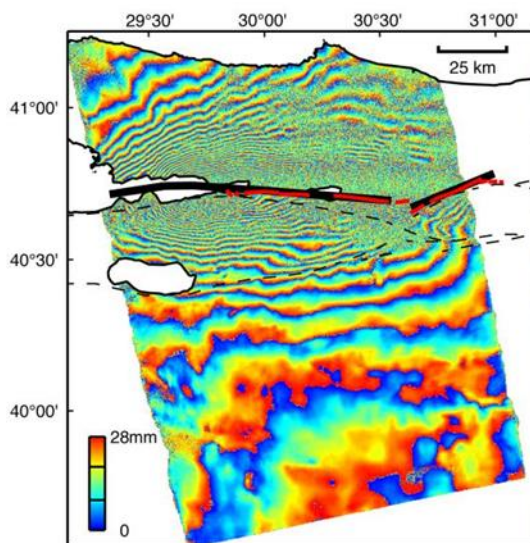


Figure 4.8 An interferogram of the Izmit Turkey, 1999 Earthquake Interferogram (Photojournal, 2001)

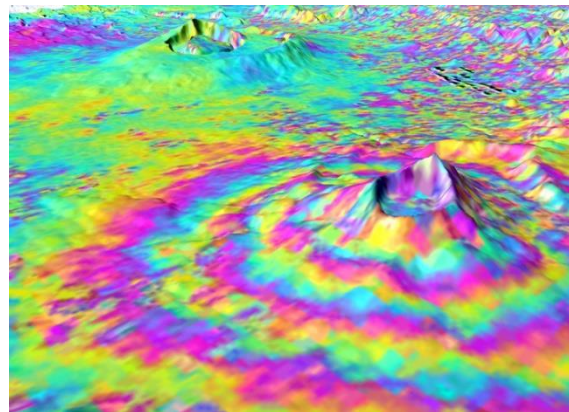


Figure 4.9 An interferogram showing small surface displacements of Kenya's Mt. Longonot Volcano (top right), legend omitted (ESA, 2010)

A series of SAR phase images of the same location can be combined into a series of interferograms which allows to follow displacement trends through time, resulting to multi-temporal InSAR. The required time interval between acquisition of SAR images can vary between 0.1 seconds to years, depending on how fast the target location is changing (Zhou, Chang, & Li, 2009; ESA Earthnet Online, 2014). Figure 4.10 gives an impression of how two images from 1st and 2nd pass (flight) of a satellite are acquired using a SAR satellite. A phase shift can be recorded and be mapped in an interferogram if the surface moves between the 1st and 2nd pass (Geoscience Australia, 2018). For two images to be used to create an interferogram the orbit configuration, the observation direction (look angle) and the processing procedure should be the same. Furthermore, the terrain slope should be small and the ground pixel should be stable. Both commercial packages and free InSAR software are available for the computing of interferograms (Zhou, Chang, & Li, 2009).

4. Synthetic Aperture Radar

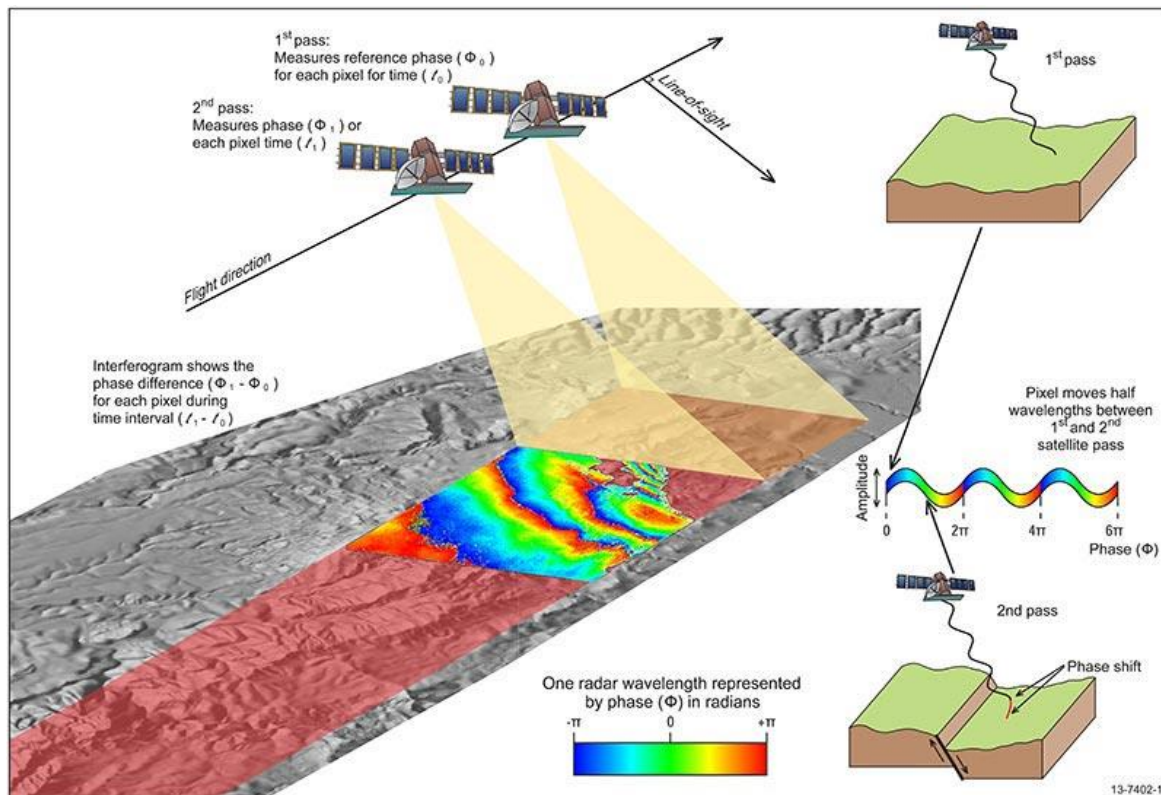


Figure 4.10 A figure depicting the acquisition of SAR images of the same area, acquired at different times (Geoscience Australia, 2018)

4.3.3 Application of InSAR (including DInSAR)

The fundamental measurement of an interferogram is the change in di-electric and/or spatial properties. These properties can change due to various forcing, from earthquakes to freezing and permafrost melting. Any factor that affects the phase of backscattered radar signal leads to an effect on the fringe pattern and the number of fringes in an interferogram. Such factors include; atmospheric effects, difference in acquisition geometry, ground surface topography and the distance between the antenna and the ground pixel. These factors can potentially be measured using the InSAR technology. Such measurements include land uplift/subsidence, surface displacements, land topography, soil moisture and water levels (Zhou, Chang, & Li, 2009). This allows the broad application of InSAR in the field of earth and environmental studies (Zhou, Chang, & Li, 2009). Studies of land subsidence using InSAR in flat arid areas are more abundant and have in general achieved greater success than in mountainous regions and slope movement studies (Smith, 2002). The DInSAR technique can be used to image up to centimetre scale ground subsidence caused by human activities such as coal mining, subsurface water groundwater extraction and petroleum extraction (Smith, 2002). InSAR can detect very subtle change with unprecedented accuracy, scale and reliability (ESA Earthnet Online, 2014). Appendix VI gives examples of InSAR applications in various fields.

4.3.4 InSAR limitations

One of the main limits of the InSAR technique has to do with temporal stability of the spatial distribution of scatters within a pixel. An example is when the moisture conditions of near surface layer changes. The spatial pattern of SAR sensitive scatters within pixel will then change over time, leading to random pattern of interferometric phase in the surroundings of a pixel, or the destruction of a fringe pattern in an interferogram. An additional limitation is related to the deformation time rate. If the relative displacement between two neighbouring pixels exceeds one fringe, this displacement cannot be detected using InSAR. This means that the maximum detectable deformation rate is one fringe per pixel. Another limitation of InSAR is that the amount of

4. Synthetic Aperture Radar

deformation inferred from the number of fringes in an interferogram are not absolute changes relative to zero deformation, but relative changes (Zhou, Chang, & Li, 2009).

4.3.5 Persistent Scatter Interferometry

A technique known as the Persistent Scatter Interferometry (PSI), handles InSAR limitations in an innovative way. PSI represents a specific class of DInSAR techniques (Crosetto et al., 2016) and provides a systematic processing strategy that can use all archived SAR data of a certain area from repeat orbits and creating a stack of differential interferograms that have a common *master image* (Zhou, Chang, & Li, 2009). This technique is the most advanced of DInSAR (Crosetto et al., 2009). It analyses the phase of PS or DS as a function of time, space and baseline. Various spatio-temporal-baseline relations of the phase components of PS to atmosphere, topography and displacement are used for successful separation of these components in an estimation procedure (Zhou, Chang, & Li, 2009). PSI is able to measure deformation only over the available PS or DS (Crosetto et al., 2016). The main results of a PSI analysis include deformation time series and deformation rate estimated over the analysed PS or DS. Figure 4.11 gives an example of a deformation velocity map and deformation time series. A residual topographic error (RTE) is another outcome of PS. RTE is the difference between the true height of the scattering phase centre of a given PS or DS and the height of the DEM at this point (Crosetto et al., 2016). The invention of PSI was a big breakthrough towards a high accuracy observation of slow moving surfaces over long time frames since it enables the identification, isolation and estimation of millimetre surface deformation from space (Zhou, Chang, & Li, 2009). The main advantages of PSI are: it allows to have a global outlook of deformation occurring in a wide area since it offers a wide-area coverage with a relatively high spatial resolution; it is very sensitive to deformations, which in terms of deformation velocity are in the region of 1 millimetre/year; there is huge historical SAR archive available, enabling the measurement of past deformation occurrences for which no other survey data could be available. The technique also has its limitations but these are not discussed in this study (Crosetto et al., 2009).

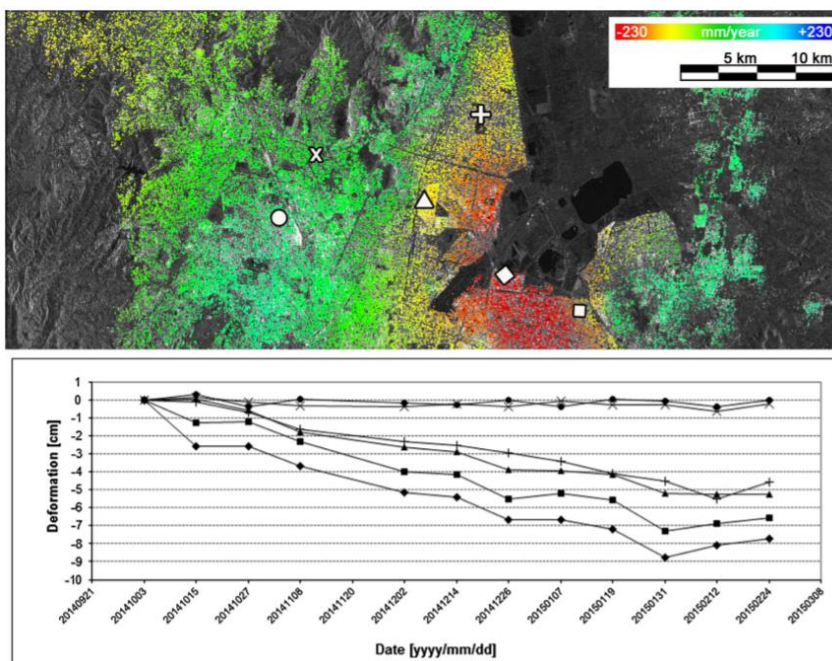


Figure 4.11 An example of a deformation rate/velocity map and deformation time series over Mexico City using SAR Sentinel-1 images (Crosetto et al., 2016)

5. Methodology

5.1 Data acquisition

5.1.1 Water level time series

Surface water level measurements in relation to the *Normaal Amsterdamse Peil (NAP)* were acquired from (Rijkswaterstaat Waterinfo, 2018) portal. From the portal one can select various water related parameters of the country's main waterways based on a certain time frame and the available measuring stations. Water level measurements were requested for measuring stations close to the study areas (Appendix VII) of this study. The study areas consist of one canal (Hartelkanaal) and 7 harbours (Donauhaven, 7e Petroloeuimhaven, Londenhaven, Brittaniëhaven, Prinses Beatrixhaven, Prins Johan Friso haven, Waalhaven and Londenhaven). After making a request, a link to a downloadable .csv file with the requested data is sent within one hour by e-mail. Rijkswaterstaat, the Ministry of Infrastructure and Water Management, has multiple measuring stations at the Port of Rotterdam. Surface water levels at these points get measured automatically. Appendix VIII shows the available measuring stations for surface water levels within the project area's surrounding for which time series can be requested. The measuring stations used in this study are represented by red points whereas the black points represent the rest of the stations. The selection of the relevant stations was based on their closeness to any study area and also based on data availability within the time periods of 2009 to 2015, since the vertical deformation time series are available within this time frame. Apart from time series acquired from the shown stations, time series from one station (measuring station Brittaniëhaven) operated by the Port of Rotterdam Authority was used. The plots in Appendix IX show the water levels for each of the used stations. The plots show similar patterns but have varying differences between upper and lower peaks.

5.1.2 Deformation time series

Deformation velocity time series generated through the PSI technique, were provided by SkyGeo from their archive portal. The portal, specific for the Port of Rotterdam, has deformation time series, at *points* where vertical deformation was detected after generating data from the TerraSAR-X satellite. The satellite acquired these data between June 2009 and November 2015. Appendix X gives more details about the TerraSAR-X satellite.

Figure 5.1 gives an example of deformation *points* at the harbour of Brittaniëhaven. The colours of the points represent estimated vertical deformation velocity (rate) in mm/year. Each point has a time series with the calculated (cumulative) deformation in mm, between 2009 and 2015 for each acquisition date. Since TerraSAR-X has a revisit time of 11 days, each month has either two or three days (acquisition dates) at which calculated deformation is available. Figure 5.2 gives an example of a graph of one deformation *point*. The red line is a linear trendline of the estimated vertical



Figure 5.1 Deformation points (Ascending PS) at Brittaniëhaven, acquired between 2009 and 2015

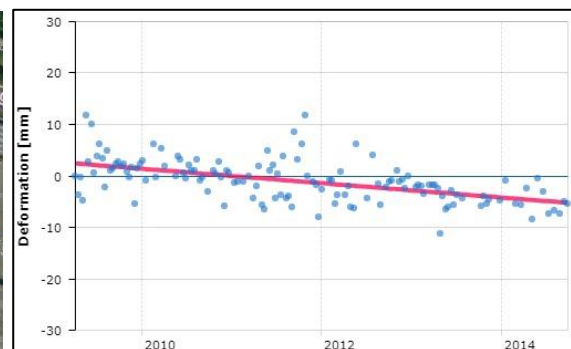


Figure 5.2 Example of estimated vertical deformation graph across the years of a point.

5. Methodology

deformation velocity of all the estimated vertical deformation time series of that point.

The value of deformation of the first observation in a time series is always zero since an assumption is made that there is no deformation. This first value is then used as a reference for the rest of the observations. Appendix XI shows the points at the different study areas. For each study area, there are vertical deformation points detected using data acquired from both the ascending and descending orbits of the TerraSAR-X satellite. As it can be seen from Appendix X there is a difference between deformation points detected using PS from the ascending and descending orbits. Notable is that descending PS points appear to be more in number than the ascending PS points at the study areas. These differences are mainly caused by difference in the total number of observations, the view angle of the satellite and differences in point quality. Furthermore, there is difference in reference points used in the geo-location of the ascending and descending points.

Differences in the number of observations can be seen in figure 5.3, which displays the number of observations/images (red lines) in the descending and ascending orbits of TerraSAR-X. It is evident that the descending orbit had more observations than the ascending orbit, meaning the descending orbit had more measurements and also longer time series. Point quality is a relative measure (between 0 and 1) of a respective deformation point. A low point quality value indicates a high amount of noise (distortion) in the time series of a point (SkyGeo, 2018). Since the descending orbit acquired more measurements (points), there are higher chances of these points to have higher point quality than those from the ascending orbit. This is because points with a lower point quality get discarded based on a defined threshold. This study uses only time series acquired from PS pixels because they are more reliable than time series acquired from DS pixels. As earlier mentioned PS pixels contain objects that have high backscatter properties and the backscatter remains consistent throughout time, making them more trustworthy than DS pixels.

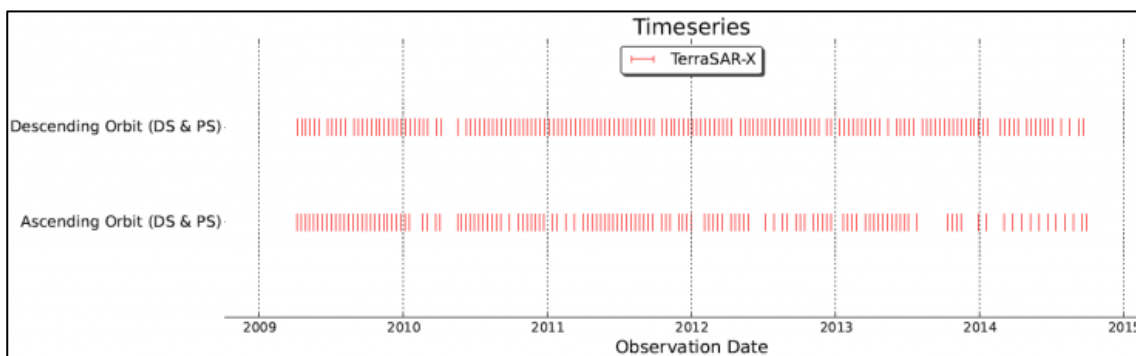


Figure 5.3 Distribution of image observations by TerraSAR-X between 2009 and 2015 (SkyGeo, 2018)

5.2 Data Analysis

5.2.1 Correlation and regression analysis

Two of the most commonly used methods to investigate the relationship between two quantitative variables are the correlation and regression analyses. Correlation analysis is a technique for assessing a possible linear association between two continuous variables. Correlation is defined as a degree of relationship between the two variables under consideration. It is measured by a statistic known as the correlation coefficient, which expresses the degree of a relationship. It is a dimensionless quantity and its value ranges between -1 and 1. The stronger the correlation, the closer the correlation coefficient gets to ± 1 . A correlation coefficient of zero denotes no linear relationship between two continuous variables whereas a correlation coefficient of -1 or $+1$ indicates a perfect linear relationship (Mukaka, 2012; SRM, 2010). As shown in 5.4, there are different types of correlation based on linearity, number of variables and degree of correlation. These types of correlation can be studied using the following methods: (1) Scatter Diagram Method, (2) Spearman's Rank Correlation Coefficient, (3) Karl Pearson's Coefficient of Correlation and (4)

5. Methodology

Method of Least Squares (SRM, 2010). This study, and also the previous study conducted by SkyGeo, used the Karl Pearson's Coefficient of Correlation also known as the Pearson's Product Momentum Correlation Coefficient or simply Pearson's Correlation, which is the most common correlation coefficient.

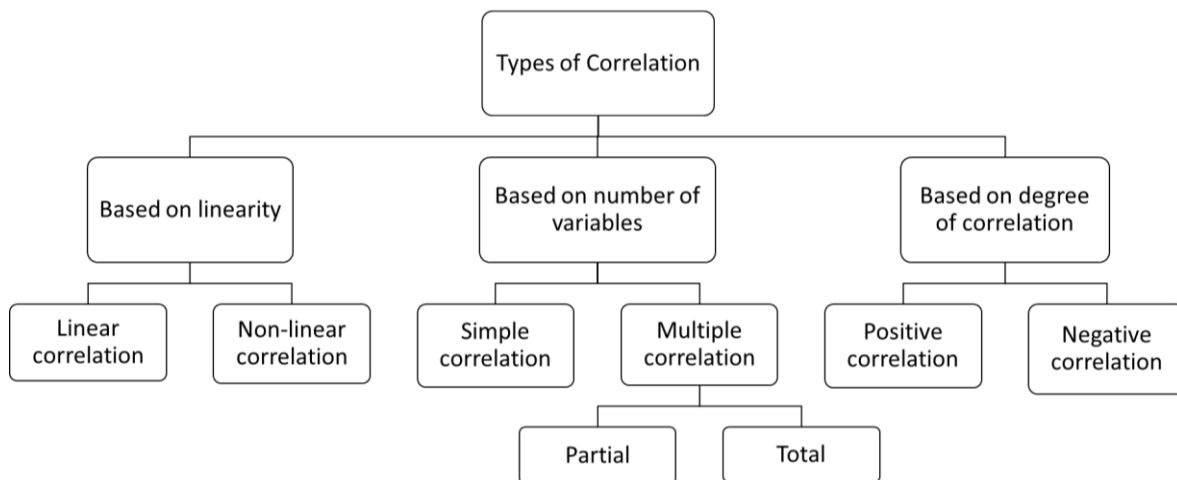


Figure 5.4 Different types of correlation

Pearson's Correlation

The Pearson's Correlation equation is given here below, where x_i and y_i are the values of x and y for the i th individual.

$$r = \frac{\sum_{i=1}^n (x_i - \bar{x})(y_i - \bar{y})}{\sqrt{\sum_{i=1}^n (x_i - \bar{x})^2 \sum_{i=1}^n (y_i - \bar{y})^2}}$$

Equation 5: Pearson's Correlation equation

Abbreviated as 'r', Pearson's Correlation measures the degree ($-1 \leq r \leq +1$) of linear relationship between two variables. It is independent of scale and origin, and is used when the considered variables are normally distributed. It however makes certain assumptions. First, it assumes that there is a linear relationship between two variables. Secondly, it assumes that a cause and effect relation exists between different forces operating on the item of the two variables (Mukaka, 2012). An advantage of r is that it summarizes the degree and direction of correlation in one value. The r also has also its limitations: (i) interpreting the correlation is difficult, (ii) the value of correlation is affected by extreme values, which may lower or exaggerate the strength of a relationship, making it inappropriate when one or both considered variables are not normally distributed, (iii) it always assumes a linear relationship between two variables (SRM, 2010).

It is important to emphasize that correlation indicates the dependence of two variables on each other. It is essential that two variables should have a cause-effect relationship, and if such does not exist then the two phenomena cannot be correlated. If the considered variables vary in such a way that movement in one goes along with the other, these variables are called cause and effect relationship. A cause and effect relation (causation) indicates correlation, correlation however does not necessarily imply causation (SRM, 2010).

Coefficient of determination

A convenient way of interpreting the value of correlation coefficient is to use the square of the Pearson's Correlation which is called the Coefficient of Determination (R^2). The maximum value of R^2 is 1 because it is possible to explain all the variation in the effect-variable but it is not possible to explain more than all of it. If $r=0.5$, $R^2=0.25$ this means that 25 % of the variation in the dependent variable (cause) has been explained by the independent variable (effect) (SRM, 2010). It is however not possible to possible find out the direction of a correlation (positive or negative) with R^2 .

5. Methodology

Regression Analysis

The goal of regression analysis is to express the relationship between two variables in the form of an equation, given the variables are related to each other. Using this method, it is possible to predict the value of unknown variable from known variable. It helps in obtaining a measure of the degree of correlation that exists between two variables. Furthermore, it helps to obtain a measure of the error involved in using the regression line as a basis for estimations. The regression line gives the best estimate of one variable from the value of any other given variable and gives the average relationship between the two variables in an equation (SRM, 2010). Figure 5.5 gives an example of correlation and regression plots, with their interpretations. The black lines, with no equations, are the regression lines, showing a fit through the correlation plots (in dots).

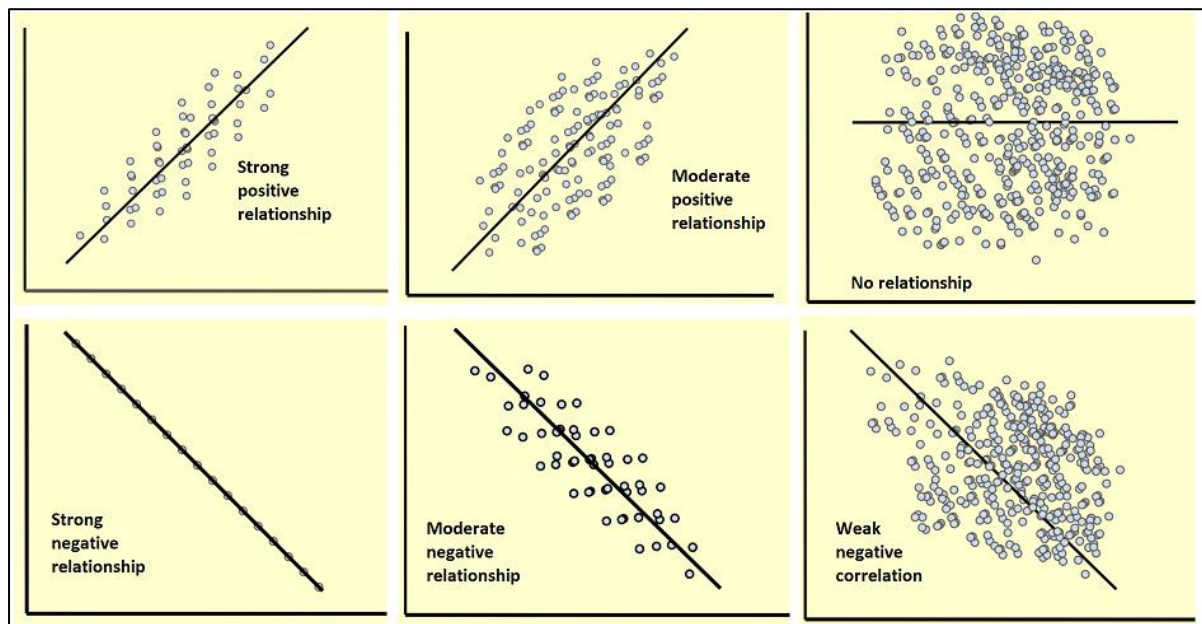


Figure 27: Examples of correlation and regression plots. Adapted from (SRM, 2010)

5.2.2 DInSAR and ocean tide loading

As mentioned in the introduction chapter, OTL is the elastic response of the earth due to redistribution of water mass from ocean tides. Using Green's function, tidal loading can be computed in the vertical/up-down (UP), north-south (NS) and east-west (EW) directions. Some of the parameters in Green's function include; ocean water density, observation of the calculation point, tidal height and longitude of the observation point (Lei et al., 2017). OTL displacements in coastal areas can be several centimetres, especially in the vertical direction (Lei et al., 2017). The relative variation of ground displacements may thus reach several centimetres in DInSAR interferograms (Peng, Wang, & Cao, 2017). Displacement of the deformable seabed happens due to the tide induced weight of water above it (Earth and Space Research, 2018).

OTL displacements and theory is beyond the scope of this study but here is however interest to gain insight into possible relationship between detected deformation points and water fluctuations caused by tidal phenomena. The change between the state of an ocean tide at its highest level (high tide), and its lowest level (low tide), causes the fluctuations of surface water levels. The previous study conducted by SkyGeo and this study applied the following hypothesis: when water levels get higher, the pressure on the sea bed gets higher, leading to an increase in vertical downward deformation.

5. Methodology

A positive correlation coefficient indicates that an increase in the first (cause) variable corresponds to an increase in the second (effect) variable. A negative correlation indicates an inverse relationship: an increase in the first variable corresponds to a decrease in the second variable (Rebekić et al., 2015). Taking this into account, a positive correlation of r suggests that an increase on surface water surface level leads to an increase in upward deformation (land uplift) whereas a negative correlation implies that an increase in surface water levels leads to an increase in vertical downward deformation (land subsidence).

5.2.3 Difference with previous study

In the previous study conducted by SkyGeo, water level time series used in the calculation of correlation was obtained from the measuring station Brittaniëhaven that is operated by the Port of Rotterdam Authority. Furthermore, entire time series of four years, from both the deformation and water level time series, were used to calculate the correlation for each deformation point located at a quay wall area. The correlation calculations were conducted in the programming language Python. This study used time series from multiple measuring stations operated by Rijkswaterstaat. Time series from multiple stations operated by the Port of Rotterdam Authority near the study areas were requested but could not be delivered on time. Table 6 shows which measuring station was assigned to which study area.

Table 3 Assignment of surface water level measuring stations to study areas

Study area	Assigned measuring station
Brittaniëhaven	Rozenburgsesluis noordzijde
Londenhaven	Rozenburgsesluis zuidzijde
Donauhaven & 7e Petroleumhaven	Scheurhaven
Prinses Beatrixhaven & Prins Johan Frisohaven	Parksluis
Hartelkanaal	Hartelbrug
Waalhaven	Parksluis

The correlation between water level and deformation time series for each deformation point was calculated annually (separate years) and also for an entire time period of 4 years. Another difference with this study is that spatial averaging of deformation time series was introduced to analyse the influence of using different measuring stations. The correlation calculations in this study were performed in the programming language R.

5.2.4 Workflow

The programming software R, version 3.4.4 was used to calculate the Pearson's Correlation (r) and the Coefficient of Determination (R^2) as well as to plot the results. The methods that were used in calculating the correlations are shown in figures 5.7 and 5.8. Using the first method, correlation was calculated using spatial averages of deformation time series of points close to the shoreline. Points that are close to the shoreline were manually selected using the QGIS Geographic Information System software after downloading the time series from the SkyGeo portal. Averages of the estimated vertical deformation velocity time series of the points were calculated based on the acquisition time of the satellite. The averaging, conducted in Microsoft Excel 2016, was done to understand the trend of the averaged estimated vertical deformation of all points at a particular time (date). The result was an average of the estimated deformation of all points at each acquisition date.

5. Methodology

It is essential to distinguish between points located on buildings and other infrastructure (high points) and points located on the ground (low points). This is because buildings and other firm structures, are more stable than features such as vegetation (SkyGeo, 2018). In this case, the low points are points closest to the shoreline/ near the quay wall areas.



Figure 5.6 A representation of difference between high and low deformation points (SkyGeo, 2018)

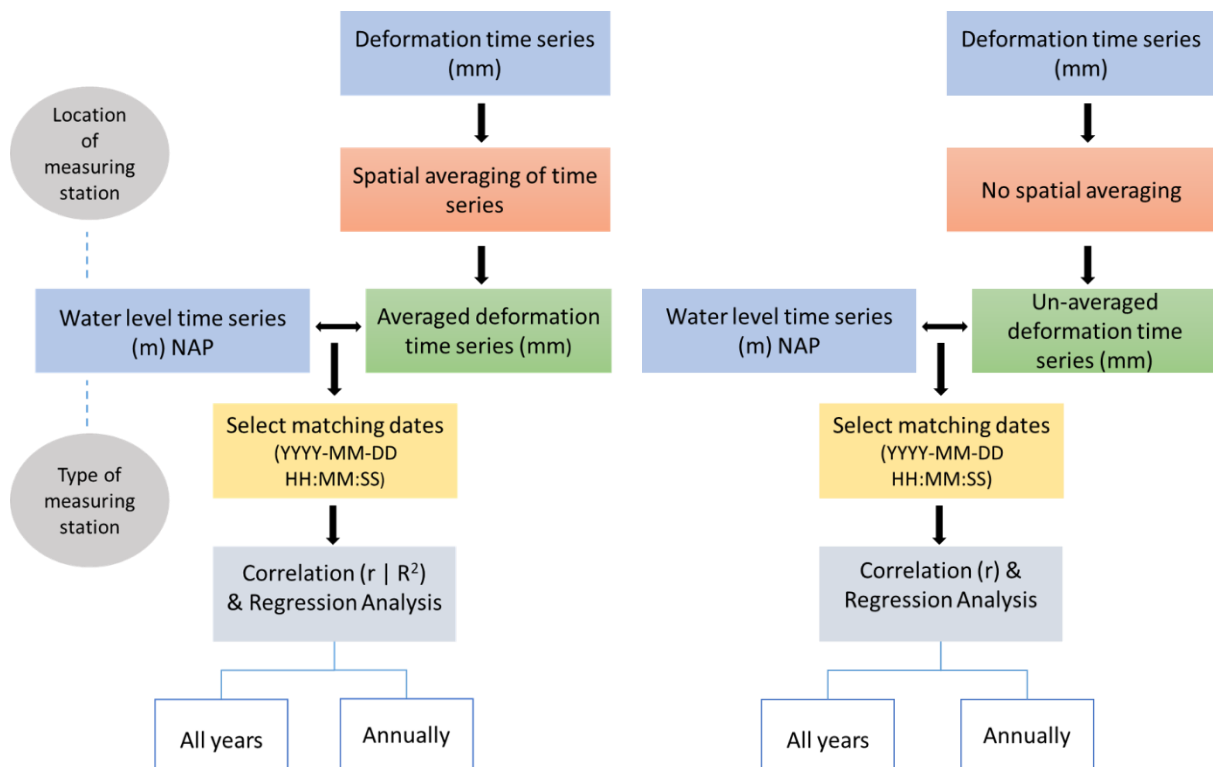


Figure 31 Flow chart of methodology 1

Figure 308 Flow chart of methodology 2

Calculating correlation after performing a spatial aggregation takes a shorter computation time. This is more efficient when testing the influence of the location of the water level measuring stations from which a time series is gained and testing the influence of the type of the measuring station. A test was conducted to find out if there are differences in correlation results when water level time series from stations operated by Rijkswaterstaat or Port of Rotterdam Authority is used. This was done since there is a difference in time step for measuring the water levels between stations operated by the two.

In the second method, time series of the same deformation points used in the first method were used but there was no spatial averaging involved. This means that each point in the end had a correlation coefficient unlike with method 1 where it is not possible to link correlation results to individual deformation points due to spatial averaging.

Using R, water level time series and the spatial averages of the vertical deformation rates were linked together in both methods. This was done by linking the observation time of the water level measurements and the acquisition time of the deformation time series. TerraSAR-X has a revisit time of 11 days and the PS time series obtained during the ascending orbit were acquired around 17:26

5. Methodology

PM, whereas PS time series obtained from the descending orbit were acquired at about 06:08 AM. As it can be seen in Appendix XII, a year mostly has 2 or 3 measurements per month, each measurement being of a different date. The measuring stations operated by Rijkswaterstaat do not have a consistent time step for conducting measurements. Some years and/or months have more measurements than others and at some days the water levels are measured more frequently than other days. There can be 5 measurements in one hour, and the next hour can have less, more or even no measurements. The measuring station operated by the Port of Rotterdam Authority has a consistent time step of 10 minutes for measuring the water levels although there are some gaps in the time series. To conduct a match with the water level time series from Rijkswaterstaat, the acquisition times from the ascending orbit were rounded up to 17:00:00 PM and those from descending orbit were rounded up to 06:00:00 AM. This was done because 17:00:00 PM and the 06:00:00 AM were the closest observation times in the water level time series, otherwise the vertical deformation time series and water level time series cannot be linked.

To conduct a match with the time series from the station operated by the Port of Rotterdam Authority, the acquisition times from the ascending orbit were rounded up to 17:20:00 PM and those from descending orbit were rounded up to 06:10:00 AM. This was done since the time series had more measurements acquired at times closer to the observation times of the satellite.

Figures 5.9 and 5.11 give examples of plots of water level and vertical deformation time series after matching the two based on observation time and acquisition times. The examples shown use vertical deformation time series of Ascending PS from Britanniëhaven and water level time series obtained from the measuring station Rozenburgseluis noordzijde. The dots in figure 5.9 represent the heights of water levels available on dates when a match was established. Appendix XIII shows plots of the spatial averages of deformation at the study areas whereas Appendix XIV and XV give the plots of deformation and water levels respectively after establishing a connection based on the acquisition times of the deformation time series and observation times of the water level time series. In Appendix XIV, the level of (downward) deformation of spatially averaged ascending PS time series are higher compared to those from descending PS time series.

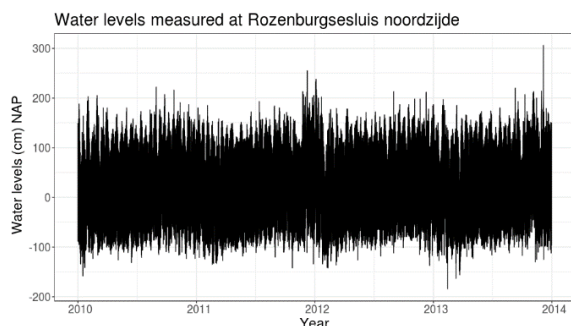


Figure 32 Measured water levels at Rozenburgseluis noordzijde station

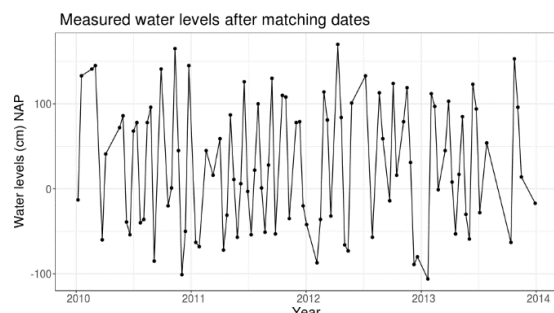


Figure 35 Water levels on dates when observation times of water levels and acquisition times of averaged deformation (Asc Ps) match

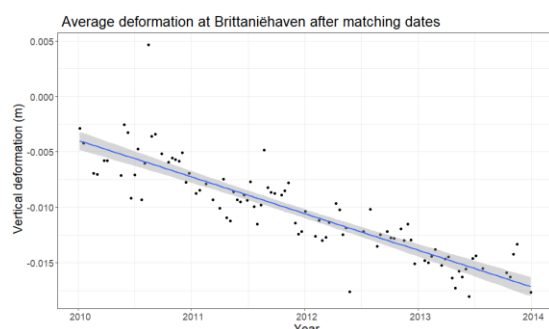


Figure 3811 Spatial averages of vertical deformation time series at Britanniëhaven (Asc Ps)

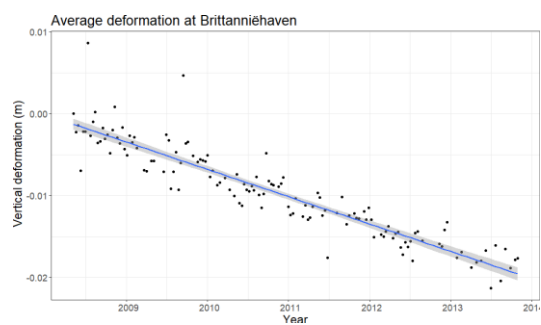


Figure 4112 Deformation at Britanniëhaven on dates when observation times of water levels and acquisition times of averaged deformation time series (Asc PS) match

6 Results

Correlation coefficients can be classified into different number of classes (between -1 and 1) to interpret them. This study uses 5 classes for positive correlation coefficients and 5 classes for the negative correlation coefficients. More or less classes compared to the ones in table 7 can be applied for interpreting the results.

Table 4 Rule of thumb applied to interpret the size of Correlation Coefficient, adapted from (Mukaka, 2012)

Coefficient range	Interpretation (class)
0.90 to 1.00	Very high positive correlation
0.70 to 0.90	High positive correlation
0.50 to 0.70	Moderate positive correlation
0.30 to 0.50	Low positive correlation
0.0 to 0.30	Negligible correlation
0.0 to - 0.30	Negligible correlation
- 0.30 to - 0.50	Low negative correlation
- 0.50 to - 0.70	Moderate negative correlation
- 0.70 to - 0.90	High negative correlation
- 0.90 to - 1.00	Very high negative correlation

6.1 Correlation between spatially averaged deformation time series and water level time series

6.1.1 Using time series from assigned water level measuring stations

Tables 5 to 10 present the results between water level time series and spatially averaged vertical deformation time series, acquired from both ascending and descending orbits, for each study area. The source of the water level time series are the measuring stations operated by Rijkswaterstaat. It is noticeable that for each table, in situations whereby descending PS time series were used, the correlation coefficients are mostly negative. Another main observation is that the results for entire time periods (2010-2013), total of four years, are mostly lower compared to an individual year. This is likely caused by differing the number of observations of each year. From all the results there is no clear trend of how the correlation coefficients increase or decrease starting from the year 2010. The year 2013 has the highest negative correlation in cases whereby descending PS time series were used. Using the classes given in table 4, most of the coefficients in the presented tables are either low or negligible. The highest coefficient, Table 5; year 2013 using Desc PS, is -0.61 which falls under the 'moderate negative correlation' class. Coefficients in the same table, in the case whereby descending PS time series were used are the higher compared to the ones in the rest of the tables. Appendix XVI gives an example of regression and correlation plots. Equations of the regression lines were omitted since they are not relevant for this study.

Table 5 Correlation results Donauhaven and 7e Petroleumhaven

YEAR	Using Asc PS time series	Using Desc PS time series
2010-2013	-0.02	-0.40
2010	-0.13	-0.51
2011	-0.04	-0.56
2012	-0.21	-0.38
2013	0.21	-0.61

6. Results

Table 6 Correlation results Londenhaven

Year	Using Asc Ps time series	Using Desc PS time series
2010-2013	0.03	0.07
2010	0.22	-0.20
2011	-0.17	0.17
2012	-0.03	-0.01
2013	0.25	-0.13

Table 7 Correlation results Brittaniëhaven

Year	Using Asc PS time series	Using Desc PS time series
2010-2013	0.0	-0.31
2010	0.10	-0.50
2011	-0.36	-0.31
2012	-0.02	-0.31
2013	-0.01	-0.53

Table 8 Correlation results Hartelkanaal

Year	Using Asc Ps time series	Using Desc PS time series
2010-2013	0.03	0.03
2010	0.21	0.11
2011	0.08	0.02
2012	-0.07	-0.09
2013	0.23	-0.34

Table 9 Correlation results Prinses Beatrixhaven and Prins Johan Friso haven

Year	Using Asc Ps time series	Using Desc PS time series
2010-2013	-0.01	-0.02
2010	0.34	-0.24
2011	-0.40	-0.20
2012	-0.08	-0.32
2013	0.30	-0.35

Table 10 Correlation results Waalhaven

Year	Using Asc Ps time series	Using Desc PS time series
2010-2013	-0.03	-0.01
2010	0.36	0.08
2011	-0.33	-0.23
2012	-0.13	-0.32
2013	0.11	-0.42

6. Results

6.1.2 Using time series from different water level measuring stations

Tables 11 and 12 present the results between spatially averaged deformation time series from Donauhaven and 7e Petroleumhaven and water level time series obtained from three different measuring stations; Scheurhaven, Rozenburgseluis Zuidzijde and Parksluis. The correlation results whereby descending PS time series were used to calculate the correlation have stronger negative results compared to those whereby ascending PS time series were used. In both tables results for Scheurhaven have the highest correlations. Most of the results in the table are either low. It is clear from both tables that results in the case whereby time series from the station Scheurhaven were used, coefficients are mostly higher compared to other stations. Of the three stations, Scheurhaven is the closest to Donauhaven and 7e Petroleumhaven.

Table 11 Correlation results at Donauhaven and 7e Petroleumhaven (using Ascending PS time series)

YEAR	Scheurhaven	Rozenburgseluis Zuidzijde	Parksluis
2010-2013	-0.02	-0.05	-0.07
2010	-0.13	-0.14	-0.14
2011	-0.04	-0.09	-0.09
2012	-0.21	-0.20	-0.13
2013	0.21	0.08	-0.04

Table 12 Correlation results at Donauhaven and 7e Petroleumhaven (using Descending PS time series)

YEAR	Scheurhaven	Rozenburgseluis Zuidzijde	Parksluis
2010-2013	-0.40	-0.25	-0.14
2010	-0.51	-0.24	-0.08
2011	-0.56	-0.33	-0.22
2012	-0.38	-0.27	-0.15
2013	-0.61	-0.51	-0.35

Tables 13 and 14 present the results between spatially averaged deformation time series of from Brittaniëhaven and water level time series obtained from the stations Scheurhaven, Rozenburgseluis noordzijde and Parksluis. The closes measuring station to the Brittaniëhaven harbour is Rozenburgseluis Noordzijde. From both tables, no clear trend can be served. The results in table 14 for Rozenburgseluis Noordzijde are mostly higher than those from the other two stations. Rozenburgseluis is the closest measuring station to the harbour of Brittaniëhaven. Majority of the correlation coefficients in all tables are either low are negligible.

Table 13 Correlation results Brittaniëhaven (using Ascending PS time series)

YEAR	Scheurhaven	Rozenburgseluis noordzijde	Parksluis
2010-2013	0.01	0.0	-0.03
2010	0.11	0.10	0.06
2011	-0.34	-0.36	-0.33
2012	-0.06	-0.02	-0.03
2013	-0.02	-0.01	0.27

6. Results

Table 14 Correlation results Britanniëhaven (Descending PS)

YEAR	Scheurhaven	Rozenburgseluis noordzijde	Parksluis
2010-2013	-0.27	-0.31	-0.10
2010	-0.49	-0.50	-0.20
2011	-0.31	-0.31	0.00
2012	-0.30	-0.31	-0.23
2013	-0.46	-0.53	-0.23

Tables 15 and 16 present the correlation results between spatially averaged deformation time series from Prinses Beatrixhaven and Prins Johan Frisohaven and water level time series obtained from the stations Scheurhaven, Rozenburgseluis zuidzijde and Parksluis. Results in table 16, whereby descending PS time series were used, have stronger negative results compared to the case whereby ascending PS time series were used. Majority of the results for Rozenburgseluis zuidzijde are higher than those of Parksluis (the closest to the harbour). Most of differences are however minimal. All the correlation coefficients from both tables are either low or negligible.

Table 15 Correlation results Prinses Beatrixhaven and Prins Johan Frisohaven (using Ascending PS time series)

YEAR	Scheurhaven	Rozenburgseluis zuidzijde	Parksluis
2010-2013	0.04	0.01	-0.01
2010	0.25	0.30	0.34
2011	-0.45	-0.47	-0.40
2012	-0.06	-0.10	-0.08
2013	0.26	0.30	0.30

Table 16 Correlation results Prinses Beatrixhaven and Prins Johan Frisohaven using (Descending PS time series)

YEAR	Scheurhaven	Rozenburgseluis zuidzijde	Parksluis
2010-2013	0.02	0.00	-0.02
2010	-0.22	-0.25	-0.24
2011	-0.24	-0.20	-0.20
2012	-0.29	-0.34	-0.32
2013	-0.67	-0.48	-0.35

6. Results

6.1.3 Using water level time series from a different type of measuring station

Tables 17 and 18 present the correlation results between spatially averaged deformation time series from Brittaniëhaven harbour and water level time series obtained from the measuring stations Scheurhaven and Brittaniëhaven. The station Brittaniëhaven is operated by the Port of Rotterdam Authority whereas the station Scheurhaven is operated by Rijkswaterstaat. The time series from Brittaniëhaven had a consistent time step and thus more measurements than those from Scheurhaven. The exact location of the measuring station Brittaniëhaven is not known but the name of the station suggests that it is close to the the Brittaniëhaven harbour. In table 17, most of the correlation results for station Brittaniëhaven are higher than those for Scheurhaven. In table 18, majority of the results for station Scheurhaven are higher than those for Brittaniëhaven. Most of the correlation coefficients in both tables are either low or negligible.

Table 17 Correlation results Brittaniëhaven (using Ascending PS time series)

YEAR	Station Scheurhaven	Station Brittaniëhaven
2010-2013	0.0	-0.03
2010	0.10	0.22
2011	-0.36	-0.18
2012	-0.02	-0.08
2013	-0.01	-0.05

Table 18 Correlation results at Brittaniëhaven (using Descending PS time series)

YEAR	Station Scheurhaven	Station Brittaniëhaven
2010-2013	-0.31	-0.17
2010	-0.50	-0.26
2011	-0.31	-0.27
2012	-0.31	-0.30
2013	-0.53	-0.55

Tables 19 and 20 present the correlation results between spatially averaged deformation time series from Donoauhaven & 7e Petroleumhaven and water level time series from the stations Scheurhaven and Brittaniëhaven. Majority of the results in table 19 show consistency in the negativity or positivity of the results but the differences in correlations when the two stations are compared are mostly minimal. In table 20 it is noticeable that there are big differences between results and furthermore most of the coefficients are negative.

Table 19 Correlation results at Donoauhaven and 7e Petroleumhaven (using Ascending PS time series)

YEAR	Station Scheurhaven	Station Brittaniëhaven
2010-2013	-0.02	-0.06
2010	-0.13	-0.14
2011	-0.04	0.03
2012	-0.21	-0.17
2013	0.21	0.08

6. Results

Table 20 Correlation results at Donauhaven (using Descending PS time series)

YEAR	Station Scheurhaven	Station Brittaniëhaven
2010-2013	-0.02	-0.32
2010	-0.13	-0.36
2011	-0.04	-0.51
2012	-0.21	-0.42
2013	0.21	-0.70

Changing rounding up time interval

Tables 21 and 22 present the results between water level time series from the station Brittaniëhaven operated by the Port of Rotterdam Authority and spatially averaged deformation time series from Donauhaven & 7e Petroleumhaven. Both tables give comparisons of correlation results in cases whereby the spatially averaged deformation time series were rounded off at different times. When the acquisition times of the ascending PS time series are rounded up to 17:20:00, Table 21, most of the coefficients are slightly higher than when rounded up to 17:00:00 PM. When the acquisition time of descending PS time series are rounded up to 06:10:00, Table 22, most of the coefficients are quite higher, compared to when the time series are rounded up to 06:00:00 AM. All of the results shown in table 21 are negligible. The coefficients in table 22 are mostly low except in the case whereby descending PS time series were used in the year 2010. These results fall under the 'high' negative class.

Table 21 Correlation results at Donauhaven and 7e Petroleumhaven (using Ascending PS time series)

YEAR	Acquisition time rounded off to 17:00:00 PM	Acquisition time rounded off to 17:20:00 PM
2010-2013	-0.06	-0.03
2010	-0.14	-0.15
2011	0.03	0.06
2012	-0.17	-0.20
2013	0.08	0.07

Table 22 Correlation results at Donauhaven and 7e Petroleumhaven (using Descending PS time series)

YEAR	Acquisition time rounded up to 06:00:00 AM	Acquisition time rounded up to 06:10:00 AM
2010-2013	-0.32	-0.35
2010	-0.36	-0.42
2011	-0.51	-0.49
2012	-0.42	-0.48
2013	-0.70	-0.71

6. Results

6.2 Correlation between unaveraged deformation time series and water level time series

Appendices XVII to XXII present frequency histograms of correlation classes and the total number of points in each class for each study area. They show the yearly correlation results between water level time series and unaveraged vertical deformation time series, acquired from both ascending and descending orbits. A vast majority of the correlation coefficients fall under the negligible and low (both negative and positive) classes. Donauhaven and 7e Petroleumhaven is the only study area with most points which have correlation coefficients that fall under high (high negative) classes. The number of points that have correlation coefficients that fall under moderate class is also highest in this study area. Appendix XXIII gives an example of how the correlation coefficient for each deformation point was visualized according to correlation classes. The first image shows the study area of Donauhaven and 7e Petroleumhaven where a linear structure (a jetty) is located between the harbour of Donauhaven and the harbour of 7e Petroleumhaven. The highest correlations were found on this structure. This is likely because the structure is less stable than the areas around it and perhaps it moves up and down as the water levels fluctuate.

Table 23 Correlation results Donauhaven and 7e Petroleumhaven

YEAR	Acquisition time rounded off to 06:00:00 AM	Acquisition time rounded off to 06:10:00 AM
2010-2013	-0.32	-0.35
2010	-0.36	-0.42
2011	-0.51	-0.49
2012	-0.42	-0.48
2013	-0.70	-0.71

7 Conclusions and discussions

7.1 Conclusions

This study looked into different factors that possibly influence the correlation between vertical deformation and water level time series obtained from different areas at the Port of Rotterdam. The main research question was follows: “What are the most influential factors that possibly influence correlation between measured surface water levels and detected vertical deformation at the Port of Rotterdam?”

The vertical deformation time series used in this study were generated using the InSAR technique. InSAR is an advanced processing technique applied to radar images acquired from SAR satellites. It is used to detect surface displacements of infrastructure and other features on the Earth’s surface. A SAR satellite sensor emits microwave radiation towards the surface of the earth which is then reflected to the sensor. Both the magnitude and the phase of the reflected signal are registered for each resolution cell. A SAR satellite can observe the same area from slightly different look angles. This is achievable by exploiting the repeated orbits of the same satellite or by using two radars mounted on the same satellite. The phase difference between two acquisition periods can be calculated and results in an interferogram from which displacements can be derived. Measurements of the travel path variations of a SAR satellite as function of its position and acquisition time enables the creation of Digital Elevation Models.

Application of InSAR is very broad since surface deformation and/or di-electric property can change due to different factors. These factors can potentially be measured using InSAR technology. This enables the application of InSAR in various fields such as geomorphology, hydrology, seismology, volcanology, glaciology, cultural heritage studies, forestry, mining, structural and environmental engineering and natural disaster and assessment. Ground deformation can for example be caused by earthquakes, land subsidence, underground mining activities and groundwater extraction. Studies of land subsidence using InSAR in flat arid areas are more abundant and have in general achieved greater success than in mountainous regions and slope movement studies. Time-series InSAR techniques such as the Persistent Scatterer Interferometry allows the estimation of displacements at millimetre-level using a series of images with the same acquisition geometry.

Spatial averaging of deformation time series allows to test different factors that possibly influence the correlation between deformation and water levels time series in a quick and efficient way due to the short computation time and less time needed to develop the scripts to compute them. Several observations were made about the degree of correlation when spatial averaging is conducted. Firstly, correlation between deformation and water level time series are mostly low or negligible. Secondly, correlation coefficients in cases whereby descending PS time series are used show a higher strength than when ascending PS time series are used. The reason behind this is not clear but there are more time series available from descending PS because there are more deformation points detected in the descending orbits than in the ascending orbit. However, the level of deformation of spatially averaged ascending PS time series from the study areas is higher compared to those from descending PS time series. Thirdly, when correlation is calculated using a one-year time series, the correlation coefficient is mostly higher compared to when a four-year time series is used. This is likely caused by the differing number of observations among the time series. Another possible cause is difference in seasonal variability of surface water levels of each year. Fourthly, when water level time series from measuring station closest to a study area is used, the coefficients are often higher compared to when a measuring station further away is used. Fifthly, when water level time series from a measuring station with a frequent and steady time step is used, the correlation coefficients are generally stronger compared to when a measuring station with an irregular and unsteady time-

7. Conclusions and discussions

step is used. The smaller the time step for measuring the water levels the, the smaller the time interval for rounding up time of the acquisition times of the satellite.

In addition, when spatial averaging is conducted, the correlation coefficients are mostly negative. This means that most of the times when water levels get higher, vertical downward deformation increases. When no spatial averaging is conducted, correlation coefficients can be visualized based on the location (x-y coordinates) of the deformation point being considered. This however takes a longer computation time and more time is needed to develop the scripts to compute them. Due to the numerous number of deformation points, it is difficult to assess possible factors that influence the strength of correlation between the water level and deformation time series. Conducting no spatial averaging however enables comparisons of classes that give the strength and direction of correlation of multiple points. Two major observations were made when no spatial averaging is conducted; (i) a vast majority of the correlation coefficients are either or negligible and (ii) most of the correlation coefficients are negative.

As mentioned above, when time series are split into separate years, the magnitude of correlation changes. Correlations calculated for individual years are most of the times significantly higher than when an entire time series of four years is used. There is a chance that the strength of correlation can increase when focussing on events with very high-water levels. A major issue is the revisit time of the satellite which limits the number of observations in the deformation time series to two or three observations per month. When deformation and water level time series are linked based on the observation time and acquisition time respectively, peak water levels are mostly not picked. The matching thus underestimates the very high-water levels. A possible way to tackle this issue is by performing a spectral analysis whereby frequency distribution of a time series from a limited set of measurements is considered by means of either non-parametric or parametric techniques. Due to limited amount of time, spectral analysis could not be conducted.

It is difficult to determine the accuracy of the correlation results and confirm them as well. This is because a major focus was laid only on the surface water levels and other factors that can be taken into consideration were ignored. The accuracy of the correlation results is questionable even though most of the correlation coefficients are either low or negligible. Interpreting Pearson's Correlation is difficult because of the assumptions made in this method. It is essential to keep in mind that correlation indicates the dependence of two variables on each other. Correlation does not necessarily imply causation (cause-effect relationship) between the variables being considered. Different number of divisions can be used to classify correlation results. For instance, a level of correlation considered low in this study, could be considered moderate when different number of classes are used to interpret the correlation coefficients. The level of correlation that would suggest that technical intervention measures or any other kind of measures that need to be taken are beyond the scope of this study.

7.2 Discussion and recommendations

There are factors (constraints), that influenced the reliability and the strength of the correlation results, which could be worked on for future research to achieve better results and increase the level of reliability. These factors are named and discussed here below:

- Possible factors that influence the strength of correlation between water level and deformation time series were tested after the deformation time series were averaged. Spatial averaging surprises the deformation signal and does not accurately represent the level of deformation for from all the deformation points. I suggest that all the factors considered in this report should be tested by conducting no spatial average. In this way the correlation results can be geo-graphically visualized, enabling patterns in results to be easily recognised.
- The major reason why I only deformation points close to the shoreline were used is because of differences in high and low points. I also consulted InSAR engineers at the company and they recommended that I use the low points. Low points are located for instance on the ground or on vegetation and are not located on features with firm foundations such as buildings. Another main reason is due to the conclusion that was drawn when a test not mentioned in this report was conducted. In that test the following hypothesis was applied: the level of correlation between time series from deformation points close to the shoreline/quay walls and water level time series is higher than the level of correlation between time series from all the deformation points. The correlation results in the case whereby deformation points close to the shoreline were used had higher levels of correlation. This hypothesis was however tested through the averaging of time series. I recommend that high points should be used when calculating correlation and this should also be done without spatial averaging of the deformation time series. This helps to identify and understand differences between results at high points and low points.
- This study is purely deterministic and assumes that surface water levels is a major factor that influences vertical deformation at the study areas. Surface water levels could just be one factor that influences vertical deformation. An appropriate way would be to create a model that takes other factors into consideration in one equation. Such factors (parameters) can include: surface water levels, ground water levels, drainage, deformation velocity, (seasonal) amplitude of the deformation signal and temperature. A possible factor that influences the level of deformation detected from ascending or descending could be related to temperature. In warm periods, structures possibly warm up leading to higher level of deformation detected in the ascending orbit (around 17:00:00 PM). In the morning, temperature effects could be minimal, affecting the level of deformation detected in the descending orbit (at about 06:00:00 AM). It could also be that horizontal deformation, which is unknown if is occurring, is related to vertical deformation. Factors such as type of material at a study area, soil type or year of construction possibly have influence on the deformation velocity. Another factor that can be considered is the relationship between surface water levels and tidal measurements in relation to NAP. Tidal measurements are available on the website of the Ministry of Infrastructure and Water Management.
- For future research, I also advice to use hypothesis testing (null and alternative hypothesis) in combination with models. This allows to focus more on the significance levels, which would point out which combination of factors do or do not affect the level of correlations.
- Lastly, I suggest the programming languages Python or MatLab be used next time when computing correlation coefficients because they can easily handle huge sets of data. The programming language R used in this study is less stable compared to these two when handling huge sets of data.

7. Conclusions and discussions

Normality

As mentioned in chapter 5, the Pearson's Correlation method should be applied between two numeric variables if the two are normally distributed (Mukaka, 2012). Some statisticians do suggest that at least one variable should be normally distributed (Sedgwick, 2012). A normality test therefore needs to be conducted before using the method. The normal/Gaussian distribution is a continuous distribution of data that has a normal curve, Figure 7.1. Some important characteristics of a normal curve are: the curve is bell shaped, it is symmetric at the centre (at around the average), the area under an entire normal curve is 1, the average, median and mode are all equal (PennState Eberly College of Science, 2018). The Shapiro-Wilk test, one of the main tests for assessing normality, was used to assess the normality of time series used in this study. This test has been found to be the most powerful test in most situations and is highly recommended (NCSS Statistical Software, 2016; Ghasemi & Zahediasl, 2012). The test is based on the correlation between the data and the corresponding normal scores (Ghasemi & Zahediasl, 2012).

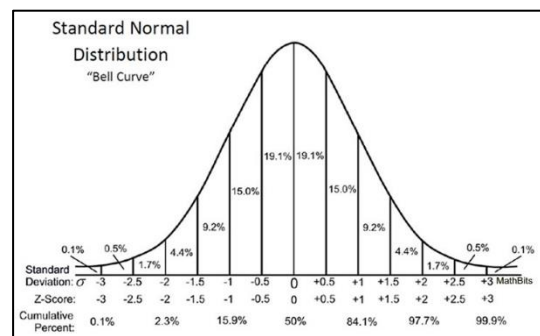


Figure 441 A representation of normal distribution (MathBitsNotebook, 2018)

$$W = \frac{(\sum_{i=1}^n a_i x_{(i)})^2}{\sum_{i=1}^n (x_i - \bar{x})^2}$$

Equation 6 Shapiro-Wilk test equation

Where: W =the correlation between given data and ideal normal scores, a_i = specific constants for each i th order statistic, x_i = ordered values and \bar{x} = sample mean. The numerator is proportional to the square of the best linear estimator of the standard deviation whereas the denominator is the sum of squares of the observations about the sample mean (NCSS Statistical Software, 2016). Apart from W , a probability value (significances of the test) also gets calculated. A null and alternative hypothesis was used to test the normality of the vertical deformation and water level time series using the Shapiro-Wilk test:

H_0 : the observed distribution fits the normal distribution

H_a : the observed distribution does not fit the normal distribution

If the probability (p) value is greater than 0.05 that implies that the data is normally distributed. If it is less than 0.05 that implies that the data is not normally distributed. Table 24 shows the probability values of deformation and water level time series pairs from the study area of Brittaniëhaven and 7e Petroleumhaven (7e PH) after a normality test was conducted. The p values highlighted in light green represent the variables for which the H_0 hypothesis was accepted while the ones highlighted in light red represent the variables for which the H_0 hypothesis got rejected. Normality tests were also conducted for the rest of the study areas and the results are similar to the ones in table 24; some time series are normally distributed and some are not. Furthermore, there is no clear trend on how the probability values differ from each other.

Table 24 Probability(p) values Brittaniëhaven and 7e PH

Year	Deformation (Desc PS) time series	Water level time series
2010-2013	0.01	0.00
2010	0.87	0.02
2011	0.89	0.75
2012	0.29	0.01
2013	0.02	0.02

7. Conclusions and discussions

Spearman vs Pearson

Spearman's Correlation coefficient has similar properties to Pearson's Correlation coefficient. It is calculated if none of the variables being considered is normally distributed, or if one of the variables is discrete or was measured on an ordinal scale (Sedgwick, 2012). Spearman's Correlation, a non-parametric (distribution free) measure, assesses how well the relationship between two variables can be described based on ranks using a monotonic function whereas the Pearson's correlation, a parametric measure, describes how well a relationship between variables exists using a linear function (Rebekić et al., 2015). Spearman's Correlation assesses how

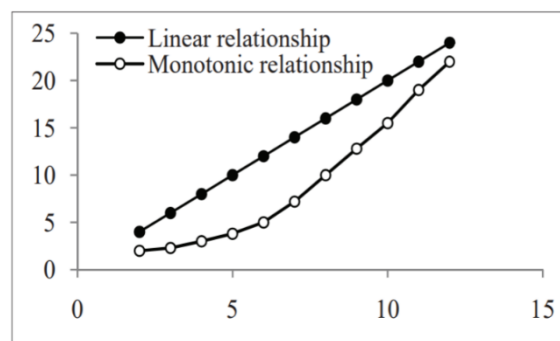


Figure 472 Linear and monotonic relationship (Rebekić et al., 2015)

well an arbitrary monotonic function can describe the relationship between two variables, without making any assumptions about the frequency distribution of the variable (Hauke & Kossowski, 2011; Rebekić et al., 2015). The method is powerful for mixed normal and non-normal distributions and is more powerful than Pearson's r in the context of non-normality (Bishara & Hittner, 2012). One of the limitations of Spearman's Correlation is that it should be used when sample sizes exceed 30.

Table 25 Number of observations Brittaniëhaven

Years	Ascending	Descending
All Years	96	121
2010	25	28
2011	27	32
2012	22	30
2013	21	30

Using table 24 as an example, it would be inefficient to use two kinds of correlations (Spearman and Pearson) based on the normality or non-normality and also based on number of observations. Table 25 shows how the number of observations for averaged deformation and water level time series from Brittaniëhaven differ from each other. Time series from the other study areas show similar patterns. Tables 26 and 27 show comparison of Spearman's and Pearson's Correlation coefficients calculated for averaged deformation time series and water level time series, regardless of the normality/non-normality or number of observations. Comparisons in table 24 do not show major differences but this is not the case in table 25. Most of the Spearman's Correlation coefficients are considerably lower than Pearson's and this would lead to the change of classification of the coefficients (rule of thumb in table 4). Both Spearman's and Pearson's correlation coefficients in the two tables are however mostly low or negligible.

Table 26 Spearman's vs Pearson's Correlation coefficients Brittaniëhaven and 7e PH (using Asc PS time series)

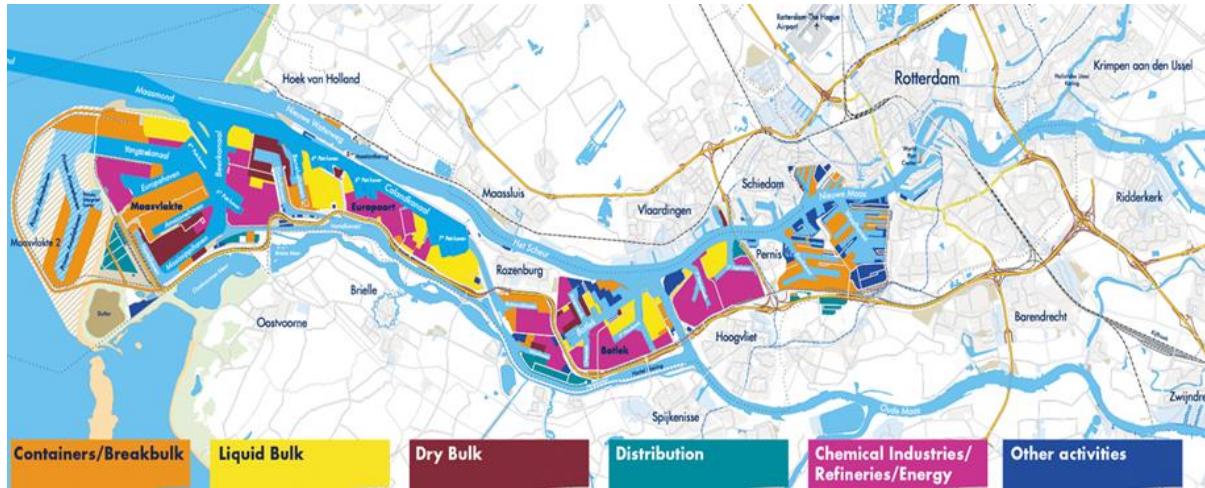
Year	Spearman's Correlation	Pearson's Correlation
2010-2013	-0.02	0.00
2010	0.09	0.10
2011	-0.36	-0.36
2012	-0.06	-0.02
2013	0.05	-0.01

Table 27 Spearman's vs Pearson's Correlation coefficients Brittaniëhaven and 7e PH (using Desc PS time series)

Year	Spearman's Correlation	Pearson's Correlation
2010-2013	-0.25	-0.31
2010	-0.47	-0.50
2011	-0.35	-0.31
2012	-0.21	-0.31
2013	-0.43	-0.53

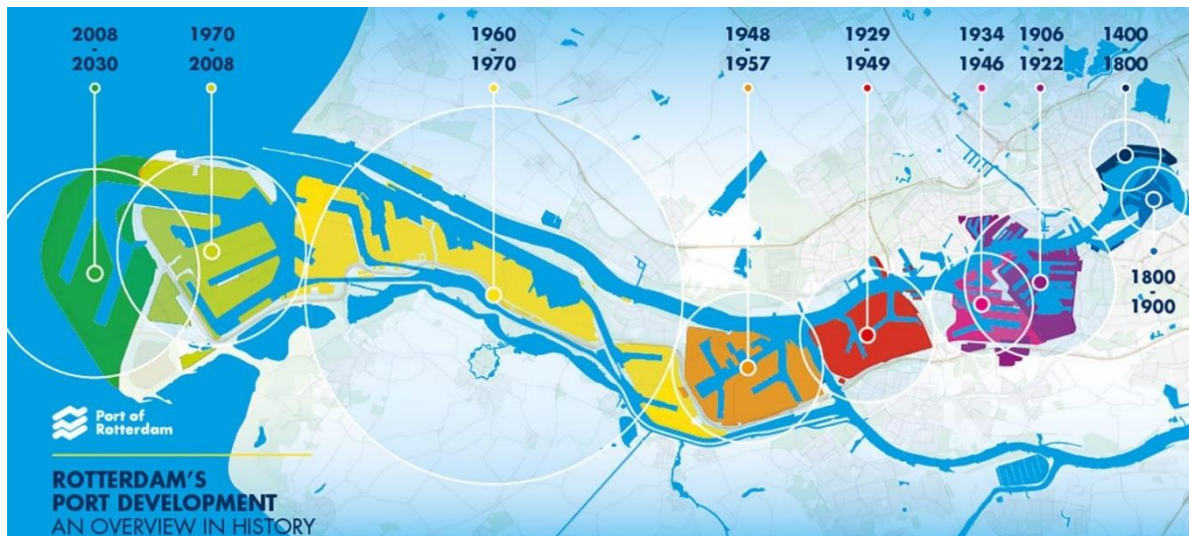
Appendices

Appendix I: Port of Rotterdam cargo handling/industries at the harbours



(Sanchez, 2015)

Appendix II: Port of Rotterdam development over the years

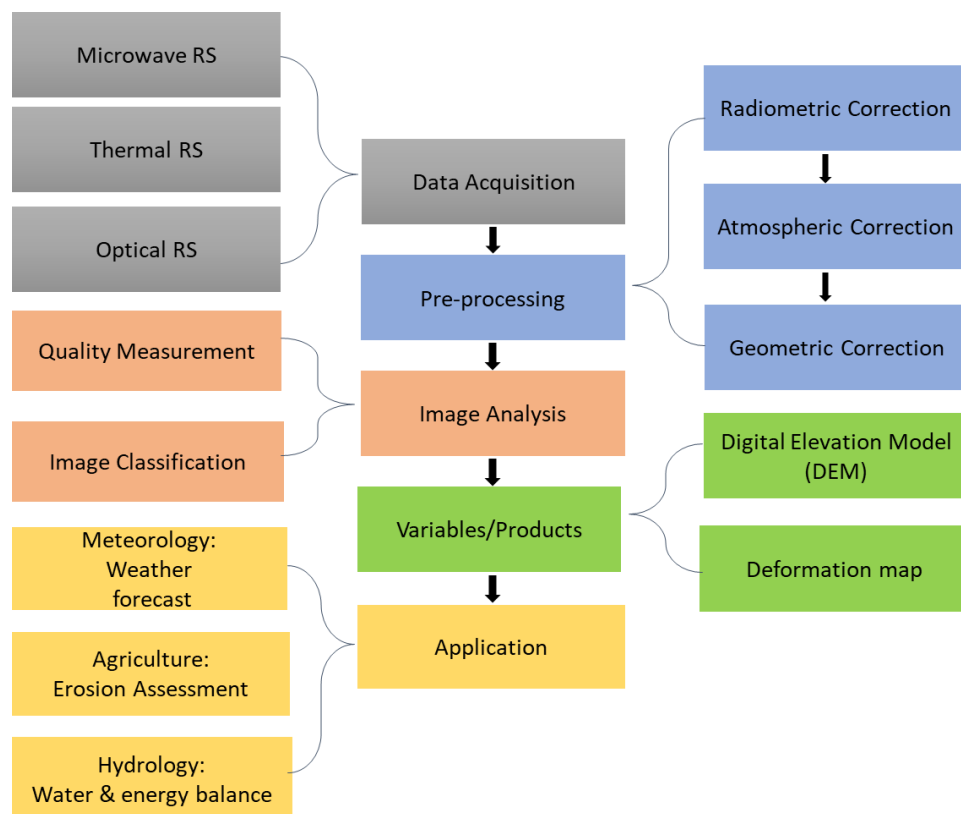


(The Port of Rotterdam, 2018)

Appendix III: Image pre-processing

After data is received from a satellite, it needs to go through several pre-processing steps before it can be analysed. Pre-processing operations, also referred to as image restoration and rectification, are meant to improve image quality and function as a basis for further analysis by rectifying certain distortions (Kooistra, 2018; Lamont-Doherty Earth Observatory, 1998). Most pre-processing algorithms are designed to handle the specific dataset they are being run on and to the final application of the image. These algorithms however follow the same general ideas; correcting for any distortion due to imaging conditions and imaging system (generally radiometric, atmospheric and geometric effects) and then analysing the images for the specific application for which the data is being used (NASA Imageseer, 2015; CRISP, 2001). Depending on a user's requirement, certain correction procedures can be carried out by the ground stations before the data gets delivered to the end user (CRISP, 2001). Appendix IV shows a flow chart of the remote sensing chain and examples of each component of the chain. The middle section, adapted from (Kooistra, 2018), are the main steps in the chain whereas the examples within each step are on the sides. Table 27 gives a summary of the general remote sensing pre-processing steps; their functions and example causes of the distortions being corrected.

Appendix IV: Remote sensing chain



Mid-section adapted from (Kooistra, 2018).

Table 28 Basic pre-processing procedures in remote sensing

Pre-processing step (Correction type)	Function	Examples of distortion cause
Radiometric	Correct for uneven sensor response (irregularities) over the whole image (CRISP, 2001)	Variations in scene illumination and viewing geometry of the satellite, atmospheric conditions, sensor noise and response (Natural Resources Canada, 2015).
Atmospheric	Compensate for effects of selectivity scattered light (Lamont-Doherty Earth Observatory, 1998)	Scattering caused by air molecules (gasses), aerosol particles, dust, smoke and rain (Kooistra, 2018)
Geometric	Correct spatial distortions in image (Lamont-Doherty Earth Observatory, 1998)	Curvature of the Earth, terrain topography, Earth rotation under the sensor during image acquisition, panoramic distortion due to the sensor's field of view (Kooistra, 2018).

Appendix V: InSAR systems and characteristics

Sensor	Repeat cycle (days)	Wavelength (cm)	Resolution (m) (azimuth x ground range)		Look angle
ALOS/PALSAR	46	23.62 cm	Fine mode 1	**10m x (7-44m)	8°-60°
			Fine mode 2	**10m x (14-88m)	
			*PL mode	**10m x (24-89)m	8°-30°
			*SC mode	100m x 100m	18°-43°
COSMO/SkyMed	16	3.125cm	*SL mode	<1m	>25°-50°
			*SM mode	<3 -15m	>25°-50°
			*SC mode	< 30-100m	>25°-50°
Envisat/ASAR	35	5.63 cm	Image mode	#30m x 30m	15°-45°
			*AP mode	#30m x 30m	15°-45°
			*WS mode	150m x 150m	17°-42°
			Wave mode	10m x 10m	15°-45°
			*GM mode	1km x 1km	17°-42°
ERS-1	3, 35, 168	5.66 cm	30m x 30m		20°-26°
ERS-2	35	5.66 cm	30m x 30m		20°-26°
JERS-1	44	33.53cm	18m x 18m		35°
RADARSAT-1	24	5.66 cm	Fine mode	9m x (8,9)m	37°-47°
			Standard mode	28m x (21-27)m	20°-49°
			Wide mode	28m x (23,27,35)m	20°-45°
			*SC narrow mode	50m x 50m	20°-49°
			*SC wide mode	100m x 100m	20°-49°
			Extended H mode	28m x 25m	52°-58°
			Extended L mode	28m x 25m	10°-22°
RADARSAT-2	24	5.55 cm	Ultra-fine mode	3m x 3m	30°-49°
			Multi-look fine mode	8m x 8m	30°-50°
			Fine mode	8m x 8m	30°-50°
			Standard mode	26m x 25m	20°-49°
			Wide mode	26m x 30m	20°-45°
			*SC narrow mode	50m x 50m	20°-46°
			*SC wide mode	100m x 100m	20°-49°
			Extended H mode	26m x 18m	49°-60°
			*Fine QP mode	8m x 12m	20°-41°
			*Standard QP mode	8m x 25m	20°-41°
Seasat	3	23.44 cm	25m x 25m		20°-26°
SIR-C/X-SAR		23.5cm 5.8cm 3.1cm	(10-50)m - variable		(20°-65°) - variable
TerraSAR-X	11	3.125cm	*SL mode	2m x (1.5-3.5)m	20°-55°
			*HR SL mode	1m x (1.5-3.5)m	20°-55°
			*SM mode	3m x (3-6)m	20°-45°
			*SC mode	16m x 16m	20°-45°

* PL – polarimetric; SC – ScanSAR; SL – spotlight; SM – stripmap; AP - alternating polarization; WS - wide swath; GM - global monitoring; QP = quad polarization; HR – high resolution;

** The azimuth resolution of 10 m is for two looks.

Resolution (azimuth x ground range) for image mode single look complex images is 6 m x 9 m; for alternating polarization single look complex images is 12 m x 9 m.

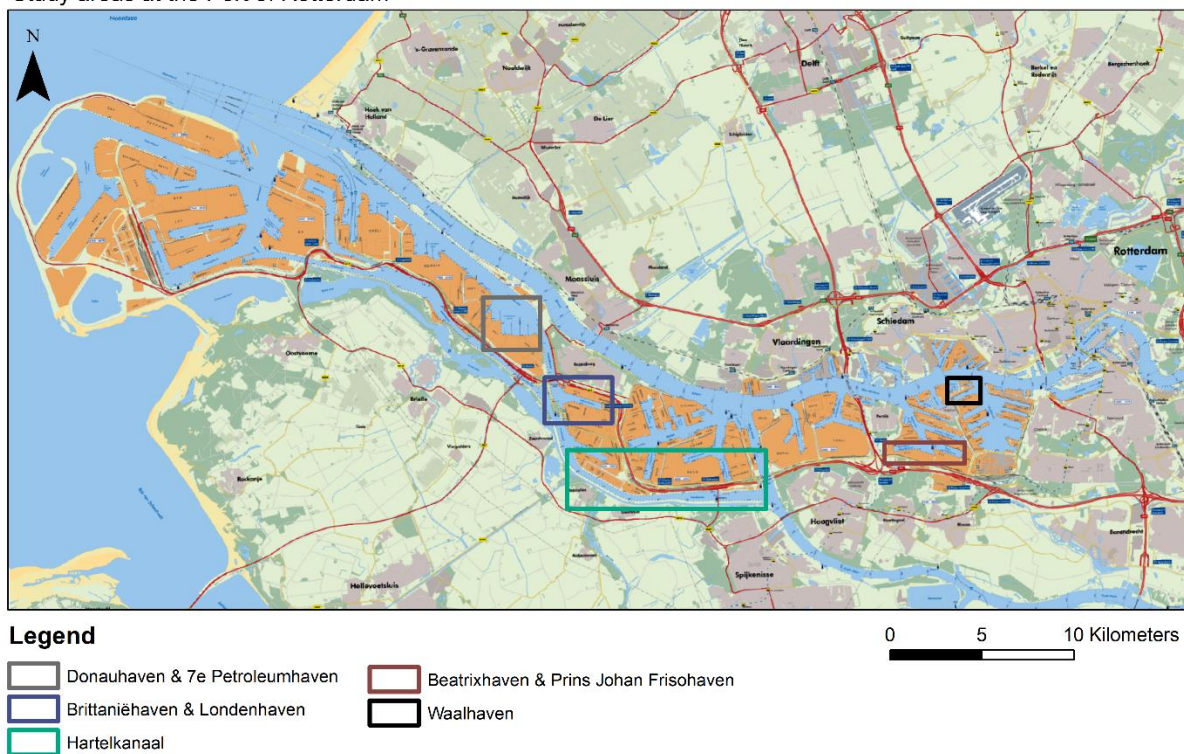
(Zhou, Chang, & Li, 2009)

Appendix VI: Applications of InSAR in different disciplines

Field/ Discipline	Monitoring applications
Geomorphology	Slow slope movements, land subsidence/uplift, erosion and depositions (Smith, 2002; Zhou, Chang, & Li, 2009).
Hydrology	Land uplift due to ground water recharge, land subsidence due to excess water extraction, soil moisture (difference), (river) inundation extent, water level change, snow cover extent and scattering properties, river ice deformation (Smith, 2002; Zhou, Chang, & Li, 2009).
Seismology	Land deformation due to earthquakes; post seismic relaxation of the lithosphere (Zhou, Chang, & Li, 2009).
Volcanology	Volcanic processes such as magma accumulation, transport and emplacement beneath volcanic structures (Zhou, Chang, & Li, 2009).
Glaciology	Glacier flow, ice sheet movement and deformation, postglacial rebound of the lithosphere (Zhou, Chang, & Li, 2009).
Cultural heritage studies	Monitoring of: sites, monuments, slow and/or rapid deformation caused by human activities, long-term environmental influences and natural disasters (Zhou, Chen, & Guo , 2017).
Forestry	Forest mapping and monitoring, canopy height (Zhou, Chang, & Li, 2009).
Mining	Land subsidence due to mining
Structural and environmental Engineering	Structural stability and ground subsidence (Zhou, Chang, & Li, 2009).
Natural disaster monitoring and assessment	Volcanoes and landslide movement (Zhou, Chang, & Li, 2009).

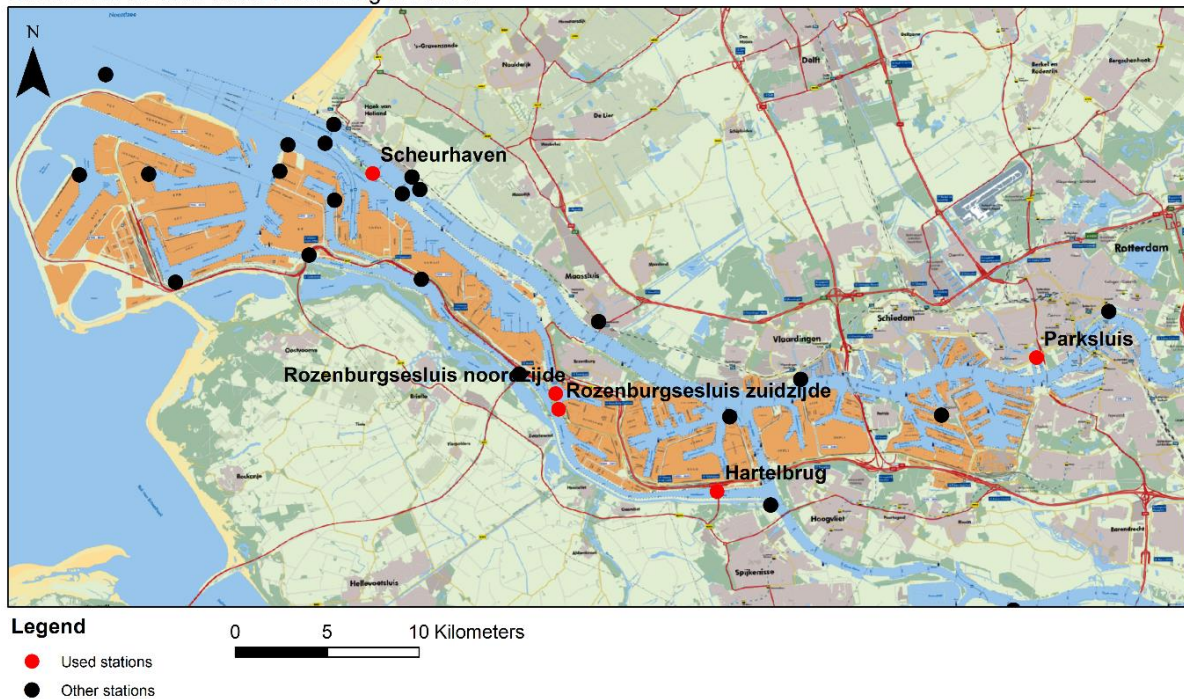
Appendix VII: Study areas at the Port of Rotterdam

Study areas at the Port of Rotterdam

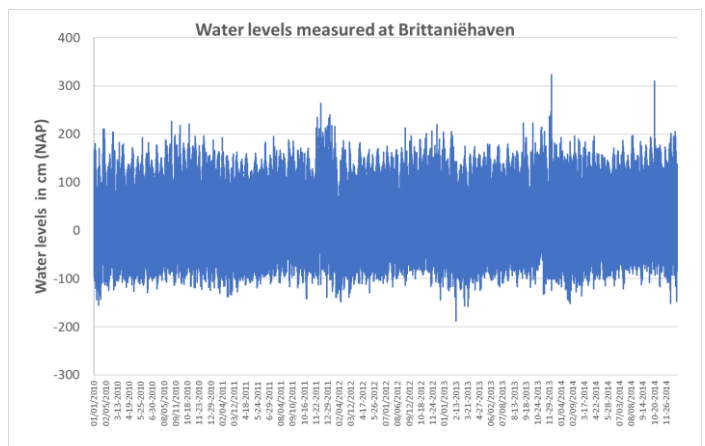
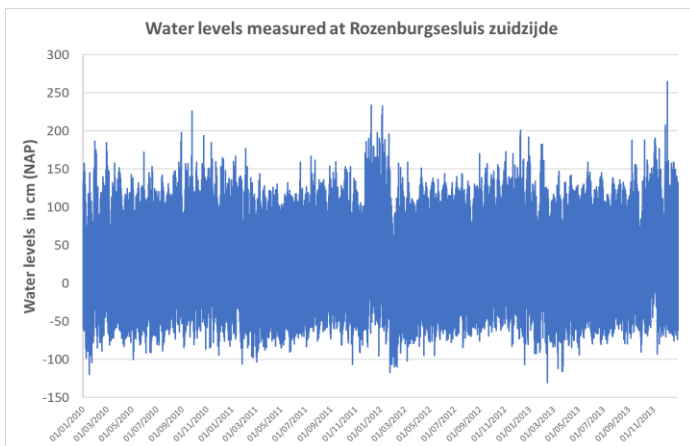
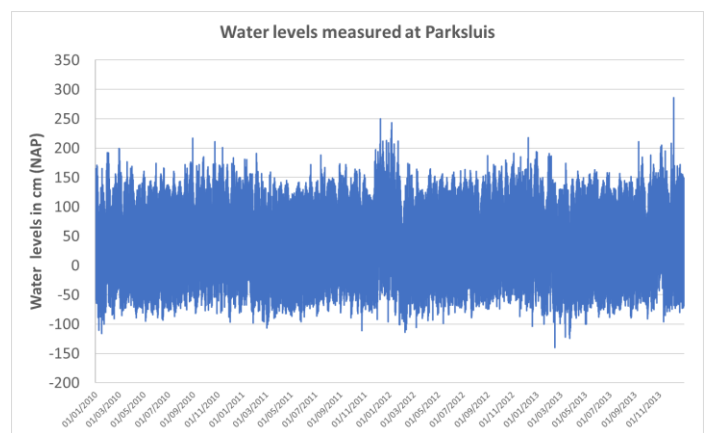
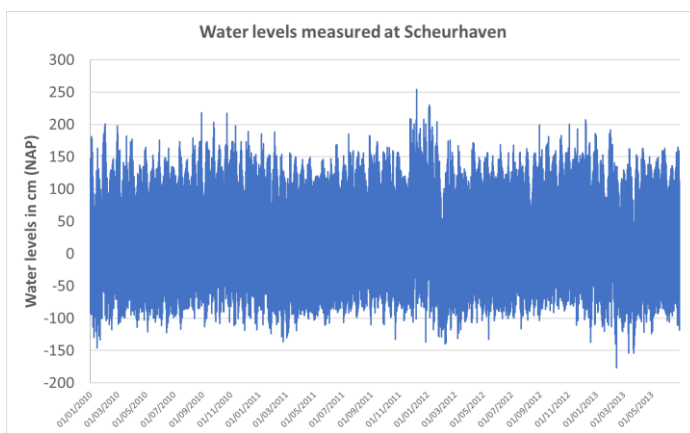
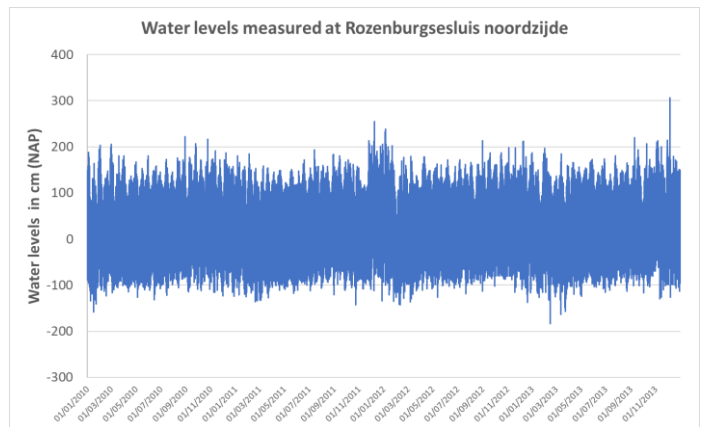
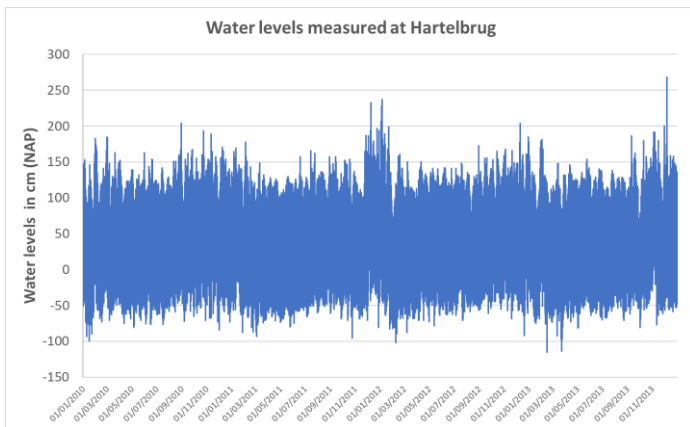


Appendix VIII: Surface water measuring locations in the project area

Location of surface water measuring locations



Appendix IX: Measured surface water levels



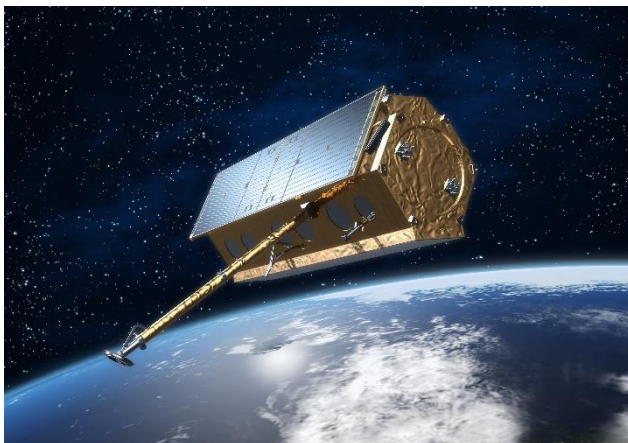
Appendix X: TerraSAR-X

The TerraSAR-X is a German Earth observation satellite that got launched in June 2007 and started its operational service in January 2008. The satellite is a joint venture carried out under a public-private partnership between the Deutsches Zentrum für Luft- und Raumfahrt, DLR (German Aerospace Centre) and EADS Astrium GmbH. In collaboration with the space agency Airbus Defence and Space, four institutes under DLR are responsible for controlling the satellite, planning and implementing the current mission as well as using the satellite's data for scientific purposes. The EADS Astrium GmbH is a private company that works as a subsidiary of Airbus S and is based in Taufkirchen, Germany. It designs, develops and manufactures satellites. EADS Astrium GmbH developed, built and launched the satellite (Airbus Defence and Space, 2018; DLR, 2014)

The satellite acquires high-resolution and wide-area radar images regardless of the weather conditions, cloud cover or absence of light (Airbus Defence and Space, 2018; DLR, 2014). Together with the TanDEM-X, it has a unique geometric accuracy that can be compared to another spaceborne sensor/ satellite. Since June 2018, the TanDEM-X together with TerraSAR-X has been collecting data for a global elevation model. Apart from the unique geometric accuracy, the main advantages of TerraSAR-X include;

- Excellent radiometric accuracy
- Easy and quick access due to a comprehensive network of ground stations and very flexible ordering options
- Flexible coverage for large areas and very high resolution for specific target areas. (Airbus Defence and Space, 2018)

TerraSAR-X serves a wide range of global markets since it is specifically optimised to meet the requirements of users; providing readily available high-quality and precise Earth observation data (Airbus Defence and Space, 2018). The objective of the satellites mission was to deliver value added SAR data in the X band for scientific and commercial applications, as well as development and research purposes (DLR, 2014). TerraSAR-X data in the fields such as; aviation, maritime monitoring, intelligence and defence, public safety, forestry, agriculture, civil engineering and land administration (Airbus Defence and Space, 2018).

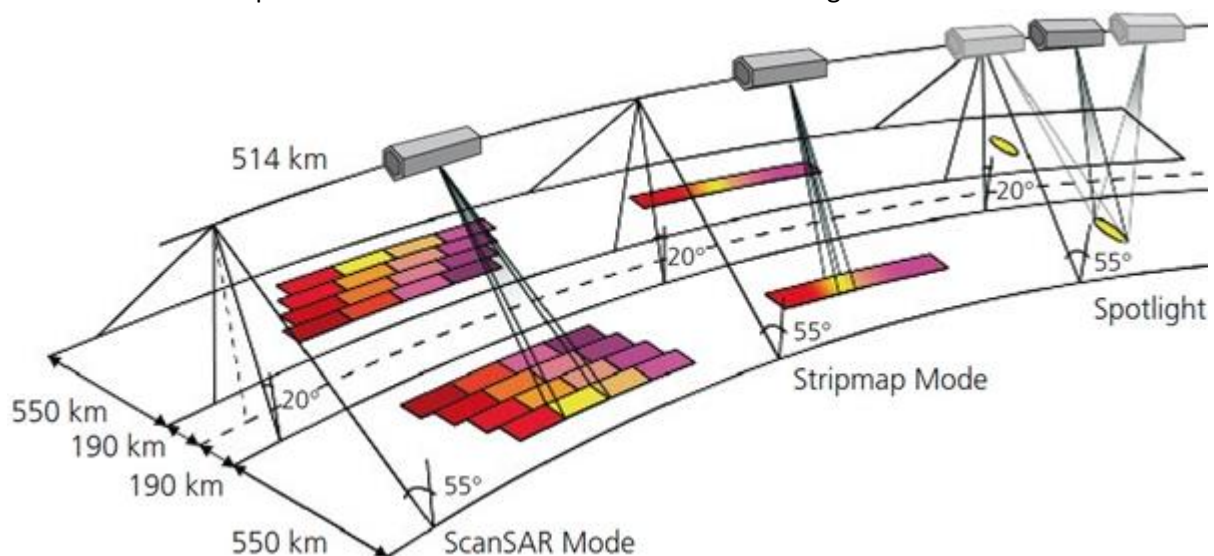


TerraSAR-X in Space (Airbus Defence and Space, 2018)

At an altitude of 514 kilometres, the satellite has a sensor with several modes of operation, enabling it to record images with different *polarisations*, *swath width* and resolutions. It is 4.9 meters long and 2.4 meters wide (DLR, 2014).

A radar sensor needs to have a resolution of one meter or better in order to represent objects that are one meter apart as separate pixels in an image. This means that TerraSAR-X would need an antenna of at least 15 kilometres in length yet the actual antenna is only five metres long. To achieve this performance, a special technique is applied in SAR satellites. The technique employs the fact that the antenna moves past the targets along the orbit of the satellite, transmitting signals at regular intervals and capturing the echoes. The echoes are first digitalised and stored on board the satellite. The recorded data is then transmitted to the DLR ground station in Germany, where the signals undergo extensive computer processing in which they are treated as if they originated from a large number of separate TerraSAR-X antennas distributed along the satellite's orbital path. By applying this computational process known as 'aperture synthesis', the virtual separate antennas are linked together to form a large 'synthetic antenna' of up to 15 kilometres in length. The result is then exactly the same as it would have been if a long antenna of 15 kilometres had really been used (DLR, 2011).

TerraSAR-X sensor operates in three different modes shown in the figure below



Modes of operation utilised by TerraSAR-X (DLR, 2011)

- ScanSAR mode: a strip of 100 kilometre is captured at a resolution of 16 meters.
- Stripmap mode: a strip of 30 kilometre is captured at a resolution between 3 and 6 metres
- Spotlight mode: 10 kilometres long and 10 kilometres wide area is recorded at a resolution of 1 to 2 metres.

(DLR, 2011)

Appendix XI: Deformation points at study areas

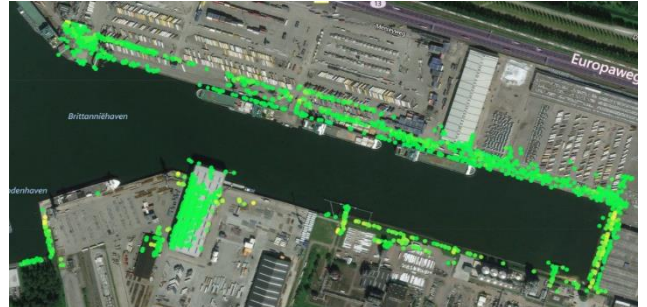
Vertical Ascending PS

Vertical Descending PS

Donauhaven and 7e Petroleumhaven



Brittaniëhaven and Londenhaven



Hartelkanaal



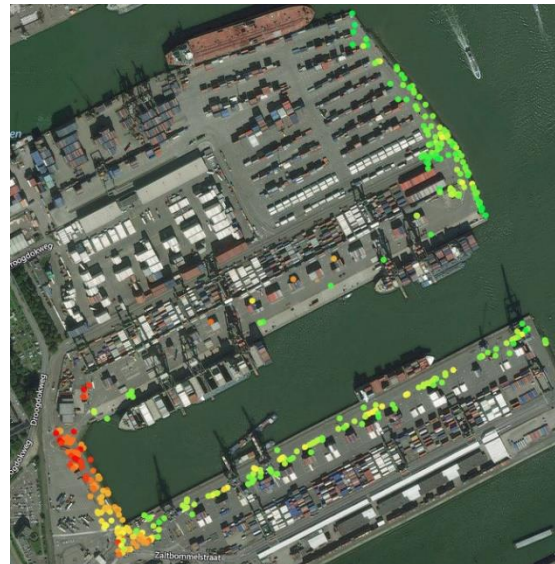
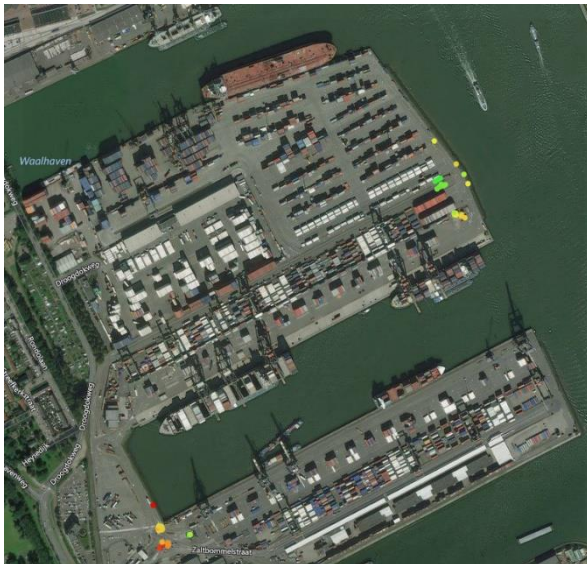
Ascending PS

Descending PS

Prins Beatrixhaven and Prins Johan Friso haven



Waalhaven

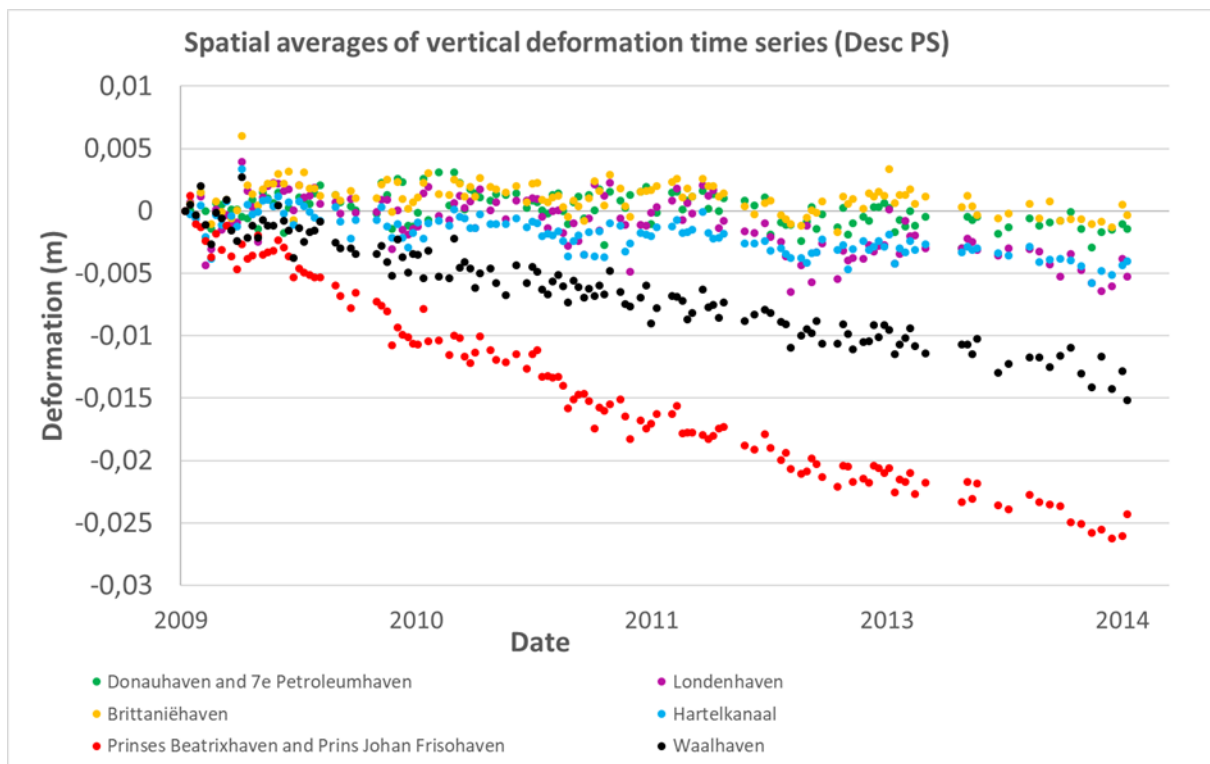
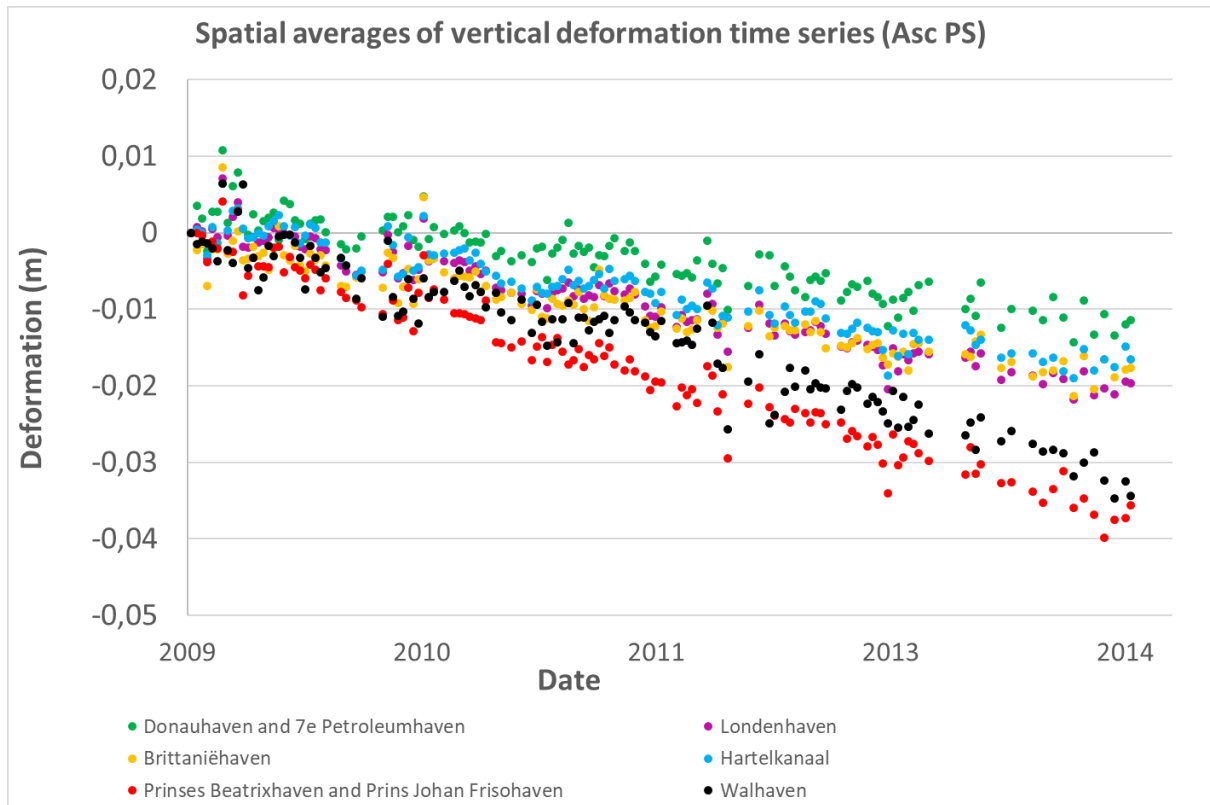


Appendix XII: Acquisition times TerraSAR-X (2009-2010)

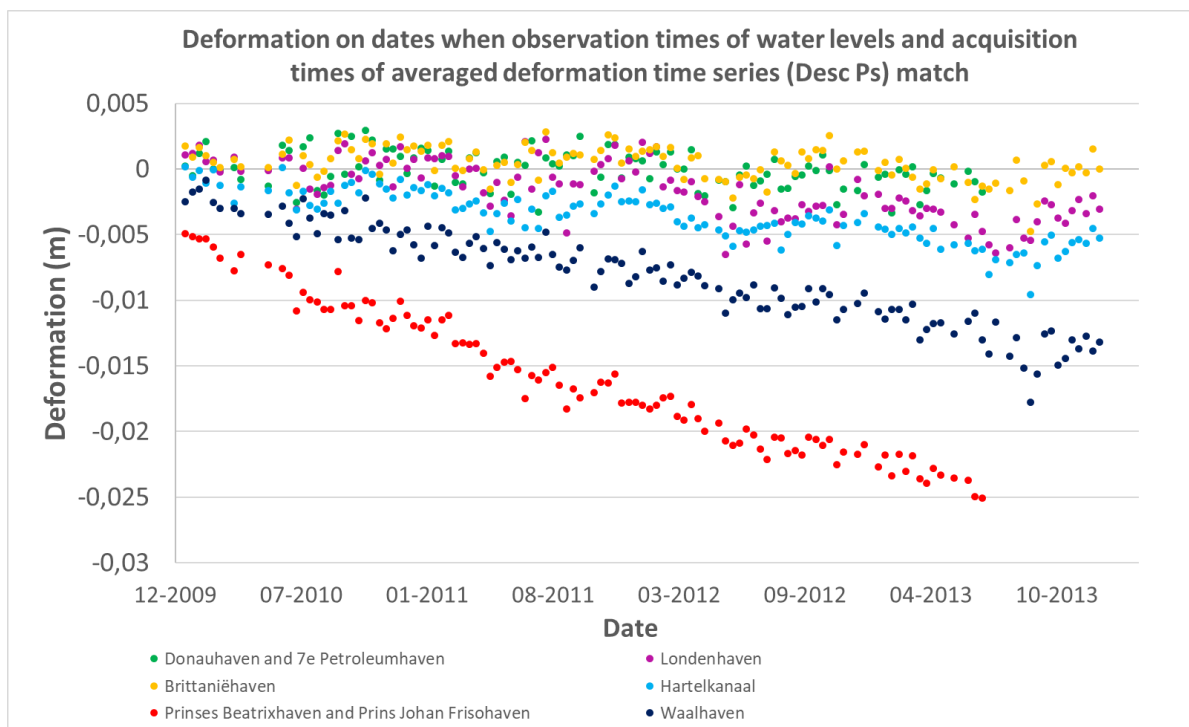
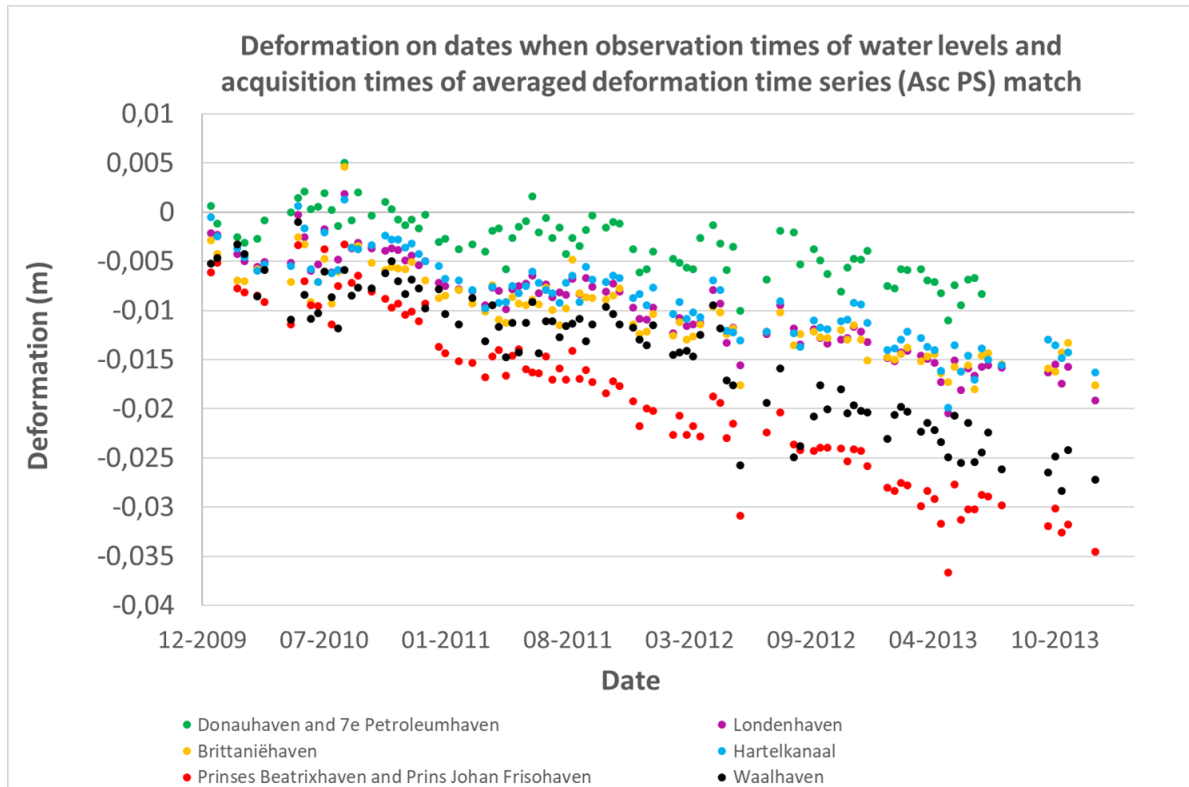
Acquisition Times Ascending Orbit	
6 Apr 2009	17:26:42
17 Apr 2009	17:26:43
28 Apr 2009	17:26:43
9 May 2009	17:26:43
20 May 2009	17:26:44
31 May 2009	17:26:44
11 Jun 2009	17:26:45
22 Jun 2009	17:26:45
3 Jul 2009	17:26:46
14 Jul 2009	17:26:46
25 Jul 2009	17:26:47
5 Aug 2009	17:26:48
16 Aug 2009	17:26:48
27 Aug 2009	17:26:49
7 Sep 2009	17:26:50
18 Sep 2009	17:26:50
29 Sep 2009	17:26:50
10 Oct 2009	17:26:51
21 Oct 2009	17:26:51
1 Nov 2009	17:26:51
12 Nov 2009	17:26:51
23 Nov 2009	17:26:50
4 Dec 2009	17:26:50
15 Dec 2009	17:26:49
26 Dec 2009	17:26:48
6 Jan 2010	17:26:47
17 Jan 2010	17:26:46
19 Feb 2010	17:26:46
2 Mar 2010	17:26:47
24 Mar 2010	17:26:48
4 Apr 2010	17:26:49
18 May 2010	17:26:50
29 May 2010	17:26:51
9 Jun 2010	17:26:51
20 Jun 2010	17:26:51
1 Jul 2010	17:26:51
12 Jul 2010	17:26:52
23 Jul 2010	17:26:52
3 Aug 2010	17:26:53
14 Aug 2010	17:26:54
25 Aug 2010	17:26:55
5 Sep 2010	17:26:55

Acquisition Times Descending Orbit	
8 April 2009	06:08:23
19 April 2009	06:08:24
30 April 2009	06:08:24
11 May 2009	06:08:25
22 May 2009	06:08:25
2 June 2009	06:08:26
24 June 2009	06:08:26
5 July 2009	06:08:27
16 July 2009	06:08:27
27 July 2009	06:08:28
7 August 2009	06:08:29
29 August 2009	06:08:30
9 September 2009	06:08:31
20 September 2009	06:08:31
1 October 2009	06:08:31
12 October 2009	06:08:32
23 October 2009	06:08:32
3 November 2009	06:08:32
14 November 2009	06:08:32
25 November 2009	06:08:31
6 December 2009	06:08:30
17 December 2009	06:08:30
28 December 2009	06:08:29
8 January 2010	06:08:28
19 January 2010	06:08:28
30 January 2010	06:08:27
10 February 2010	06:08:27
21 February 2010	06:08:28
4 March 2010	06:08:28
26 March 2010	06:08:28
6 April 2010	06:08:30
20 May 2010	06:08:32
11 June 2010	06:08:32
22 June 2010	06:08:32
3 July 2010	06:08:32
14 July 2010	06:08:33
25 July 2010	06:08:33
5 August 2010	06:08:35
16 August 2010	06:08:35
27 August 2010	06:08:36
7 September 2010	06:08:36
18 September 2010	06:08:37
29 September 2010	06:08:36
10 October 2010	06:08:37
21 October 2010	06:08:37
1 November 2010	06:08:37
12 November 2010	06:08:37

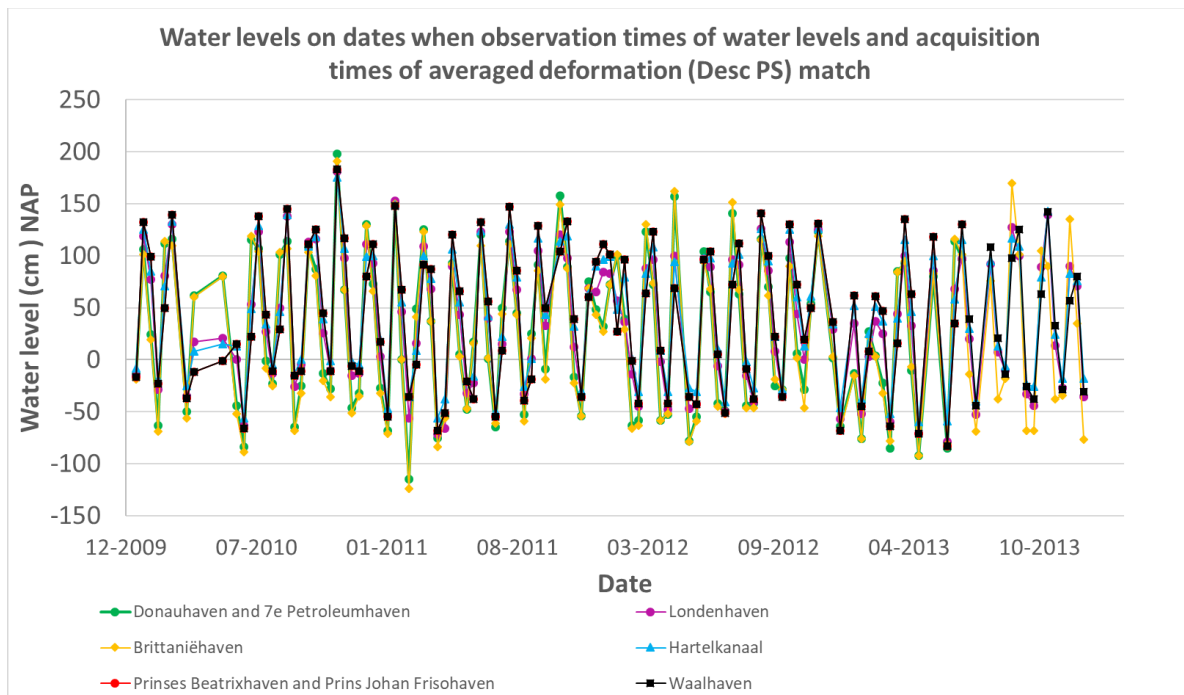
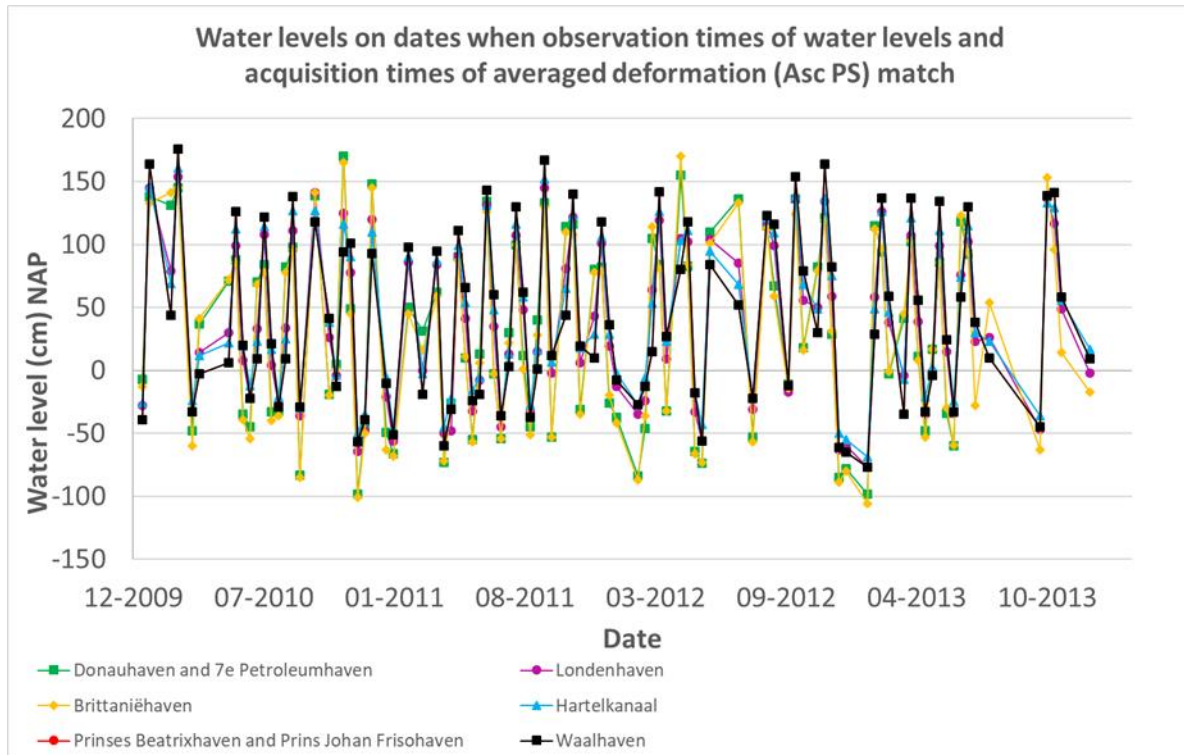
Appendix XIII: Spatial averages of vertical deformation time series



Appendix XIV: Vertical deformation on dates when connection with water levels were established

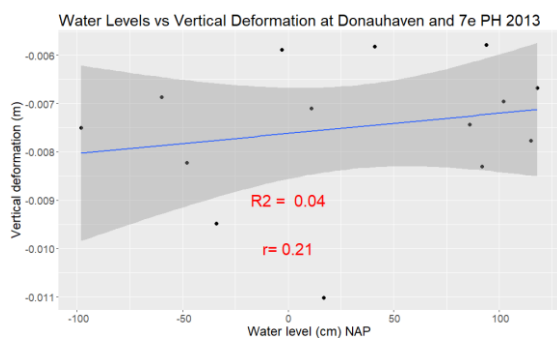
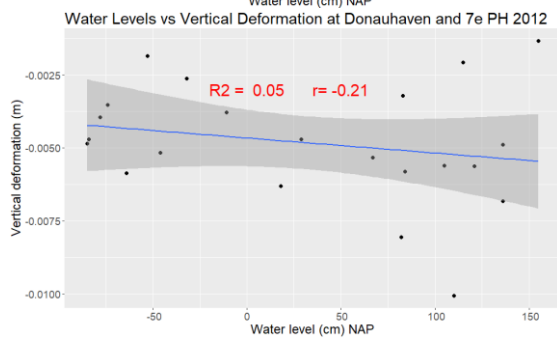
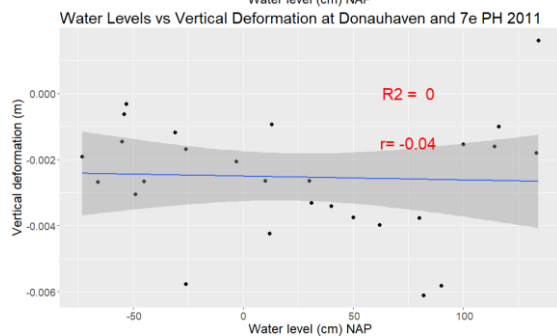
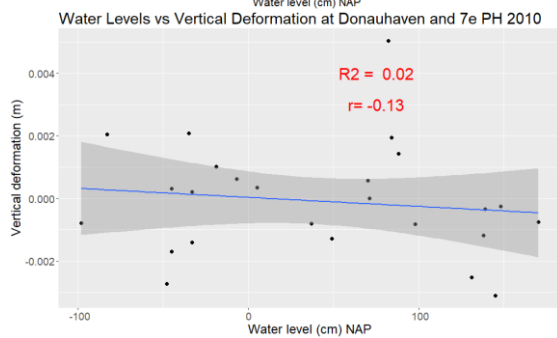
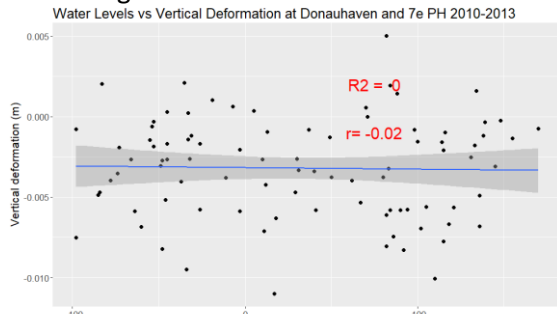


Appendix XV: Water levels on dates when connection with averaged deformation were established

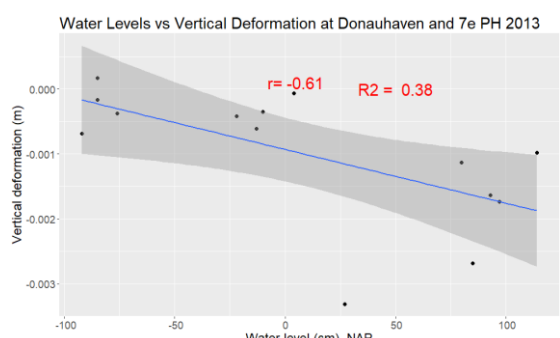
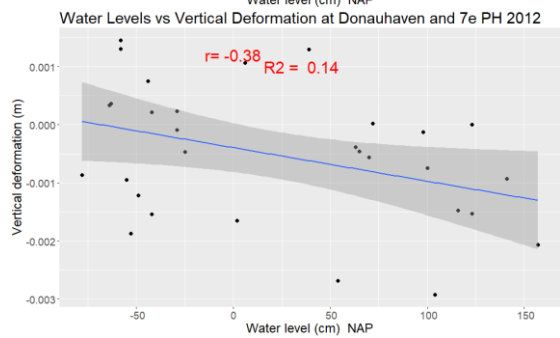
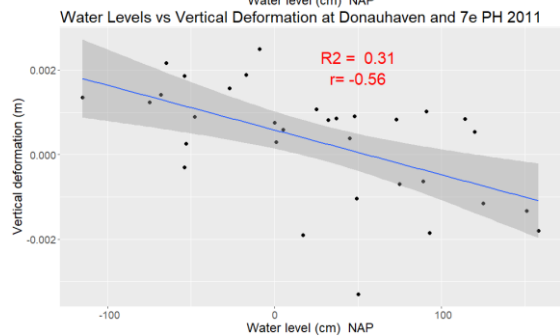
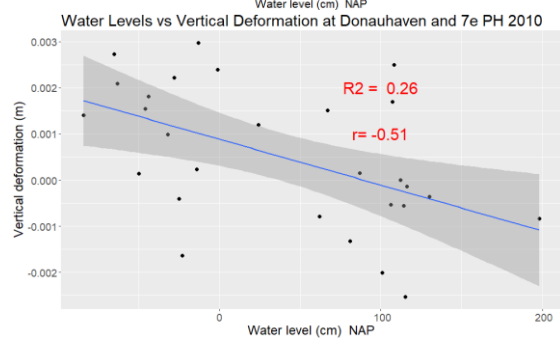
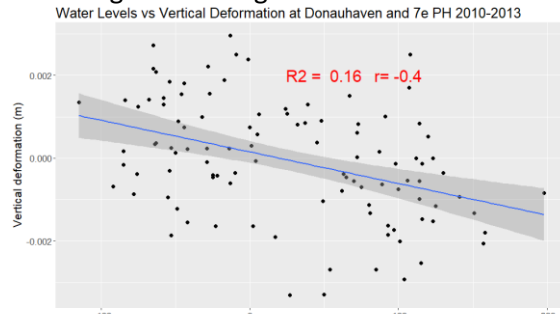


Appendix XVI: Results Donauhaven and 7e Petroleumhaven (7e PH); regression and correlation plots

Ascending PS time series

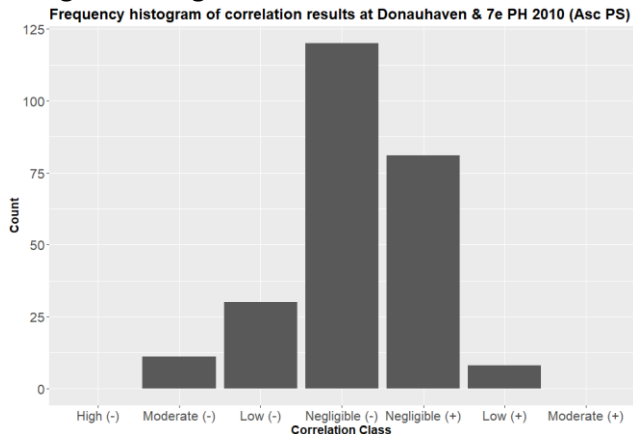


Using Descending time series

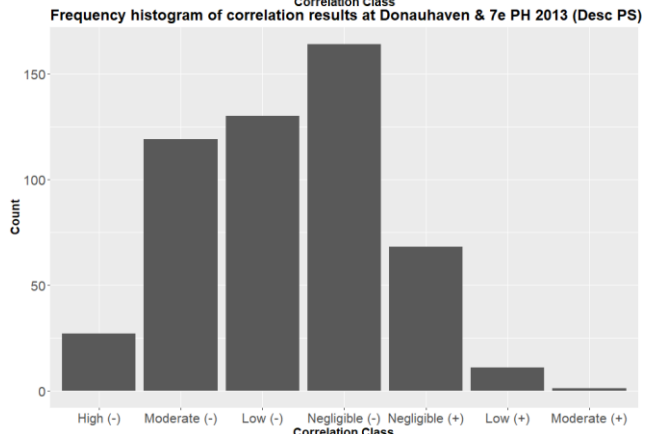
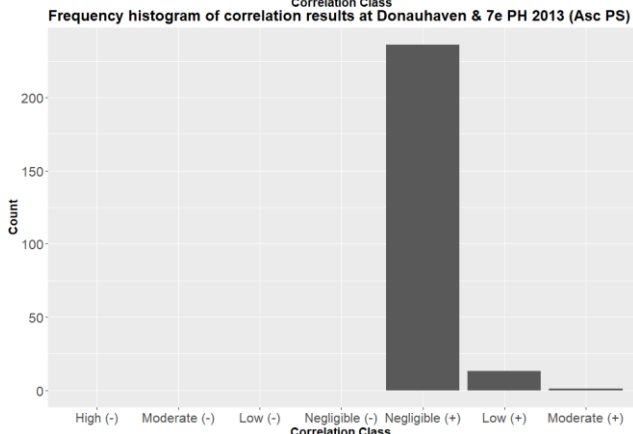
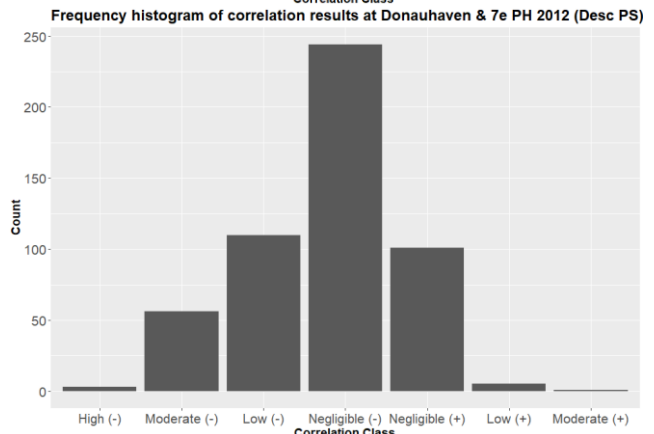
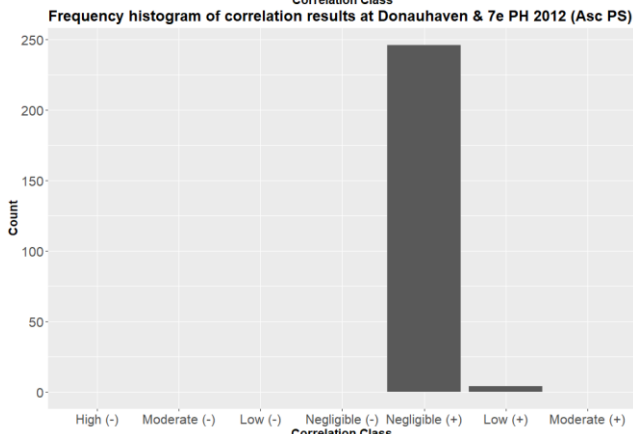
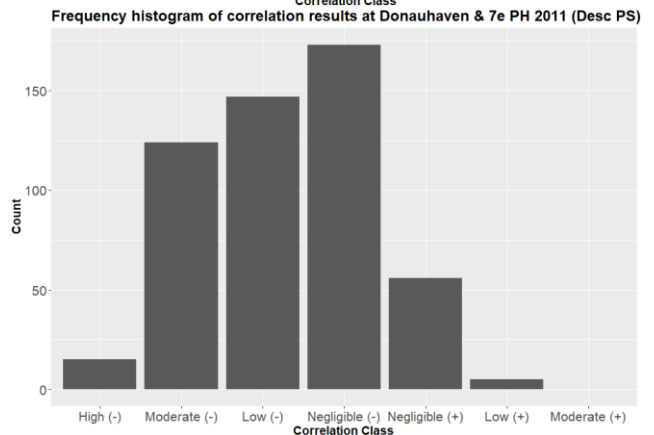
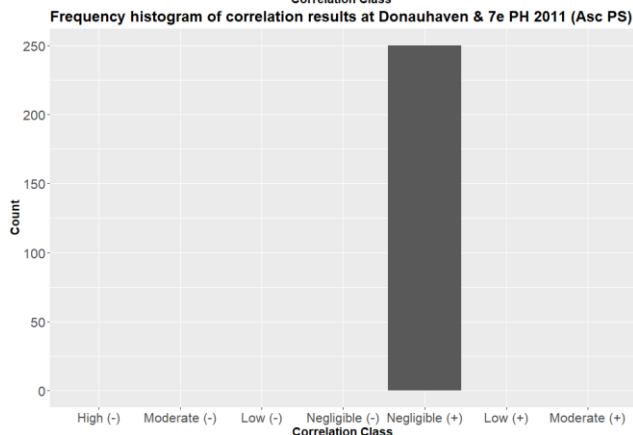
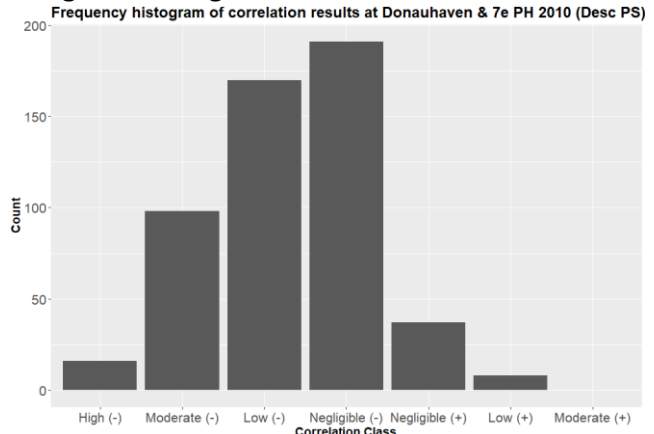


Appendix XVII: Frequency histograms Donauhaven and 7e Petroleumhaven

Using Ascending PS time series

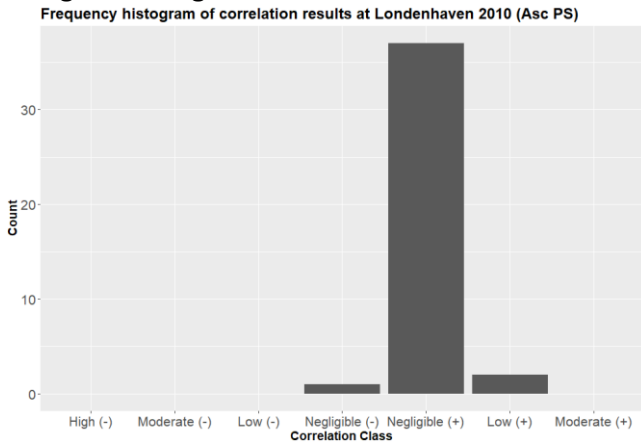


Using Descending PS time sires

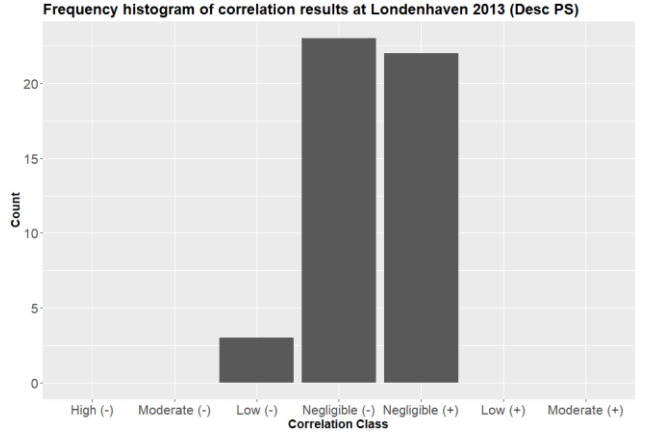
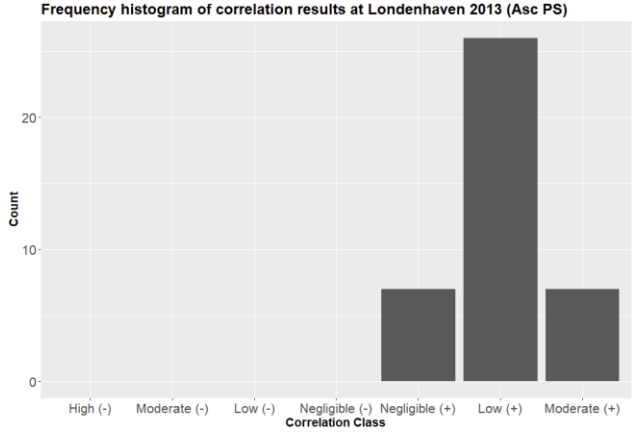
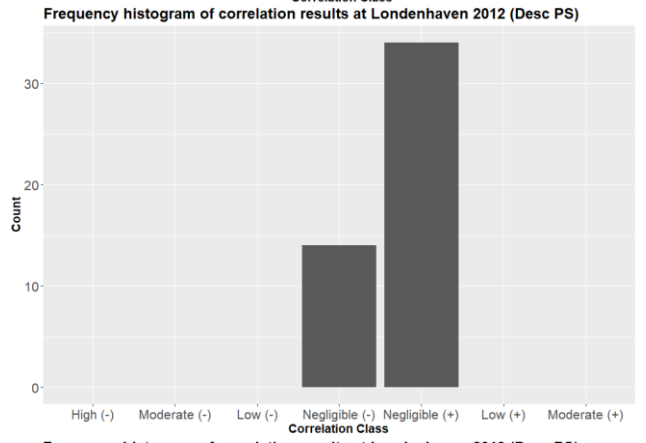
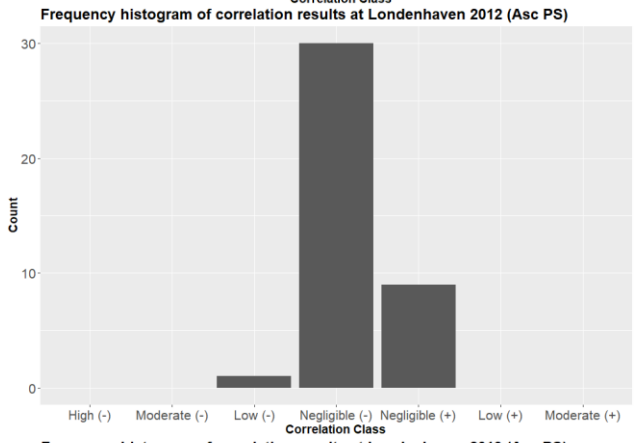
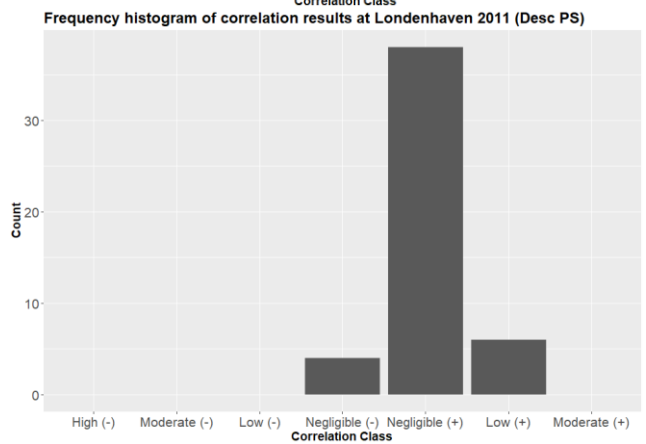
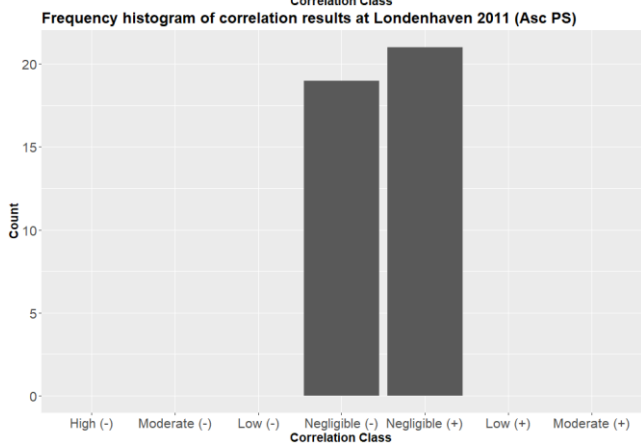
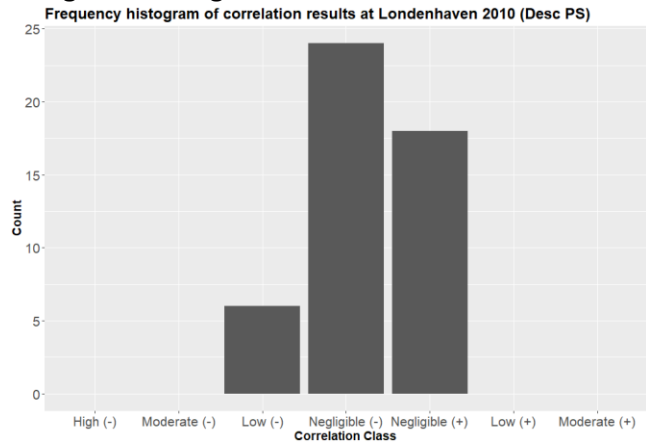


Appendix XVIII: Frequency histograms Londenhaven

Using Ascending PS time series

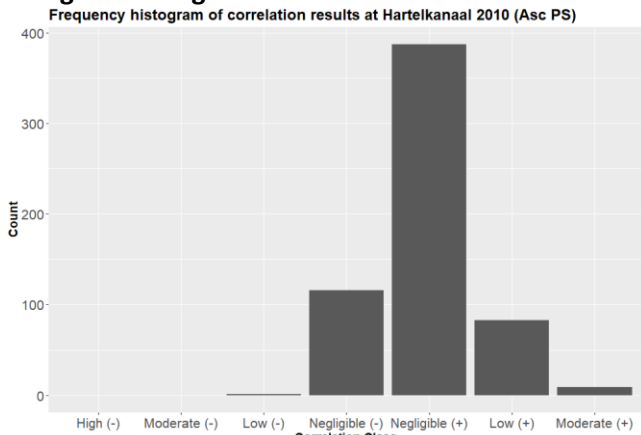


Using Descending PS time series

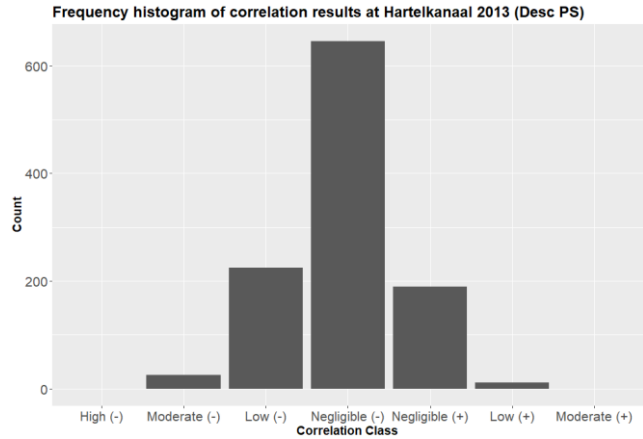
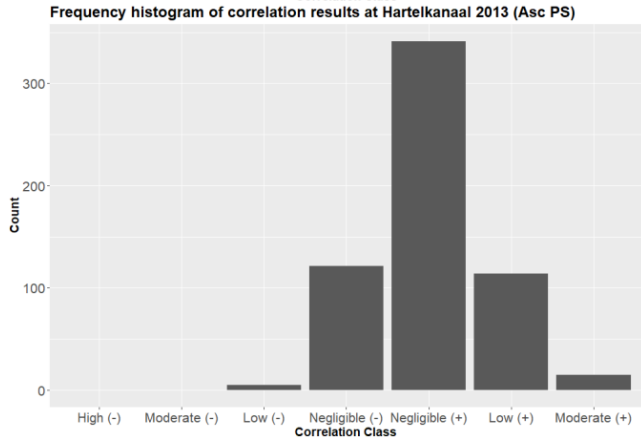
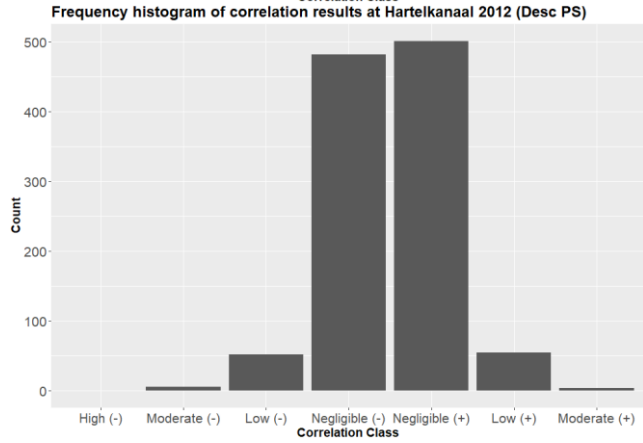
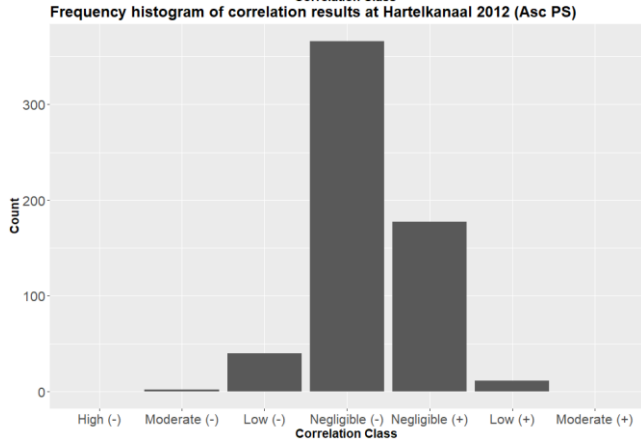
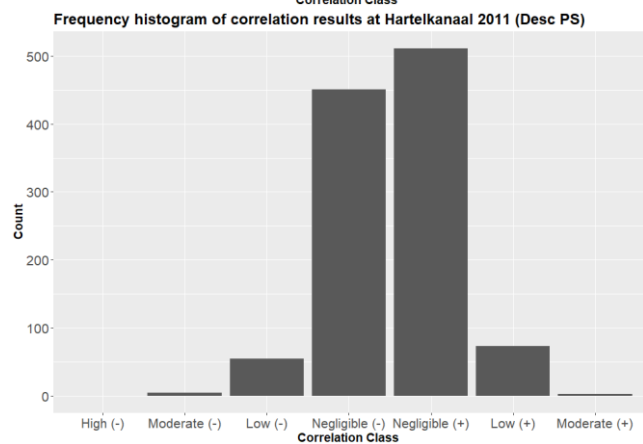
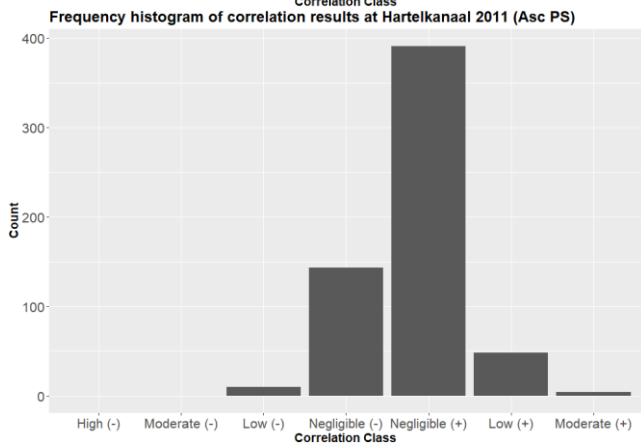
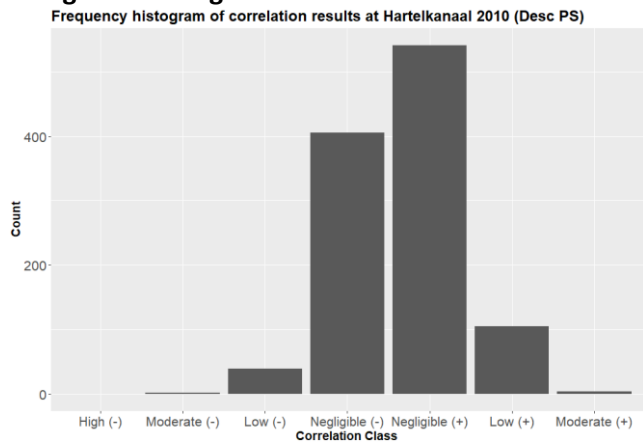


Appendix XIX: Frequency histograms Brittaniëhaven

Using Ascending PS time series

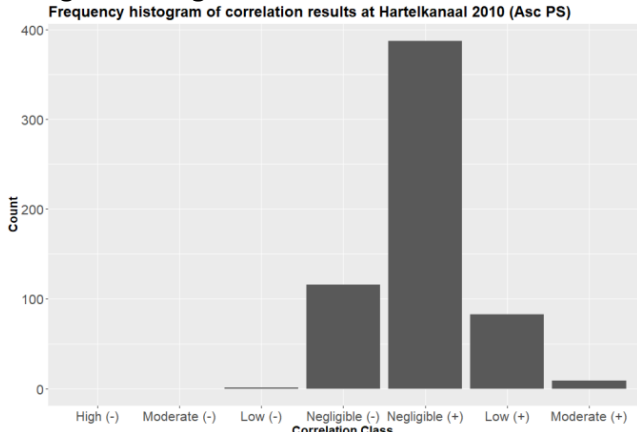


Using Descending PS time series

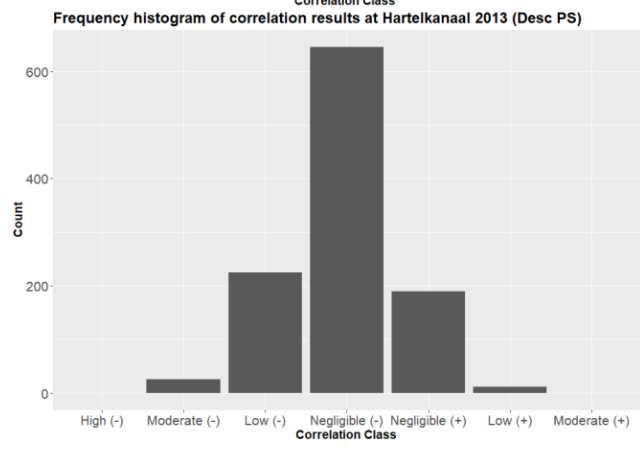
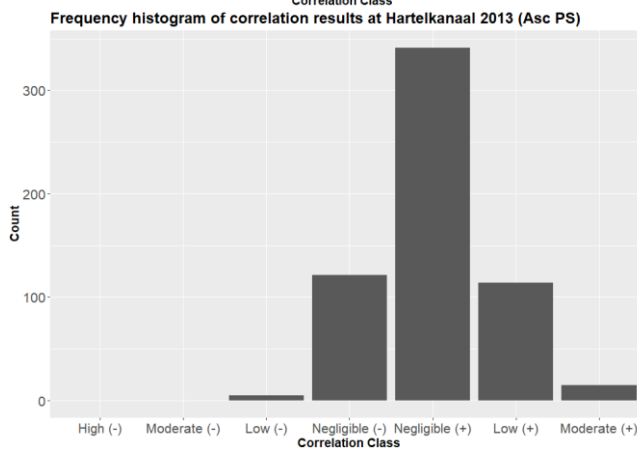
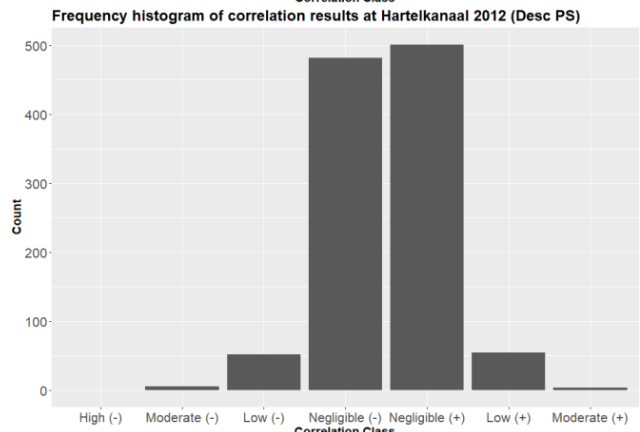
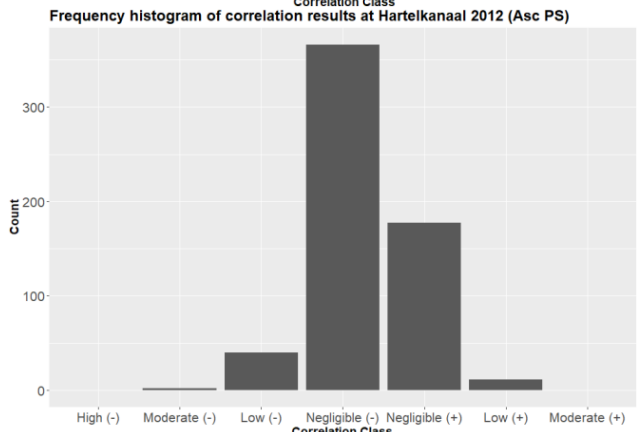
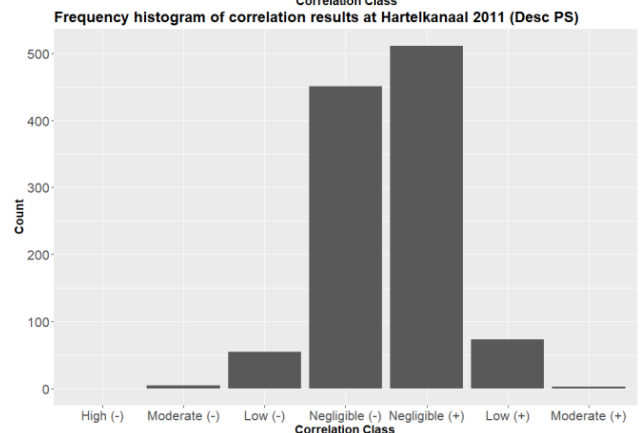
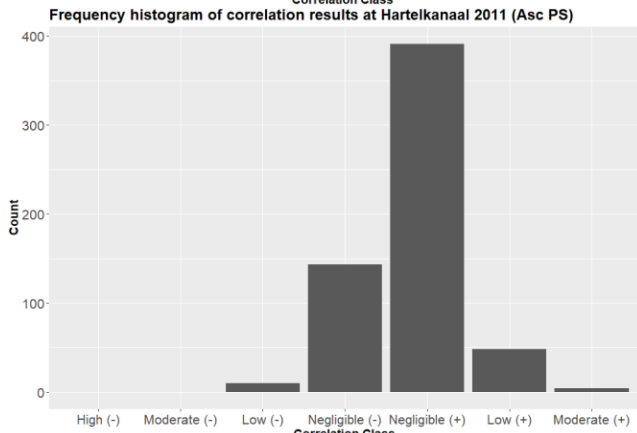
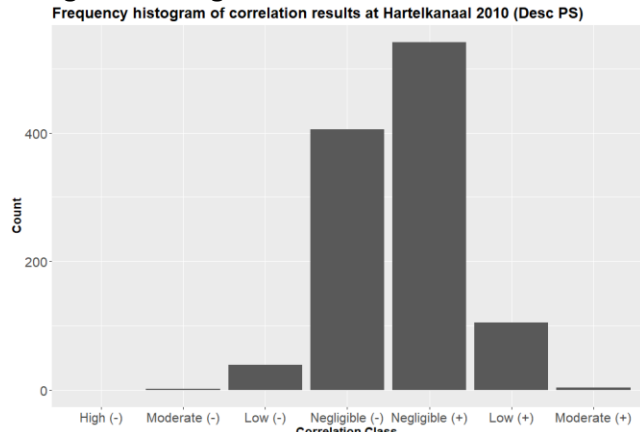


Appendix XX: Frequency histograms Hartelkanaal

Using Ascending PS time series



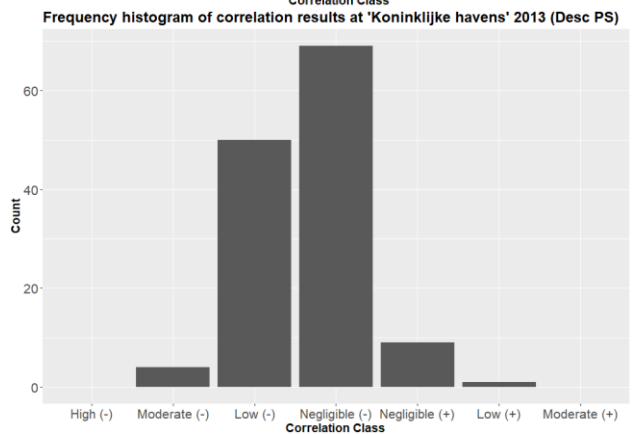
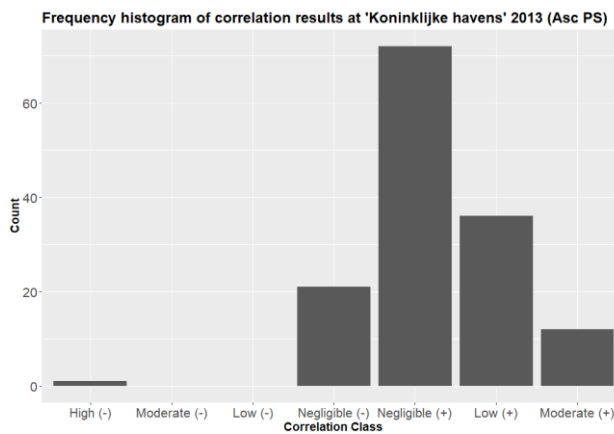
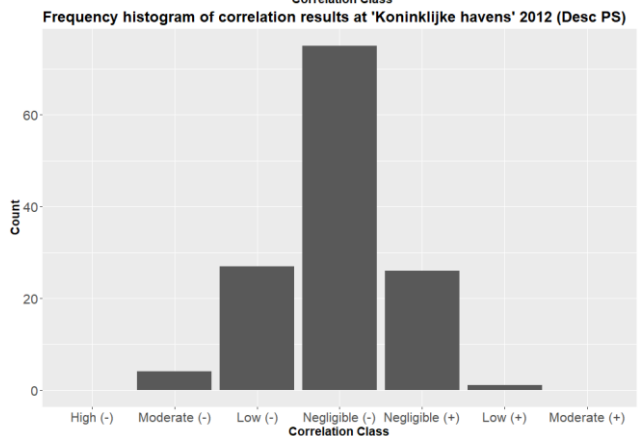
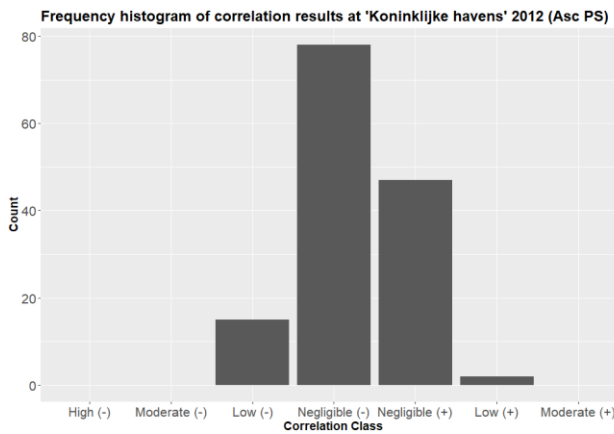
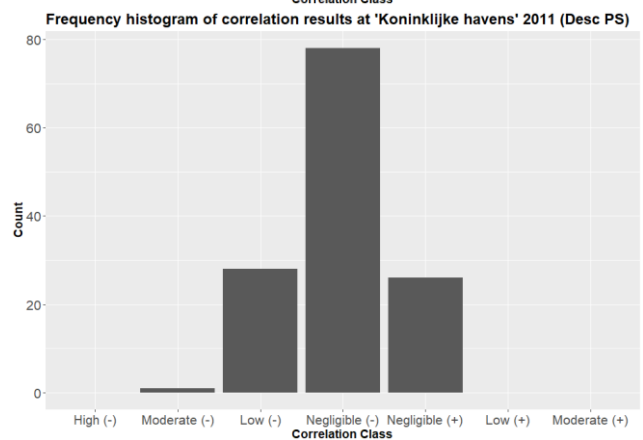
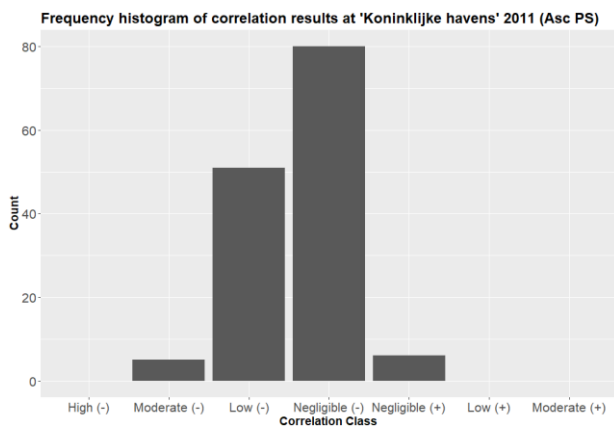
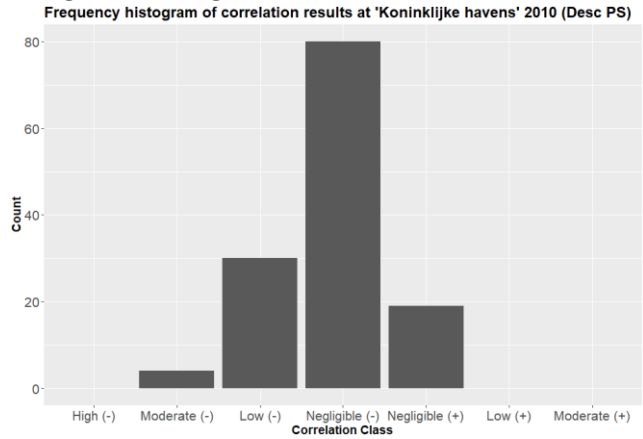
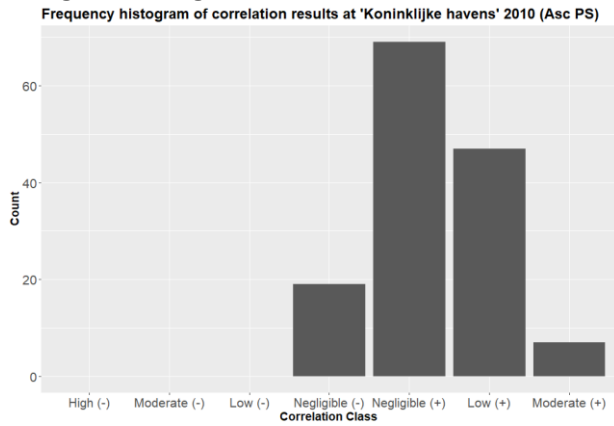
Using Descending PS time series



Appendix XXI: Frequency histograms Prinses Beatrixhaven and Prins Johan Friso haven

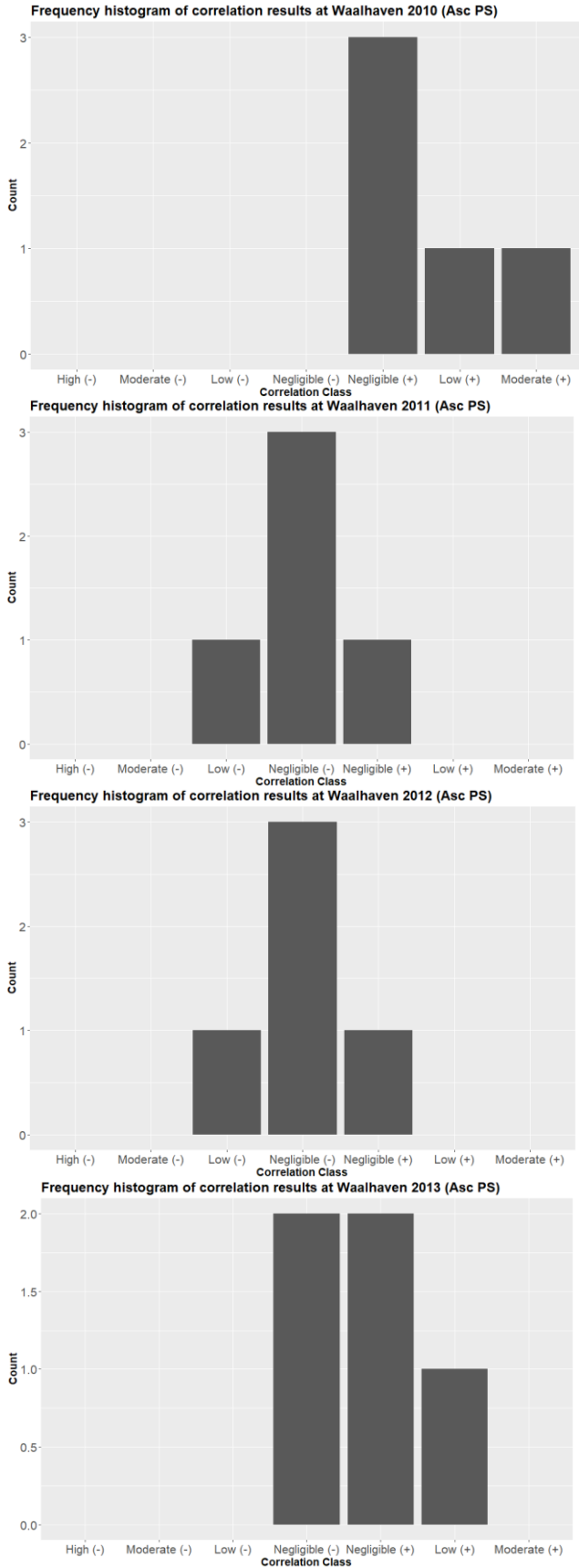
Using Ascending PS time series

Using Descending PS time series

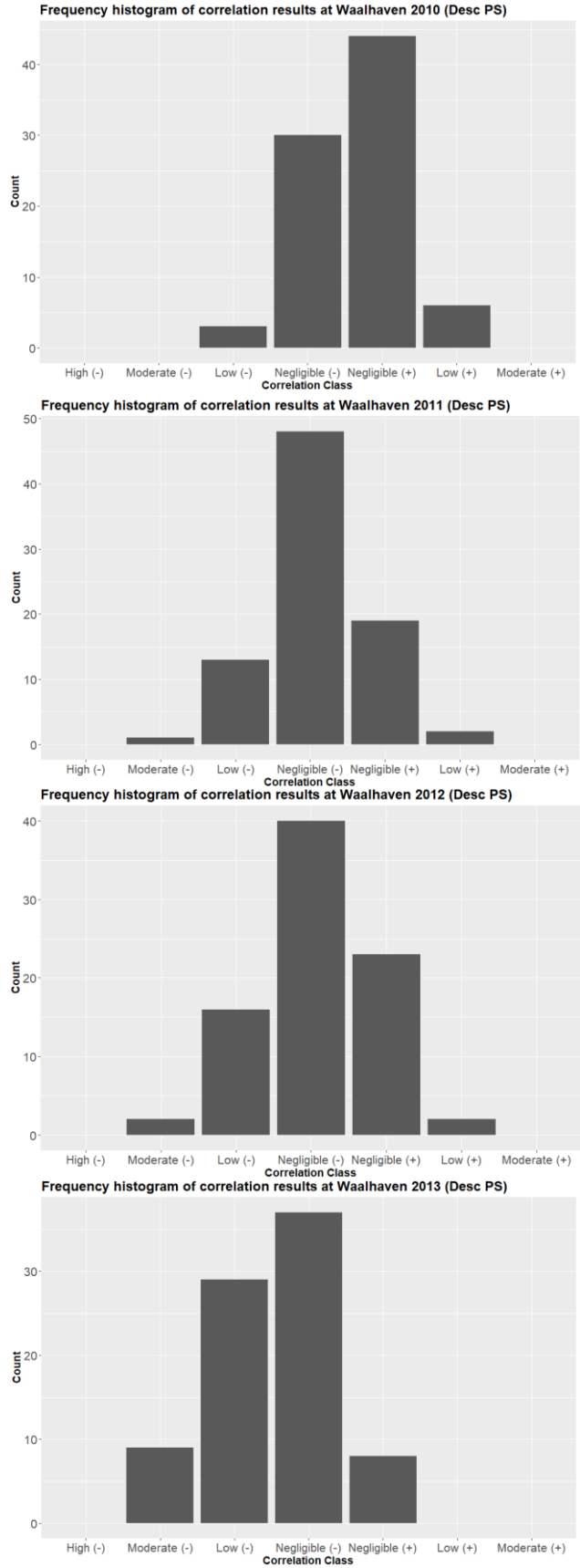


Appendix XXII: Frequency histograms Waalhaven

Using Ascending PS time series



Using Descending PS time series

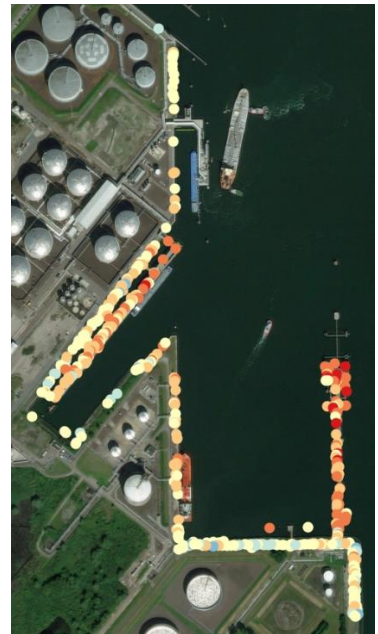
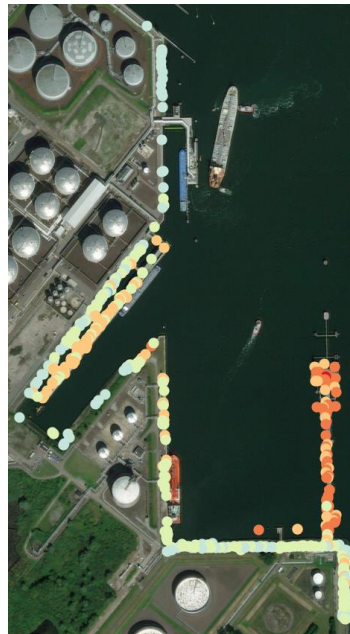


Appendix XXIII: Correlation per point Donauhaven and 7e Petroleumhaven
(using Descending PS time series)

Study area

2010-2013

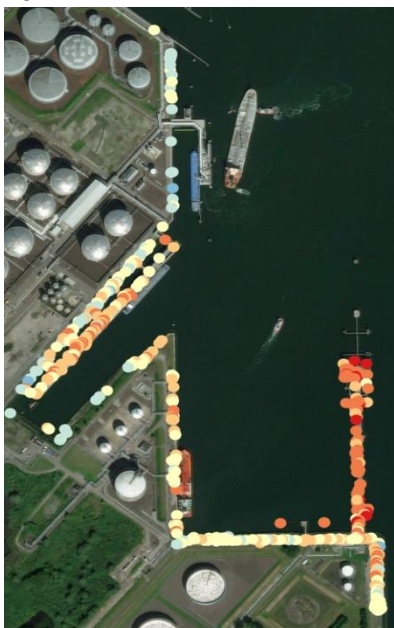
2010



2011

2012

2013



Legend

- High negative correlation
- Moderate negative correlation
- Low negative correlation
- Negligible correlation
- Negligible correlation
- Low positive correlaaton
- Moderate positive correlation

References

- Zhou, X., Chang, N.-B., & Li, S. (2009). Applications of SAR Interferometry in Earth and Environmental Science Research. *Sensors*, 1876-1911. doi:<https://doi.org/10.3390/s90301876>
- Airbus Defence and Space. (2018). *Airbus Defence and Space*. Retrieved April 2018, from [www.intelligence-airbusds.com: https://www.intelligence-airbusds.com/en/3085-terrasar-x-paz-constellation](https://www.intelligence-airbusds.com/en/3085-terrasar-x-paz-constellation)
- Airbus Defence and Space. (2018). *Airbus Defence and Space*. Retrieved April 2018, from [https://www.intelligence-airbusds.com: https://www.intelligence-airbusds.com/terrasar-x/](https://www.intelligence-airbusds.com/terrasar-x/)
- Baumann, P. R. (2010). *The State University of New York*. Retrieved March 2018, from [suny.oneonta.edu: http://www.oneonta.edu/faculty/baumanpr/geosat2/RS-Introduction/RS-Introduction.html](http://www.oneonta.edu/faculty/baumanpr/geosat2/RS-Introduction/RS-Introduction.html)
- Bishara, A. J., & Hittner, J. B. (2012). Testing the Significance of a Correlation with Non-normal Data: Comparison of Pearson, Spearman, Transformation, and Resampling Approaches. *Psychological Methods*, 399-417. doi:10.1037/a0028087
- Brinkman, M. (2016, August 22). *blackboard.wur.nl*. Retrieved May 2018, from [blackboard.wur.nl: https://blackboard.wur.nl](https://blackboard.wur.nl)
- Business Dictionary. (2018). *Business Dictionary*. Retrieved from [www.businessdictionary.com: http://www.businessdictionary.com/definition/non-destructive-testing.html](http://www.businessdictionary.com/definition/non-destructive-testing.html)
- CRISP. (2001). *Centre for Remote Imaging Sensing and Processing (CRISP)*. Retrieved March 2018, from [crisp.nus.edu.sg: https://crisp.nus.edu.sg/~research/tutorial/process.htm](https://crisp.nus.edu.sg/~research/tutorial/process.htm)
- Crosetto, M., Monserrat, O., Jungner, A., & Crippa, B. (2009). *Persistent Scatterer Interferometry: Potential and Limits*. Institute of Geomatics | University of Milan, Av. del Canal Olímpic | Department of Earth Sciences, Castelldefels | Milan. Retrieved May 2018, from <https://www.semanticscholar.org/paper/Persistent-Scatterer-Interferometry%3A-Potential-and-Crosetto-Monserrat/8751fcad5e0dec33ef633a5dc15d12a8b3cf2489>
- Crosetto, M., Monserrat, O., Cuevas-González, M., Devanthéry, N., & Crippa, B. (2016, May). Persistent Scatterer Interferometry: A review. *ISPRS Journal of Photogrammetry and Remote Sensing*, 115, 78-89. doi:<https://doi.org/10.1016/j.isprsjprs.2015.10.011>
- De Gijt, J. G., & Broeken, M. L. (2014). Determination of design water levels. In J. G. De Gijt, & M. L. Broeken, *Quay Walls* (p. 261). Rotterdam: CRC Press. Retrieved March 2018, from <https://books.google.nl/books?id=K3xcAgAAQBAJ&pg=PA261&lpg=PA261&dq=tides+fluctuating+water+levels+quay+walls&source=bl&ots=LtZFVYonc&sig=qllDmYjfkahAcMfZyQ27A0HKODU&hl=nl&sa=X&ved=0ahUKEwlrLyGovzaAhXBLVAKHXxxAV0Q6AEIKDAA#v=onepage&q=tides%20fluctuating>
- De Gijt, J. G., & Broeken, M. L. (2014). Main types of quay walls. In J. G. De Gijt, & M. L. Broeken, *Quay Walls* (2 ed., pp. 47-48). Rotterdam: CRC Press. Retrieved April 2018, from <https://books.google.nl/books?id=K3xcAgAAQBAJ&pg=PA261&lpg=PA261&dq=tides+fluctua>

ting+water+levels+quay+walls&source=bl&ots=LtZFYonc&sig=qllDmYjfkahAcMfZyQ27A0H
kODU&hl=nl&sa=X&ved=0ahUKEwilrLyGovzaAhXBLVAKHXxxAVOQ6AEIKDAA#v=onepage&q=
tides%20fluctuating

Dictionary.com. (2018). *Dictionary.com*. Retrieved May 2018, from [www.dictionary.com](http://www.dictionary.com/browse/ground-track):
<http://www.dictionary.com/browse/ground-track>

DLR. (2011, June 27). *DLR*. Retrieved June 2018, from <https://www.dlr.de>:
https://www.dlr.de/dlr/en/desktopdefault.aspx/tabid-10382/570_read-431/#/gallery/356

DLR. (2014, March 21). *DLR*. Retrieved April 2018, from <http://www.dlr.de>:
http://www.dlr.de/dlr/en/desktopdefault.aspx/tabid-10377/565_read-436/#/gallery/350

Dwarakish, G. S., & Salim, A. M. (2015). Review on the Role of Ports in the Development of a Nation.
Aquatic Procedia, 4, 295-301. doi:<https://doi.org/10.1016/j.aqpro.2015.02.040>

Earth and Space Research. (2018). *Earth and Space Research*. Retrieved June 2018, from
<https://www.esr.org>: https://www.esr.org/data-products/antarctic_tg_database/ocean-tide-and-ocean-tide-loading/

EARTHDATA. (2018, April 16). *EARTHDATA*. Retrieved April 2018, from <https://earthdata.nasa.gov>:
<https://earthdata.nasa.gov/user-resources/remote-sensors>

EESemi.com. (2005). *EESemi.com*. Retrieved June 2018, from www.eesemi.com:
<http://eesemi.com/dielectric-constant.htm>

ESA. (2005, March 11). *Space in images*. Retrieved May 2018, from www.esa.int:
http://www.esa.int/spaceinimages/Images/2005/12/Interferogram_of_Bam_earthquake

ESA. (2010, Februar 07). *Space in images*. Retrieved May 2018, from www.esa.int:
http://m.esa.int/spaceinimages/Images/2010/06/Volcanic_uplift

ESA. (2018). *ESA Education*. Retrieved April 2018, from [m.esa.int](http://www.esa.int)/ESA:
http://www.esa.int/Education/7._Active_sensors

ESA Earth Watching. (2018). *ESA Earth Watching*. Retrieved May 2018, from
earth.esa.int/web/earth-watching: <https://earth.esa.int/web/earth-watching/image-of-the-week/content/-/article/cairo-egypt-sentinel>

ESA Earthnet Online. (2014, July 24). *ESA Earthnet Online*. Retrieved April 17, 2018, from ESA
Earthnet Online: <https://earth.esa.int/handbooks/asar/CNTR5-2.html#eph.asar.gloss.radsar:SAR>

ESA Earthnet Online. (2018). *ESA Earthnet Online*. Retrieved April 2018, from earth.esa.int:
https://earth.esa.int/web/guest/missions/esa-operational-eo-missions/ers/instruments/sar/applications/radar-courses/content-2/-/asset_publisher/qIBc6NYRXfnG/content/radar-course-2-parameters-affecting-radar-backscatter

- ESA Sentinel Online. (2018). *ESA Sentinel Online*. Retrieved May 2018, from www.sentinel.esa.int/web/sentinel/home:
<https://sentinel.esa.int/web/sentinel/missions/sentinel-1/overview>
- Ferretti, A., Monti-Guarnieri, A., Prati, C., & Rocca, F. (2007). *InSAR Principles: Guidelines for SAR Interferometry Processing and Interpretation*. Politecnico di Milano, Dipartimento di Elettronica ed Informazione. Milan: ESA Publications. Retrieved April 2018, from https://www.esa.int/esapub/tm/tm19/TM-19_ptA.pdf
- Geoscience Australia. (2018). *Geoscience Australia*. Retrieved from www.ga.gov.au:
<http://www.ga.gov.au/scientific-topics/positioning-navigation/geodesy/geodetic-techniques/interferometric-synthetic-aperture-radar>
- Ghasemi, A., & Zahediasl, S. (2012). Normality Tests for Statistical Analysis: A Guide for Non-Statisticians. *International Journal of Endocrinology*, 486–489. doi: 10.5812/ijem.3505
- Hauke, J., & Kossowski, T. (2011). Comparison Of Values Of Pearson's and Spearman's Correlation Coefficients On The Same Sets Of Data. *Quaestiones Geographicae*, 87-93. doi:10.2478/v10117-011-0021-1
- Havenbedrijf Rotterdam. (2018). *Port of Rotterdam*. Retrieved April 2018, from www.portofrotterdam.com/nl: <https://www.portofrotterdam.com/nl/de-haven/havenontwikkeling/waalhaven-gebiedsontwikkeling>
- ITS. (1996, August 23). *Institute For Telecommunication Sciences*. Retrieved June 2018, from <https://www.its.blrdoc.gov>: https://www.its.blrdoc.gov/fs-1037/dir-029/_4335.htm
- Kooistra, L. (2018). *Laboratory of Geo-information Science and Remote Sensing*. Retrieved from www.wur.nl/en/Research-Results/Chair-groups/Environmental-Sciences/Laboratory-of-Geo-information-Science-and-Remote-Sensing.htm:
http://scomp5063.wur.nl/courses/grs10306/Clevers/RS%20CH4%20Preprocessing/IGI_preprocessing%20RS%20ppt.pdf
- Lamont-Doherty Earth Observatory. (1998, August 20). *Remote Sensing Glossary*. Retrieved April 2018, from <http://www.ldeo.columbia.edu>:
<http://www.ldeo.columbia.edu/res/fac/rsvlab/glossary.html>
- Lei, M., Wang, Q., Liu, X., Xu, B., & Zhang, H. (2017, January). Influence of ocean tidal loading on InSAR offshore areas deformation monitoring. *Geodesy and Geodynamics*, 70-76. doi:<https://doi.org/10.1016/j.geog.2016.09.004>
- MathBitsNotebook. (2018). *MathBitsNotebook*. Retrieved June 2018, from mathbitsnotebook.com:
<https://mathbitsnotebook.com/Algebra2/Statistics/STstandardNormalDistribution.html>
- Merk, O. (2010). *The Competitiveness of Global Port-Cities: Synthesis Report*. Organisation for Economic Co-operation and Development (OECD). Retrieved April 2018, from <https://www.oecd.org/cfe/regional-policy/Competitiveness-of-Global-Port-Cities-Synthesis-Report.pdf>

- Mukaka, M. (2012, September). A guide to appropriate use of Correlation coefficient in medical research. *Malawi Medical Journal*, 69–71. Retrieved May 2018, from <https://www.ncbi.nlm.nih.gov/pmc/articles/PMC3576830/#R2>
- NASA Earth Observatory. (2018). *NASA Earth Observatory*. (S. Graham, Editor) Retrieved April 17, 2018, from earthobservatory.nasa.gov: <https://earthobservatory.nasa.gov/Features/RemoteSensing/remote.php>
- NASA Earth Observatory. (2018). *NASA Earth Observatory*. (S. Graham, Editor) Retrieved April 17, 2018, from earthobservatory.nasa.gov: <https://earthobservatory.nasa.gov/Features/RemoteSensing/remote.php>
- NASA Earth Observatory. (2018). *NASA Earth Observatory*. Retrieved May 2018, from www.earthobservatory.nasa.gov: <https://earthobservatory.nasa.gov/Features/ShuttleRetrospective/page7.php>
- NASA Imageseer. (2015, February 12). *NASA Imageseer*. Retrieved March 2018, from imageseer.nasa.gov: <https://imageseer.nasa.gov/imagepedia/articles.php?article=Pre-Processing+Techniques>
- National Research Council of Italy. (2018). *National Research Council of Italy*. Retrieved April 2018, from www.irea.cnr.it: http://www.irea.cnr.it/en/index.php?option=com_k2&view=item&id=77:differential-synthetic-aperture-radar-interferometry&Itemid=139
- Natural Resources Canada. (2015, Decemeber 12). *Natural Resources Canada*. Retrieved April 2018, from National Resources Canada: <http://www.nrcan.gc.ca/node/9309>
- NCSS Statistical Software. (2016, 30 June). *NCSS Statistical Software*. Retrieved May 2018, from <https://www.ncss.com>: https://ncss-wpengine.netdna-ssl.com/wp-content/themes/ncss/pdf/Procedures/NCSS/Normality_Tests.pdf
- Peng, W., Wang, Q., & Cao, Y. (2017, January). Analysis of Ocean Tide Loading in Differential InSAR Measurements. *Remote Sensing*, 2-9. doi:<https://doi.org/10.3390/rs9020101>
- PennState Eberly College of Science. (2018). *STAT 414/415*. Retrieved May 2018, from <https://newonlinecourses.science.psu.edu/statprogram/>: <https://onlinecourses.science.psu.edu/stat414/node/149/>
- PennState Eberly College of Science. (2018). *STAT 501*. Retrieved May 2018, from <https://newonlinecourses.science.psu.edu/stat501/node/256/>
- Photojournal. (2001, March 30). *Photojournal*. Retrieved May 2018, from www.jpl.nasa.gov/index.php: <https://photojournal.jpl.nasa.gov/catalog/PIA00557>
- Port of Rotterdam. (2018). *Port of Rotterdam*. Retrieved March 2018, from www.portofrotterdam.com: <https://www.portofrotterdam.com/en/downloads/grafische-kaarten-en-luchtfotos/port-of-rotterdam>

- radartutorial.eu. (2018). *radartutorial.eu*. Retrieved May 2018, from <http://www.radartutorial.eu: http://www.radartutorial.eu/01.basics/The%20Radar%20Range%20Equation.en.html>
- Rebekić, A., Lončarić, Z., Petrović, S., & Marić, S. (2015). *Pearson's or spearman's correlation coefficient – which one to*. Agricultural Institute Osijek, Faculty of Agriculture in Osijek. Osijek: Agricultural Institute Osijek. doi:<http://dx.doi.org/10.18047/poljo.21.2.8>
- Richwien, W. (2008). Design Concepts for Quay Walls For Large Vessels. *Chinese-German Joint Symposium on Hydraulic and Ocean Engineering* (pp. 90-94). Darmstadt: Institute of Soil Mechanics and Foundation Engineering, University Duisburg-Essen, Essen. Retrieved April 2018, from <http://www.comc.ncku.edu.tw/joint/joint2008/papers/18.pdf>
- Rijkswaterstaat Waterinfo. (2018). *Rijkswaterstaat Waterinfo*. Retrieved March 2018, from waterinfo.rws.nl: http://waterinfo.rws.nl/#!/nav/bulkdownload/parameters/Waterhoogten/
- Roque, D., Perrisin, D., Falcao, A. P., Fonseca, A. M., Henriques, M. J., & Franco, J. (2015). Dam Regional Safety Warning Using Time-Series InSAR Techniques. (pp. 1-8). Lisbon, Portugal: Second International Dam World Conference. Retrieved January 2018, from https://www.researchgate.net/publication/317620924_DAM_REGIONAL_SAFETY_WARNING_USING_TIME-SERIES_INSAR_TECHNIQUES
- Sapling Learning. (2018). *Sapling Learning*. Retrieved April 2018, from sites.google.com/site/chempendix/: <https://sites.google.com/site/chempendix/em-spectrum>
- Sedgwick, P. (2012, July). *BMJ*. doi:[10.1136/bmj.e4483](https://doi.org/10.1136/bmj.e4483)
- SkyGeo. (2018). *SkyGeo*. Retrieved March April, from www.skygeo.com: https://skygeo.com/insar-technical-background/
- SkyGeo. (2018). *skygeo.com*. Retrieved March 2018, from [skygeo.com: https://skygeo.com/company/](https://skygeo.com/company/)
- Smith, L. C. (2002). Emerging Applications of Interferometric Synthetic Aperture Radar (InSAR) in Geomorphology and Hydrology. *Annals of the Association of American Geographers*, 395-398. Retrieved May 2018, from <https://pdfs.semanticscholar.org/116d/faf41b646b7f91007e54f43f29de12c7acec.pdf>
- Sousa, J. J., Ruiz, A. M., Bakoň, M., Lazecky, M., Hlaváčová, I., Patrício, G., . . . Perissin, D. (2016). Potential of C-Band SAR Interferometry for Dam Monitoring. *Procedia Computer Science*, 100, 1103 - 1114. doi:<https://doi.org/10.1016/j.procs.2016.09.258>
- Sousa, J., Hlaváčová, I., Bakoň, M., Lazecký, M., Patrício, G., Guimarães, P., . . . Bento, R. (2014). Potential of Multi-temporal InSAR Techniques for Bridges and Dams Monitoring. *Procedia Technology*, 16, 834 - 831. doi:<https://doi.org/10.1016/j.protcy.2014.10.033>
- SRM. (2010, October 10). *SRM Institute of Science and Technology*. Retrieved May 2018, from <http://www.srmuniv.ac.in: http://www.srmuniv.ac.in/sites/default/files/downloads/CORRELATION.pdf>

The Port of Rotterdam. (2018). *The Port of Rotterdam*. Retrieved from

<https://www.portofrotterdam.com>: <https://www.portofrotterdam.com/en/asia/why-rotterdam>

Yeh, T.-K., Hwang, C., Huang, J.-F., Chao, B. F., & Chang, M.-H. (2011). Vertical Displacement due to Ocean Tidal Loading Around Taiwan Based on GPS Observations. *Terrestrial, Atmospheric and Oceanic Sciences (TAO)*, 22, 373-382. doi:10.3319/TAO.2011.01.27.01(T)

Zhou, W., Chen, F., & Guo, H. (2017). Differential Radar Interferometry for Structural and Ground Deformation Monitoring: A New Tool for the Conservation and Sustainability of Cultural Heritage Sites. *Sustainability*, 1712-1729. doi:<https://doi.org/10.3390/su7021712>